

UNIVERSIDAD DE VIGO
DEPARTAMENTO DE FÍSICA APLICADA
EPhyslab

Universida_deVigo

PhD Thesis

**Differences in warming trends between coastal upwelling areas
and the adjacent ocean**

Memoria Presentada por
Francisco J. Santos González
para optar al título de *DOCTOR POR LA UNIVERSIDAD DE VIGO*
CON MENCIÓN INTERNACIONAL
Junio, 2013.

Informe del director

Dr. Ramón Gómez Gesteira catedrático del Departamento de Física Aplicada de la Universidad de Vigo y Dra. Maite deCastro profesora del Departamento de Física Aplicada de la Universidad de Vigo:

CERTIFICAN

Que la presente memoria "Differences in warming trends between coastal upwelling areas and the adjacent ocean", resume el trabajo de investigación realizado, bajo su dirección, por DON FRANCISCO J. SANTOS GONZÁLEZ en el departamento de Física Aplicada en el programa de doctorado de Ciencias del Clima: Meteorología, Oceanografía Física y Cambio Climático de la Facultad de Ciencias de Ourense para optar al título de "DOCTOR POR LA UNIVERSIDAD DE VIGO CON MENCIÓN INTERNACIONAL" .

Y para que conste y en cumplimiento de la legislación vigente, firma el presente informe en Ourense, a 6 de Marzo del 2013.

Fdo. Dr. Ramón Gómez Gesteira

Fdo. Dra. María Teresa deCastro Rodríguez

“It would not be nothing without the people around me, they make me better every day”.

“NO PAIN NO GLORY”.

Acknowledgements

To my parents *Manolo and Mari* “ Thank you for life, thanks for your effort and your commitment to take me here and thank you for being as you are, without you and a little person who looks after me from heaven I would be nothing”

“My sister and brother *Patri and Cesar*, for your encouragement, for your support and you are more than brothers to me.”.

“To *Moncho Gómez Gesteira and Maite DeCastro* for the opportunity given to me, for their patience and understanding. Thanks also for all the fun times we spent together”.

“To *Lorena Meijide and Juan Santás*, that great partners who has contributed with so much good sense to my life”.

“To *Guille* for our life together, I just want to say Thank You Brother”.

“To *Lucía Barandela* thank you for this nice present, but I am sure that our future together will be awesome”.

“To *Lorena Díaz, Santy, Montse & Glo* for so many times spent together and all the encouragement received”.

“To *Anxo, Alejandro, Angel, Jose, Inés, Alexandre, Isabel & Xurxo* the large group that I have accepted me and every moment spent with them.”

“Thanks to *Ana Belen, Angie, Ainara, Begoña, Adrián, Bety, Carlos Percival, Diego, Estrella, Eva, Igor, Lucía Díaz, Marina, Raquel, Rai, Ronal, Silvia Álvarez & Yago* for all the moments together with you all, for all the confidence and encouragement you have given me”.

“And Most especially thanks to my bikes, my best psychologist, haha”.

“This work was supported by the Xunta de Galicia under Research Grants No and was also supported by Xunta de Galicia under Programa de Consolidación e Estruturação de Unidades de Investigación (Grupos de Referencia Competitiva). 10PXIB383169PR cofinanced by European Regional Development Fund (FEDER).”.

Resumen en Castellano

El cambio climático ha sido uno de los temas más analizados por los climatólogos y oceanógrafos durante finales del siglo *XX* y comienzos del siglo *XXI*, tal y como queda recogido en los diferentes informes del *Intergovernmental Panel on Climate Change* (IPCC) ([IPCC 1990];[IPCC 1996]; [IPCC 2001];[IPCC2007]). La principal conclusión a la que se llega es que la temperatura ha ido incrementando durante la segunda mitad del siglo *XX* y que este incremento es mayor que cualquier otro observado para un periodo de 50 años en los últimos 500 años [IPCC2007]. Además, numerosos estudios resaltan que las últimas cuatro décadas han sido el periodo de mayor calentamiento jamás observado. Los océanos también se han visto afectados por este calentamiento y juegan un papel importante en el cambio climático, ya que actúan como un gran almacén de calor debido a la gran capacidad calorífica del agua. Este cuarto informe del IPCC también establece que *"el incremento de la temperatura superficial del mar a lo largo del siglo *XX* es aproximadamente la mitad del incremento medio de la temperatura del aire en la superficie de la tierra"* y *"el contenido global de calor del océano se ha incrementado desde 1950, periodo a partir del cual están disponibles observaciones precisas de la temperatura del mar a nivel sub-superficial"*. Debe tenerse en cuenta que, *"la capacidad de calor de los océanos es sobre 1,000 veces mayor que la de la atmósfera, y el calor neto absorbido por los*

océanos desde 1960 es sobre unas 20 veces mayor que el absorbido por la atmosfera [Levitus 2005]. Esta cantidad tan grande de calor, la cual está principalmente contenida en las capas superficiales del océano, juega un papel crucial en el cambio climático, en particular en variaciones a escala decadal”.

Las variables más usadas para analizar el calentamiento del océano han sido la temperatura superficial (SST) y el contenido de calor (cuyos cambios son aproximadamente proporcionales al promedio de los cambios de temperatura en un volumen de agua). Ambas variables son complementarias proporcionando información sobre la tendencia de la SST y del calor almacenado en el océano entre la superficie y profundidades entre 700 y 3,000 *m*. En general, la mayoría de los autores [Levitus 2005], consideraban que un gran porcentaje de este calor almacenado se concentraba en los primeros 700 *m* mientras que la capa entre 1,000–3,000 *m* solo proporcionaba el 9% del incremento global. Recientemente, algunos autores como [Katsman 2011] han encontrado que existen cambios importantes en el contenido de calor por debajo de 700 *m*. La comparación en los cambios en el contenido de calor para profundidades entre 0–700 *m* y 700–2000 *m* se puede encontrar en [Levitus 2012]. La SST es también un parámetro fundamental en el intercambio de calor entre el océano y la atmosfera. Además, la SST está influenciada por parámetros climáticos, meteorológicos, hidrodinámicos y batimétricos.

Durante el último siglo, se ha realizado un gran esfuerzo en el desarrollo de series de SST con cobertura global, primero mediante medidas voluntarias de barcos, derivas y boyas ([Brohan 2006];[Smith 2008]) y después con datos de satélites. Se han realizado también grandes esfuerzos para corregir las incertidumbres debidas a diversos factores tales como: cambios en las rutas de los barcos después de abrir los canales de Panamá y de Suez, escasez de muestreos durante las guerras mundiales, diferencias

en la recolección de agua y más recientemente, la incertidumbre provocada por la presencia de aerosoles y la cobertura nubosa, que producen un sesgo negativo en la temperatura, y por el hecho de que los satélites recogen temperaturas de la capa superficial en vez de temperaturas cercanas a ella, (para entender completamente los diferentes sesgos y métodos para corregirlos ver: ([Kushnir 1994];[Folland 1995];[Kapala 1998];[Smith 2002]; [Smith 2003]; [Smith 2004];[Smith 2005];[Worley 2005];[Kent 2005];[Kent 2006a]; [Kent 2006b];[Brohan 2006];[Smith 2008])).

Del análisis de la tendencia de la SST se desprende que tiene una dependencia muy alta tanto de la escala temporal como de la escala espacial seleccionada ([Parker 1994];[Smith 1994];[Casey 2001]). Además, las tendencias de la SST están lejos de ser lineales, y se pueden observar tendencias opuestas si se consideran diferentes estrategias de ajuste (lineal, senoide) o diferentes periodos de tiempo (ver *Appendix I*).

Aunque en las últimas décadas la base de datos más utilizada ha sido la *World Ocean Database* [Levitus 2005], recientemente también se han comenzado a utilizar bases de datos obtenidas de proyectos de asimilación de datos como *Simple Ocean Data Assimilation (SODA)*, las cuales han reanalizado datos de diferentes fuentes (barcos oceanográficos, satélites, modelos de simulación) proporcionándonos un mapeado uniforme y medidas regulares de variables tanto observadas directamente como variables indirectas. Este tipo de datos de asimilación proporcionan una valiosa información desde la superficie hasta una profundidad de 5,375 m (40 niveles). De esta manera, es posible obtener una visión completa de los diferentes procesos hidrográficos mediante el análisis de patrones tanto globales ([Carton 2008]; [Zheng 2009]) como a escalas más pequeñas ([Zheng 2010];[Patti 2010]; [Giese 2011]).

El calentamiento global no es uniforme ni en el tiempo ni en el espacio ([Folland 1984];[Folland 1992];[Nicholls 1996];[Casey 2001]). Así, por ejem-

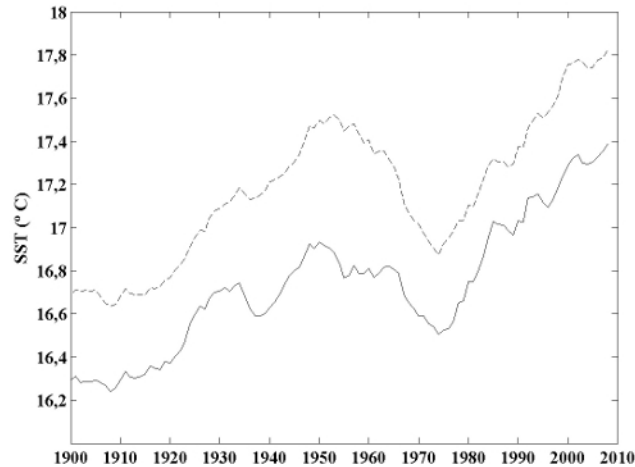


Figure 1: *Evolución costera (línea gris) y oceánica (línea negra) de la SST en el Atlántico norte para el periodo 1900–2010. La SST costera (oceánica) se ha promediado latitudinalmente desde 37 hasta 47°N en los 9°W (15°W). Para facilitar la visualización se ha realizado una media móvil a ± 60 meses.*

plo, se han detectado varios ciclos de calentamiento y enfriamiento en la región del Atlántico Norte durante el siglo XX Fig.1 tanto a escalas globales como regionales ([IPCC2007];[Rayner 2006];[GarciaSoto 2002]; [deCastro 2009];[Gesteira 2011]).

El primer periodo de calentamiento comprende desde 1910 hasta 1945 y fue seguido por un periodo de enfriamiento, el segundo periodo de calentamiento comenzó durante los años 70.

De acuerdo con el cuarto informe del IPCC, "Durante el periodo comprendido entre 1961 hasta 2003, la temperatura global del océano ha aumentado 0.10°C considerando el intervalo desde la superficie hasta una profundidad de 700 m. De acuerdo con el tercer informe del IPCC Third Assessment Report (TAR), el contenido de calor global (0-3,000 m) se in-

crementó durante el mismo periodo, lo que es equivalente a absorber energía a una velocidad de $0.21 \pm 0.04 \text{ W m}^2$ promediando a toda la superficie de la Tierra. Dos tercios de esta energía se absorbió en los primeros 700 m del océano. Las observaciones del contenido global de calor muestran una considerable variabilidad tanto inter-anual como inter-decadal sobreimpuestas a tendencias a más largo plazo. El periodo desde 1993 hasta 2003 tiene la mayor tasa de calentamiento relativo al periodo que comprende desde 1961 hasta 2003, pero desde el 2003 se aprecia un cierto enfriamiento”.

El calentamiento del océano varía en un amplio rango de escalas temporales, desde escala estacional, decadal hasta centenaria y a escalas aún más largas. Los principales modos de variabilidad climática en cada área (*El Niño-Southern Oscillation (ENSO)*, *la Pacific Decadal Oscillation (PDO)*, *la North Atlantic Oscillation (NAO)*, *la Souther Annular Mode (SAM)*, *la Eastern Atlantic Mode (EA)*) fuerzan a los océanos, causando cambios en la circulación del océano mediante cambios en los patrones de vientos y cambios en la densidad de la superficie del océano.

Por otro lado, el calentamiento global no tiene una uniformidad espacial para todos los océanos, con unas regiones calentándose más rápido y otras más lento que la media global ([Levitus 2000];[Palttridge 1981]). En particular, el Océano Atlántico es el mayor responsable del incremento del contenido de calor a nivel mundial ([Nerem 1999];[Levitus 2000];[Strong 2000]). Existe un gradiente latitudinal en el incremento de SST con un mayor calentamiento en el Hemisferio Norte que en el Sur [Strong 2000]. De acuerdo con el cuarto informe del IPCC, *”Nuevos análisis de datos proxy para el Hemisferio Norte indican que el incremento en la temperatura para el siglo XX es probablemente el mayor registrado durante los últimos 1,000 años. También es probable que en el Hemisferio Norte, los 90s hayan sido la década más calurosa y el año 1998 el más caluroso”*. En la Fig.2 se muestra el calentamiento del océano Atlántico para el periodo desde 1900 hasta 2009.

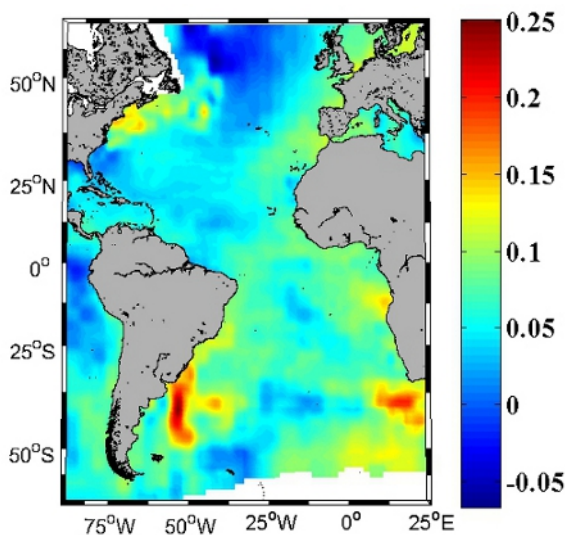


Figure 2: *Tendencia de la SST para el Atlántico, para el periodo 1900-2009, calculada con la base HadISST.*

El aumento en la SST también se muestra para la región del Atlántico Norte para dos periodos diferentes (Fig.3), desde 1900 hasta 2009 (*izquierda*) y desde 1979 hasta 2009 (*derecha*). En ambas figuras se observa un calentamiento en toda la región siendo más intenso durante las últimas décadas.

Estas diferencias entre áreas macroscópicas (hemisferios y océanos) son aún más marcadas a escalas regionales debido tanto a forzamientos locales como a forzamientos remotos tales como cambios en los vientos, corrientes oceánicas, variaciones en la profundidad de la termohalina y el afloramiento ([Cole 2000];[Lemos 2004];[Ginzburg 2004];[SantosA 2005];[Gesteira 2008a];[deCastro 2008a]). Más recientemente, autores como ([Relvas 2009];[Santos 2011a];[Santos 2012a]) describieron la existencia de diferentes velocidades de calentamiento entre zonas costeras y zonas oceánicas a la misma latitud, en regiones donde el afloramiento costero tiene un papel importante.

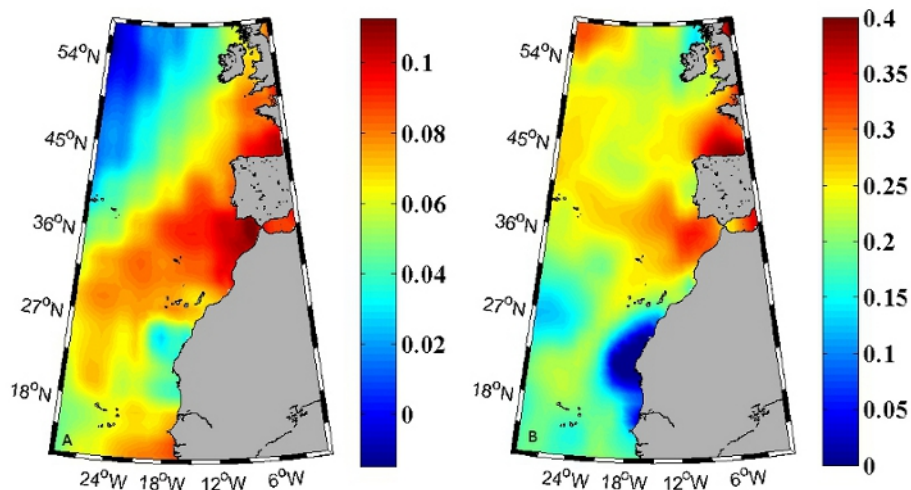


Figure 3: *Tendencia de la SST para el Atlántico Norte, para el periodo 1900-2009 (izquierda) y para el periodo 1975-2009 (derecha), calculada con la base HadISST.* De este modo, [Relvas 2009] detectó débiles tendencias al calentamiento en zonas costeras a lo largo de la parte sur de la costa oeste de la Península Ibérica (WIP).

El efecto producido por el afloramiento en la SST es posiblemente la característica oceanográfica más importante a lo largo de los cuatro mayores ecosistemas de afloramiento del mundo (*Canary Upwelling Ecosystem (CUE)*, *Benguela Upwelling Ecosystem (BUE)*, *California Current System (CCS)*, y *Peru-Humboldt Ecosystem*) ya que conlleva el reemplazo del agua superficial caliente por agua sub-superficial más fría. De acuerdo con algunos autores, los cambios en el gradiente térmico entre la tierra y el océano pueden ser los responsables de los cambios observados en la intensidad del afloramiento ([Bakun 1990];[Mendelssohn 2002];[McGregor 2007]).

Los vientos que soplan desde el norte a lo largo de las costas con orientación Norte-Sur tienden a desplazar las corrientes superficiales hacia la derecha de la dirección del viento, arrastrando las aguas superficiales ha-

cia el océano, esto ocurre en el hemisferio Norte, en el hemisferio sur ocurriría lo contrario. Como las aguas superficiales se desplazan hacia fuera de costa, aguas sub-superficiales se desplazan hacia arriba para sustituirlas. Este tipo de aguas que suben para sustituir a las aguas desplazadas suelen ser más frías, ricas en nutrientes, y muy productivas biológicamente. El afloramiento costero tiene principalmente dos efectos ecológicos. Por un lado, el afloramiento proporciona aguas ricas en nutrientes a la superficie lo cual hace aparecer el fitoplancton. El fitoplancton constituye una fuente de energía muy importante para muchas poblaciones de animales, como peces, mamíferos y pájaros marinos. Por otro lado, el afloramiento que mueve las aguas superficiales mar adentro, también puede mover las larvas de algunos animales marinos que viven cerca de costa a largas distancias de su habitat natural reduciendo sus posibilidades de supervivencia. Por estas razones, las regiones de afloramiento costero constituyen uno de los ecosistemas más productivos del mundo y soportan la mayor parte de la pesca mundial. Aunque las regiones de afloramiento costero representan solo el 1% de la superficie del océano, contribuyen al 20% de la pesca mundial [Pauly 1995]. Pero también, son regiones donde se produce el esparcimiento de larvas de especies costeras evitando su supervivencia. (Parte de esta información es obtenida desde la *NOAA Ocean Explorer: Sanctuary Quest*).

Por las razones arriba descritas, diversos autores han analizado la variabilidad del afloramiento a lo largo de la costa de los cuatro mayores sistemas de afloramiento del mundo obteniendo que es altamente dependiente del periodo de tiempo, de la región y de las estrategias de ajuste escogidas al analizar tendencias.

Estudios previos han mostrado resultados contradictorios en el ecosistema de afloramiento Canario. [Bakun 1990] encontró una intensificación en los vientos favorables al afloramiento para el periodo 1948–1979 y [McGregor 2007] obtuvo un enfriamiento de $0.5-1^{\circ}C$ durante el siglo *XX*

asociado a un aumento del afloramiento costero. Por el contrario, [Lemos 2004] y [Lemos 2006] encontraron un debilitamiento significativo en los vientos favorables al afloramiento para periodos de tiempo similares (para el periodo 1940–2000 y para el periodo 1901–2000, respectivamente). Además, [Gesteira 2008b] detectó un cierto debilitamiento en la intensidad del índice de afloramiento, siendo más pronunciado durante las últimas décadas. En el ecosistema de afloramiento de California [Schwing 1997] y [Mendelsohn 2002] encontraron un incremento en el afloramiento costero durante la estación de máxima intensidad, observando tendencias opuestas en cambios de la SST a largo plazo. Además, [diLorenzo 2005] también destacó el fortalecimiento de vientos favorables al afloramiento vinculado al calentamiento de la SST a largo plazo para esta región. Finalmente, [Pardo 2011] no encontró ninguna tendencia clara en la región de California durante las últimas seis décadas.

A día de hoy y hasta donde conocemos, solamente unos pocos estudios han analizado las componentes físicas de la tendencia del afloramiento costero en las regiones de Perú y de Benguela. [Pardo 2011] analizó la región de Perú para el periodo comprendido desde 1948 hasta 2009, mostrando un debilitamiento en el afloramiento con un pequeño calentamiento de la SST o incluso una tendencia al enfriamiento. El mismo autor encontró un incremento del afloramiento con un ligero incremento de la SST en la zona de Benguela. [Patti 2010] encontró un marcado incremento en el estrés del viento en ambas regiones, con un incremento en la estabilidad de la columna de agua.

El incremento de la temperatura del océano es especialmente importante en las áreas costeras debido a su importante impacto en los ecosistemas costeros ([Honkoop 1998];[Diederich 2005]). Recientemente, [Lima 2012], detectó que durante las últimas tres décadas, el $\sim 71.6\%$ de las zonas costeras del mundo experimentaron un calentamiento de $0.25 \pm 0.13^\circ C$

por década, el 6.8% un enfriamiento de $-0.11 \pm 0.10^{\circ}C$ *por década* y el restante 22.2% no sufrió ningún cambio significativo. Aparte de los cambios en la temperatura media, la frecuencia de las temperaturas extremas en el océano como eventos extremadamente cálidos o fríos son fundamentales para determinar los escenarios y las políticas para mitigar el impacto humano y comprender los cambios en el ecosistema marino costero ([Philippart 2003];[Frank 2005];[Thieltges 2006];[Occhipinti 2007]). Por esta razón, autores como [Lima 2012] han analizado el incremento (decrecimiento) en la frecuencia de días con eventos extremadamente cálidos (fríos) a lo largo del mundo en general y del margen Este Atlántico en particular.

El estudio de las temperaturas extremas sobre la tierra ha sido ampliamente considerado en el contexto de olas de calor y en el del impacto sobre la mortalidad ([Dessai 2002];[GarciaHerrera 2005];[Diaz 2006];[Trigo 2009]; [Barriopedro 2011];[deCastro 2011]). Además su variabilidad ha sido analizada durante los últimos 50 años, de acuerdo con el cuarto informe del IPCC, *"Fenómenos como días fríos, noches frías y heladas, se han convertido en menos frecuentes, mientras que los días cálidos, noches cálidas y olas de calor, se han convertido en más frecuentes probablemente a finales del siglo XX y muy probablemente debido a la contribución humana"*. Hasta donde nosotros sabemos, existen pocos estudios centrados en valores extremos de SST, tanto en la zona costera como en la zona oceánica, a pesar de que sus implicaciones son muy importantes para el ecosistema marino ([Lima 2006];[Lima 2007];[Wetthey 2011]).

El objetivo de este estudio es describir las diferencias en la evolución de SST entre la costa y el océano en el Atlántico Norte, en particular, a lo largo de la costa oeste de la Península Ibérica. El oeste de la Península Ibérica (37° hasta $43^{\circ}N$) está considerado como la zona más al norte influenciada por uno de los mayores ecosistemas de afloramiento del mundo, el (*Eastern North Atlantic Upwelling System*), que actúa a lo largo de

la costa Noroeste de África y la costa Atlántica de la Península Ibérica ([Nykjaer 1994];[SantosA 2005];[Álvarez 2008a]). Estos estudios han demostrado que en esta región el afloramiento es principalmente estacionario, y que ocurre con mayor probabilidad entre Abril y Septiembre.

La variabilidad de la SST observada tanto en zonas costeras como oceánicas durante el último siglo se ha analizado en función del afloramiento y de la intensidad de la circulación termohalina. Posteriormente también se han estudiado las diferencias en la variabilidad de la temperatura y del contenido de calor entre zonas costeras y oceánicas para los primeros 700 *m* desde 1975 hasta 2006 obteniendo información sobre los cambios producidos en la estructura vertical. Hasta donde sabemos, no se ha realizado nunca un estudio similar en esta región dónde solo se habían considerado patrones de SST.

Por otro lado, se han analizado los cambios observados en las masas de agua más relevantes a lo largo de la costa continental Atlántica de la Península Iberia (ENACW y MW) desde los años setenta. Para este propósito, se ha analizado la tendencia de la salinidad y de la temperatura correspondientes a la isopicna de ENACW y MW para determinar la velocidad de cambio de estas masas de agua. Este análisis permite conocer la influencia de esas masas de agua en las tendencias de los perfiles verticales del agua atlántica.

El estudio del calentamiento del océano en esta región continúa con el análisis de tendencias en la frecuencia de días de valores de SST extremadamente altos durante la era satelital (1982–2011). Más específicamente, se han analizado las diferencias entre la tendencia costera y oceánica tanto a escala anual como estacional.

A continuación se han realizado estudios similares primero para la sub-región Marroquí del ecosistema de afloramiento Canario y después a lo largo del sistema de afloramiento de Benguela. Ambas zonas están caracterizadas

por tener un afloramiento permanente aunque con variaciones estacionales. En la sub-región Marroquí del ecosistema de afloramiento Canario, se han analizado las diferencias regionales en la velocidad de calentamiento de la SST entre zonas costeras y oceánicas para la misma latitud en función de forzamientos locales como el viento y la temperatura del aire y forzamientos remotos como patrones de circulación atmosférica desde 1982 hasta 2010. Por último, se han analizado las diferencias en las tendencias del SST entre las zonas costeras y oceánicas a lo largo del sistema de afloramiento de Benguela analizando el papel clave jugado por el afloramiento costero.

Investigaciones futuras, que constituirán la continuación del análisis llevado a cabo en este manuscrito, deberían analizar las diferencias observadas en la tendencia de la temperatura y salinidad para zonas costeras y oceánicas en otras regiones de afloramiento como California, Perú, Somalia y la costa oeste de Australia, teniendo en cuenta tanto factores remotos (modos atmosféricos, circulación oceánica) como locales (viento y afloramiento).

Abstract

In the last part of 20th century and in the beginning of the 21st, the scientific community agrees that world ocean is warming, being this warming more intense from seventies on. This warming is not uniform either in time or in space; it is not the same in all parts of the world. In particular, the Atlantic Ocean contributes most to the increase of heat content, being responsible for one third of the increase in the heat content observed from 1955 to 1998. These differences among macroscopic areas (hemispheres and oceans) are even more marked at regional scale due to local and remote forcing factors like changes in winds, ocean currents, thermohaline depth and upwelling.

The aim of the present study is to describe the differences in SST evolution at coastal and ocean locations in the North Atlantic region, in particular, along the western coast of the Iberian Peninsula. The western coast of the Iberian Peninsula ($37^{\circ}N$ to $43^{\circ}N$) may be regarded as the northern boundary of influence of one of the major upwelling system in the world (the Eastern North Atlantic Upwelling System), that acts all along the northwest coast of Africa and the Atlantic coast of the Iberian Peninsula ([Nykjaer 1994];[SantosA 2005];[Álvarez 2008a]). These studies have shown that upwelling in this region is mainly a seasonal event that occurs with higher probability from April to September.

The SST variability observed during the last century both at coastal and ocean locations will be analyzed in terms of upwelling and the thermohaline circulation intensity. Then, the differences in the variability of temperature and heat content between coastal and ocean locations will be analyzed for the upper 700 *m* from 1975 to 2006 providing information about the vertical structure of temperature changes. As far as we know a similar analysis has never been done before in this area, where only SST patterns had been considered. Changes in the water masses more relevant along the Atlantic continental shelf of the Iberian Peninsula (ENACW and MW) will be also analyzed from seventies on. For this purpose, trends in salinity and temperature corresponding to the ENACW and MW isopycnal will be analyzed to determine the rate of change of ENACW and MW. This analysis will allow knowing the influence of water masses in trends of Atlantic water vertical profiles. The study of ocean warming in this region will continue analyzing the existence of trends in the frequency of extreme hot days over the satellite era (1982–2011). More specifically, the differences between ocean and coastal trends will be analyzed both at seasonal and annual scale.

Similar studies will be extended first to the Moroccan sub- region of the Canary Upwelling Ecosystem and then along the Benguela Current System. Both regions characterized by persistent upwelling through the year although with seasonal variations. In the Moroccan sub- region of the Canary Upwelling Ecosystem, regional differences in the SST warming rates between coast and ocean locations at the same latitude will be analyzed in terms of local forcing factors like wind and air temperature and remote forcing factors like atmospheric circulation patterns from 1982 to 2010. Finally, the differences in coastal and ocean SST trends will be studied along the Benguela Current System analyzing the key role played by the persistent coastal upwelling.

New research, which will constitute a continuation of the analysis car-

ried out in this manuscript, should be addressed to analyze the differences observed in temperature and salinity trends at coastal and ocean locations in other upwelling regions like the California Current System, Peru, the Somalia coast or the western coast of Australia taking into account remote (atmospheric modes, ocean circulations) and local (wind, upwelling) forcing factors.

INTRODUCTION

Climate change has been the most analyzed topic by climatologists and oceanographers during the last decades of the 20th century and the beginning of the 21st as it was summarized in the different Intergovernmental Panel on Climate Change (IPCC) reports ([IPCC 1990];[IPCC 1996]; [IPCC 2001];[IPCC2007]). The main conclusion is the increment of temperature observed during the second half of the 20th century which is higher than during any other 50 *years* period in the last 500 *years* [IPCC2007]. In addition, numerous studies have highlighted that the last four decades were the most intense warming period ever observed. The world's oceans are involved in this warming and play a key role in climate change acting as a great heat store. According to the fourth IPCC report, *"the increase in sea surface temperature over the 20th century is about half that of the mean land surface air temperature" and "the global ocean heat content has increased since the late 1950s, the period for which adequate observations of sub-surface ocean temperatures have been available" In addition, "the ocean's heat capacity is about 1,000 times larger than that of the atmosphere, and the oceans net heat uptake since 1960 is around 20 times greater than that of the atmosphere [Levitus 2005]. This large amount of heat, which has been mainly stored in the upper layers of the ocean, plays a crucial role in climate change, in particular in variations on seasonal to decadal time scales"*.

The variables most widely used to analyze the ocean warming have been the sea surface temperature (SST) and the ocean heat content (whose change is closely proportional to the average temperature change in a volume of seawater). Both variables are complementary providing information about surface temperature trends and heat stored in the ocean between surface and a depth which typically ranges from 700 to 3,000 *m*. In general, most of authors consider the upper 700 *m* since, according to [Levitus 2005], a great percentage of the warming is stored in the first 700 *m* while the layer 1000–3000 *m* provides only the 9% of the global increase. This picture was corroborated by further studies ([Domingues 2008];[Levitus 2009]; [Lyman 2010]). Only recently, some authors [Katsman 2011] have claimed that there has been a significant heat content increase below 700 *m*. A clear comparison between heat content changes for depths 0–700 *m* and 700–2000 *m* can be seen in [Levitus 2012]. SST is also a fundamental parameter in the ocean- atmosphere heat exchange and hence in the climatic regulation. In addition, SST is influenced by climatic, meteorological, hydrodynamic and bathymetric parameters.

During the last century, a great effort has been devoted to develop reliable SST series with global coverage, first by means of measurements from voluntary observation ships, drifters and moored buoys ([Brohan 2006]; [Smith 2008]) and then by means of satellite-derived data. Great efforts were also devoted to correct uncertainties in the SST data due to several factors as: changes in the ship routes after the opening of Panama and Suez Canals, sampling sparseness during the world wars, differences in water collection and more recently, uncertainties due to the presence of aerosols and clouds, which can cause a cool bias, and to the fact that satellite instruments record skin temperature instead of near-surface temperature (for a complete understanding of the different bias and the methods to correct them see: ([Kushnir 1994];[Folland 1995];[Kapala 1998];[Smith 2002]; [Smith 2003];

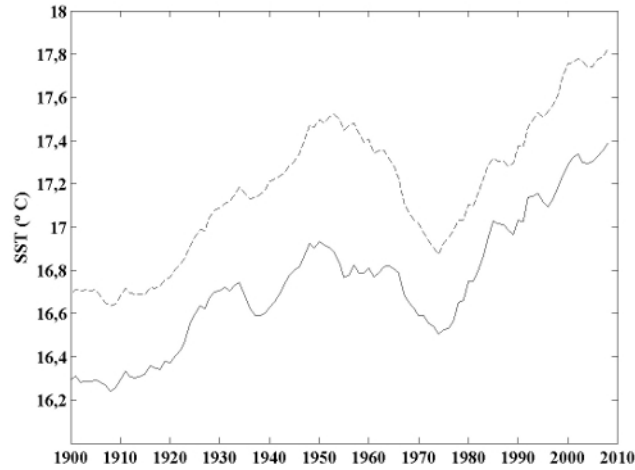


Figure 4: Time evolution of coastal (*gray line*) and oceanic (*black line*) Sea Surface Temperature in the North Atlantic from 1900 to 2010. Coastal (oceanic) SST is the latitudinal average from 37 to $42^{\circ}N$ at $9^{\circ}W$ ($15^{\circ}W$). A running average of ± 60 month where used.

[Smith 2004];[Smith 2005];[Worley 2005];[Kent 2005];[Kent 2006a];
[Kent 2006b];[Brohan 2006];[Smith 2008]).

Studies carried out trying to quantify SST trends have shown to be highly dependent on spatial and temporal scales ([Parker 1994];[Smith 1994]; [Casey 2001]). In addition, SST trends are far from being linear, and opposite trends can be obtained when considering different fitting strategies (linear, sinusoid) or different periods of time (see *Appendix I*).

Although the most commonly used ocean database for the last decades, has been the World Ocean Database [Levitus 2005], more recently, some data assimilation projects, like Simple Ocean Data Assimilation (SODA), have reanalyzed data from different sources (oceanographic cruises, satellite, model simulations) providing us with uniformly mapped and regularly available samples of not only di-

rectly observed variables but also indirect variables. These data assimilation projects provide valuable information beneath the sea surface at a depth of 5,375 m (40 levels). In this way, it is possible to obtain a complete view of the different-scale hydrographic processes by analyzing ocean patterns both at global ([Carton 2008];[Zheng 2009]) and basin scale ([Zheng 2010];[Patti 2010];[Giese 2011]).

Ocean global warming was not uniform either in time or in space ([Folland 1984];[Folland 1992];[Parker 1994];[Nicholls 1996];[Casey 2001]). Thus for example, several warming-cooling cycles were detected in the North Atlantic region over the 20th century both at global and regional scales ([IPCC2007];[Rayner 2006];[GarciaSoto 2002];[deCastro 2009]; [Gesteira 2011]). The first warming occurred during the period 1910 to 1945 and was followed by a period of cooling; the second warming period began during the 70s.

According to the fourth IPCC report, *"Over the period 1961 to 2003, global ocean temperature has risen by 0.10°C from the surface to a depth of 700 m. Consistent with the Third Assessment Report (TAR), global ocean heat content (0–3,000 m) has increased during the same period, equivalent to absorbing energy at a rate of $0.21 \pm 0.04 \text{ W m}^2$ globally averaged over the Earth's surface. Two-thirds of this energy is absorbed between the surface and a depth of 700 m. Global ocean heat content observations show considerable inter-annual and inter-decadal variability superimposed on the longer-term trend. Relative to 1961 to 2003, the period 1993 to 2003 has high rates of warming but since 2003 there has been some cooling"*

Ocean warming varies over a broad range of time scales, from seasonal, decadal to centennial and longer. The main modes of climate variability in each area (El Niño-Southern Oscillation (ENSO), the Pacific Decadal Oscillation (PDO), the North Atlantic Oscillation (NAO), the Southern Annular Mode (SAM), the Eastern Atlantic Mode (EA)) force the oceans

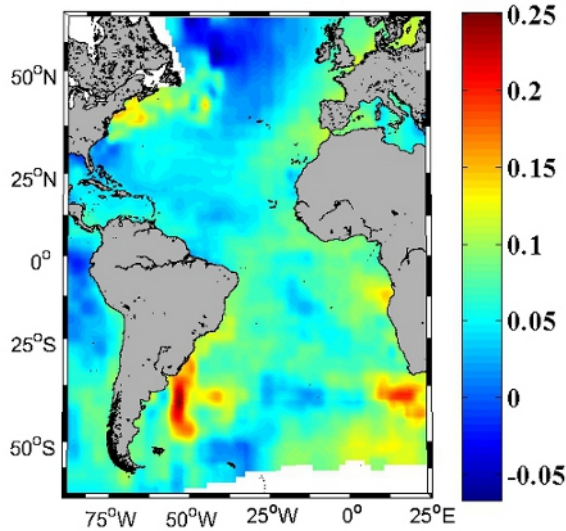


Figure 5: Sea surface Temperature trend over the period 1900–2009 calculated from the HadISST database.

causing changes in ocean circulation through changes in winds patterns and changes in surface ocean density.

On the other hand, global warming is not spatially uniformly distributed all over the world’s oceans with some regions warming faster or slower than the global average ([Levitus 2000];[Palttridge 1981]). In particular, the Atlantic Ocean contributes most to the increase of the heat content ([Nerem 1999];[Levitus 2000];[Strong 2000]. There is a latitudinal gradient in the SST increase with greater warming in the northern Hemisphere than in the southern one [Strong 2000]). According to the fourth IPCC report, *“new analyses of proxy data for the Northern Hemisphere indicate that the increase in temperature in the 20th century is likely to have been the largest of any century during the past 1,000 years. It is also likely that, in the Northern Hemisphere, the 1990s was the warmest decade and 1998 the warmest year”*. The SST warming for the Atlantic ocean is shown in Fig.5 from 1900 to 2009.

SST warming was also calculated in the North Atlantic region for two different periods of time, from 1900 to 2009 (*left*) and from 1979 to 2009 (*right*). Both figures show warming in most of the region being stronger during the last decades.

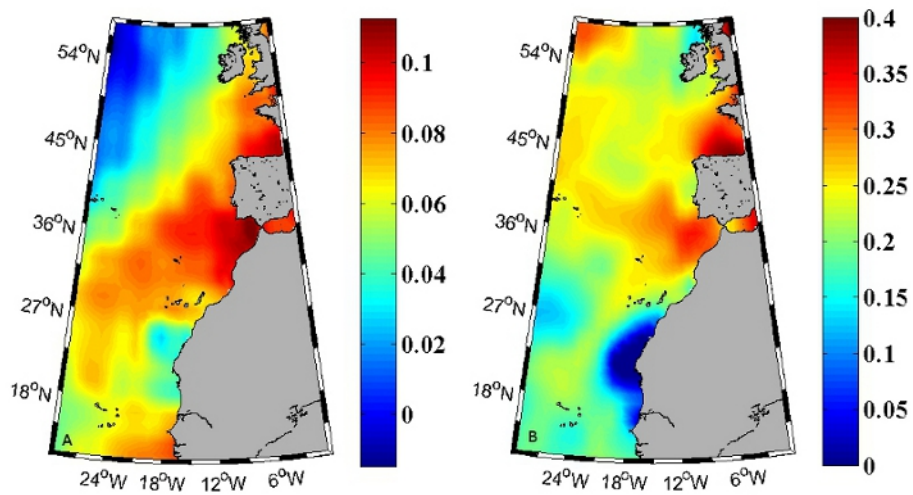


Figure 6: Sea Surface Temperature trend in the North Atlantic, over the period 1900–2009 (*left*) and over the period 1975–2009 (*right*), taken from the HadISST database.

These differences among macroscopic areas (hemispheres and oceans) are even more marked at regional scales due to local and remote forcing factors like changes in winds, ocean currents, thermohaline depth and upwelling ([Cole 2000];[Lemos 2004];[Ginzburg 2004];[SantosA 2005];[Gesteira 2008a];[deCastro 2008a]). More recently, some authors ([Relvas 2009];[Santos 2011a];[Santos 2012a]) have described the existence of different warming rates at oceanic and coastal locations at the same latitude in areas where coastal upwelling plays a key role. Thus, [Relvas 2009] detected weaker warming trends at coastal locations along the southern part of the western Iberian Peninsula (WIP).

Upwelling forcing on SST is possibly the most important oceanographic feature along the four major eastern coastal upwelling ecosystems in the world (Canary Upwelling Ecosystem, CUE, Benguela Upwelling Ecosystem, BUE, the California Current System, CCS, and the Peru- Humboldt Ecosystem) since it involves the replacement of warmer surface water by cooler subsurface water. Even, according to some authors, changes in the thermal gradient between land and ocean can be responsible of changes observed in upwelling intensity ([Bakun 1990];[Mendelsohn 2002];[McGregor 2007]).

Winds that blow from the north along a coastline oriented North-South tend to drive ocean surface currents to the right of the wind direction pushing surface waters offshore, this happens in the northern hemisphere, the opposite happens in the south. As surface waters are pushed offshore, water is drawn from below to replace them. The subsurface water that rises to the surface is typically colder, rich in nutrients, and biologically productive. Coastal upwelling has two especially important ecological effects. On the one hand, upwelling brings up nutrient-rich waters to the surface which support blooms of phytoplankton. The phytoplankton blooms constitute the ultimate energy base for large animal populations, like fish, marine mam-

mals and seabirds. On the other hand, upwelling that moves surface water offshore can drift larvae of marine animals, which live near shore, long distances away from their natural habitat reducing their possibilities of survive. From this it follows that coastal upwelling ecosystems are some of the most productive ecosystems in the world and support many of the world's most important fisheries. Although coastal upwelling regions account for only 1% of the ocean surface, they contribute approximately 20% of the world's fisheries landings [Pauly 1995]. But also, disperses the offspring of coastal species avoiding their survival. (Information partially obtained from the NOAA Ocean Explorer: Sanctuary Quest).

For the reasons above described, the upwelling variability has been analyzed along the coast of the major eastern boundary upwelling systems in the world showing to be highly dependent on the period of time, space and the fitting strategies used.

In the Canary upwelling ecosystem contradictory results were obtained from previous studies. [Bakun 1990] found an intensification of the upwelling favorable winds from 1948 to 1979 and [McGregor 2007] obtained a cooling of $0.5-1^{\circ}C$ during the 20th century associated to an increase of the coastal upwelling. On the contrary, [Lemos 2004] and [Lemos 2006] found a significant weakening of the upwelling favorable winds during similar periods of time (from 1940 to 2000 and from 1901 to 2000, respectively). Besides, [Gesteira 2008b] detected a weakening in the upwelling intensity from 1967 to 2006 and [Pardo 2011] reported a decrease in the upwelling index, which is even more pronounced during the last four decades. In the California current system, [Schwing 1997] and [Mendelssohn 2002] found an increase of the coastal upwelling during the favored season linked to opposite trends in the long-term changes of SST. In addition, [diLorenzo 2005] also remarked the strengthening of upwelling favorable winds linked to the long term SST warming in this region. Finally, [Pardo 2011] did not find a clear trend in

the California region during the last six decades.

To date, and as far as we know, only a few studies have dealt with the physical component of coastal upwelling trends in Peru and Benguela regions. [Pardo 2011] analyzed the Peru region from 1948 to 2009, showing the weakening of upwelling accompanied by a slight SST warming or even cooling trend. The same authors found an enhancement of upwelling with a slight SST warming in the Benguela region. [Patti 2010] found a marked increase in wind stress in both regions, with an increase in the water column stability.

The increase of sea temperature is especially important in coastal areas due to its severe impact in coastal ecosystems ([Honkoop 1998]; [Diederich 2005]). Recently [Lima 2012], detected that during the last three decades, $\sim 71.6\%$ of the world coastal locations have experienced a warming trend of $0.25 \pm 0.13^\circ C$ per decade, 6.8% a cooling of $-0.11 \pm 0.10^\circ C$ per decade and that the remaining 22.2% have not suffered any significant variation. Apart from changes in mean temperature, the frequency of extreme sea temperatures like extremely hot or cold events is fundamental to determine scenarios and policies to mitigate human impacts and to understand changes in coastal marine ecosystems ([Philippart 2003];[Frank 2005];[Thieltges 2006]; [Occhipinti 2007]). Thus, the increase (decrease) in the frequency of extreme hot (cold) days along the Eastern Atlantic margin was analyzed by [Lima 2012].

The study of extreme temperatures over land has been widely discussed in the context of heat waves and its impact on mortality ([Dessai 2002]; [GarciaHerrera 2005];[Diaz 2006];[Trigo 2009];[Barriopedro 2011]; [deCastro 2011]). In addition its variability was analyzed over the last 50 years, according to the fourth IPCC report, "*Cold days, cold nights and frost have become less frequent, while hot days, hot nights and heat waves have become more frequent likely in late 20th century and more likely due to*

a human contribution". As far as we know, there are very few studies focused of extreme SST events, both near coast and at the ocean, despite its implications for marine ecosystems can be remarkable ([Lima 2006];[Lima 2007]; [Wethey 2011]).

The aim of the present study is to describe the differences in SST evolution at coastal and ocean locations in the North Atlantic region, in particular, along the western coast of the Iberian Peninsula. The analysis of coastal and oceanic SST trends is carried out in terms of local forcing factors like wind or air temperature and remote forcing factors like atmospheric circulation or the thermohaline circulation intensity. Similar studies are carried out in other regions like the Moroccan sub- region of the Canary Upwelling Ecosystem and the Benguela Upwelling Ecosystem.

For this purpose the study was organized as follows:

- A complete description of atmospheric and oceanographic databases used was presented in *chapter 2*. A detailed description of the principal atmospheric modes of variability in the northern Hemisphere was also included.
- The principal water masses around de Atlantic coast of the Iberian Peninsula (ENACW and MW) were characterized in *chapter 3*. In addition, changes in ENACW and MW in the upper 700 *m* from the seventies on were analyzed.
- The differences in the warming trend between ocean and coastal SST for the WIP were analyzed in *chapter 4* from 1900 to 2008 in terms of upwelling and the thermohaline circulation intensity. Then, the differences in the variability of temperature and heat content between coastal and ocean locations was analyzed in the upper 700 *m* from 1975 to 2006, providing information about the vertical structure of temperature changes. Finally, the existence of trends in the frequency

of extreme hot days over the period 1982 to 2011 was analyzed. In particular, the differences between ocean and coastal trends was studied both at seasonal and annual scale.

- *Chapter 4* deals with the regional differences in the SST warming rates between coast and ocean locations at the same latitude in the Moroccan sub- region of the Canary Upwelling Ecosystem and along the Benguela Current System in terms of local forcing factors like wind, air temperature or upwelling and remote forcing factors like atmospheric circulation patterns.

Contents

Contents	xxxi
List of Figures	xxxv
1 DATABASE	1
1.1 <i>Ocean database</i>	1
1.1.1 HadleyISST	1
1.1.2 Pathfinder	2
1.1.3 SODA	6
1.2 <i>Oceanographic Modes</i>	8
1.2.1 Atlantic Multidecadal Oscillation (AMO)	8
1.3 <i>Atmospheric database</i>	9
1.3.1 National Center of Atmospheric Research/National Center for Environmental Prediction(NCEP/NCAR)	9
1.3.2 Pacific Fisheries Enviromental Laboratory (PFEL) .	12
1.3.3 Climate Forecast System Reanalysis (CFSR)	12
1.4 <i>Atmospheric Modes</i>	14
1.4.1 North Atlantic Multidecadal Oscillation (NAO) . . .	15
1.4.2 East Atlantic pattern (EA)	16
1.4.3 Scandinavia pattern (SCA)	16

CONTENTS

1.4.4	East Atlantic/Western Russia pattern (EA/WR) . . .	17
1.4.5	Polar/Eurasia pattern (POL)	17
1.4.6	Southern Hemisphere Annular Mode (SAM)	17
2	Evolution of water masses along the Atlantic Arc	19
2.1	<i>Water Masses</i>	19
2.1.1	Surface waters	19
2.1.2	Intermediate waters	22
2.1.3	Deep waters	22
2.2	<i>Changes in Water masses</i>	23
2.3	<i>Changes in ENACW and MW along the Atlantic coast of the Iberian Peninsula</i>	26
2.3.1	Motivation	26
2.3.2	Methods	26
2.3.3	Trends in the vertical profiles of the Atlantic water	28
2.3.4	Trends in ENACW and MW	32
2.4	<i>Changes in ENACW along the Bay of Biscay</i>	34
2.4.1	Motivation	34
2.4.2	Methods	34
2.4.3	Trends in ENACW	35
2.4.4	Conclusions	42
3	Differences between ocean and coastal SST	45
3.1	<i>Differences between ocean and coastal SST</i>	45
3.1.1	Motivation	45
3.1.2	Methods	45
3.1.3	Results and Discussion	48
3.1.4	Conclusions	55

CONTENTS

3.2	<i>Variability of coastal and ocean water temperature in the upper 700 m.</i>	57
3.2.1	Motivation	57
3.2.2	Methods	57
3.2.3	Results and Discussion	59
3.2.4	Conclusions	68
3.3	<i>Changes in the frequency of extreme sea temperatures events from 1982 to 2011</i>	69
3.3.1	Motivation	69
3.3.2	Methods	69
3.3.3	Results and Discussion	72
3.3.4	Conclusions	79
4	Differences between ocean and coastal SST in other areas	81
4.1	<i>Differences between ocean and coastal SST in the Canary Upwelling Ecosystem</i>	81
4.1.1	Motivation	81
4.1.2	Methods	81
4.1.3	Results and Discussion	83
4.1.4	Conclusions	91
4.2	<i>Differences between ocean and coastal SST in the Benguela Upwelling Ecosystem (BUE)</i>	93
4.2.1	Motivation	93
4.2.2	Methods	93
4.2.3	Results and Discussion	95
4.2.4	Conclusions	104
A	Upwelling along the western coast of the Iberian Peninsula	107
A.1	Motivation	107

A.2	Methods	107
A.3	Results and Discussion	109
A.4	Conclusions	114
B	Acronym and abbreviation list	115
C	List of Publications	119
	Bibliography	121

List of Figures

1	<i>Evolución costera (línea gris) y oceánica (línea negra) de la SST en el Atlántico norte para el periodo 1900–2010. La SST costera (oceánica) se ha promediado latitudinalmente desde 37 hasta 47°N en los 9°W (15°W). Para facilitar la visualización se ha realizado una media móvil a ± 60 meses. . . .</i>	vi
2	<i>Tendencia de la SST para el Atlántico, para el periodo 1900–2009, calculada con la base HadISST.</i>	viii
3	<i>Tendencia de la SST para el Atlántico Norte, para el periodo 1900–2009 (izquierda) y para el periodo 1975–2009 (derecha), calculada con la base HadISST.</i>	ix
4	Time evolution of coastal (<i>gray line</i>) and oceanic (<i>black line</i>) Sea Surface Temperature in the North Atlantic from 1900 to 2010. Coastal (oceanic) SST is the latitudinal average from 37 to 42°N at 9°W (15°W). A running average of ± 60 month where used.	xxi
5	Sea surface Temperature trend over the period 1900–2009 calculated from the HadISST database.	xxiii
6	Sea Surface Temperature trend in the North Atlantic, over the period 1900–2009 (<i>left</i>) and over the period 1975–2009 (<i>right</i>), taken from the HadISST database.	xxiv

LIST OF FIGURES

1.1	Mean SST calculated with the HadISST1.1 database for the North Atlantic for the period 1900–2000	1
1.2	Mean SST for the period from 1982–2010 for the Arc Atlantic, calculated with: a) Advanced Very-high Resolution Radiometer (AVHRR) database Pathfinder 5.2, b) Advanced Very-High Resolution Radiometer (AVHRR) database Pathfinder OI 1.4	5
1.3	Mean SST calculated with Simple Ocean Data Assimilation (SODA) database for the North Atlantic, for the period from 1960–2005	6
1.4	Atlantic multidecadal Oscillation index has been traditionally calculated as the average of SST anomaly for the North Atlantic north of the equator [Enfield 2001]	9
1.5	National Center of Atmospheric Research/National Center for Environmental Prediction (NCEP/NCAR). a) Mean SLP T (in $10^5 Pa$) for the period 1970 to 2009. b) Air temperature trend ($^{\circ}C$ per decade) for the Canary region, calculated from 1982 to 2010	11
1.6	Ekman transport field ($m^3s^{-1}km^{-1}$) averaged using PFEL data for the period 1981 to 2009	12
2.1	T–S diagram of the water masses present in the Bay of Biscay at $3.25^{\circ}W$ and $44.75^{\circ}N$ from 1975 to 2006 till a depth of 700 m. ENACW is highlighted by means of gray dots. This water mass was identified by salinity and temperature values which generate a density ranging from 27.0 to $27.2 kg m^{-3}$	21
2.2	Bathymetry of $0-20.5^{\circ}W$ and $36.5-48.5^{\circ}N$	24

LIST OF FIGURES

2.3 Time evolution of the temperature anomaly ($^{\circ}C$) along the Atlantic Coast of the Iberian Peninsula over the period 1975–2008. *Black line* represents the temperature average to those depths characterized by ENACW (from 5 m to 700 m) and *gray line* represents the temperature average to those depths characterized by MW (from 728 m to 3,125 m) 25

2.4 Vertical profile of a) temperature trends ($^{\circ}C$ per decade), b) salinity trends (*psu per decade*) for the entire Bay of Biscay from 1975 to 2006. Circles represent trends with a significance level greater than 95%. 26

2.5 Vertical profiles of temperature trends ($^{\circ}C$ per decade) along the Atlantic coast (from 37.75 to $42.75^{\circ}N$) of the IP over the period 1975–2008 (*left pannels*). Vertical profiles of temperature ($^{\circ}C$ per decade) along the Atlantic coast of the IP at coastal (*black line*) and ocean (*gray line*) location (*right pannels*). Temperature trend at coastal (oceanic) locations was calculated averaging temperature values at the three latitudes nearest (farthest). 29

2.6 Vertical profiles of salinity trends (*psu per decade*) along the Atlantic coast (from 37.75 to $42.75^{\circ}N$) of the IP over the period 1975–2008 (*left pannels*). Vertical profiles of salinity (*psu per decade*) along the Atlantic coast of the IP at coastal (*black line*) and ocean (*gray line*) location (*right pannels*). Salinity trend at coastal (oceanic) locations was calculated averaging salinity values at the three latitudes nearest (farthest). 31

LIST OF FIGURES

2.7 Annual temperature (*left pannels*) and salinity (*right pannels*) trends (*°C per decade* and *psu per decade*) corresponding from top to bottom to ENACW, uppwer MW and lower MC along the atlantic coast of the IP from 1975 to 2008. Black dots represent the grid points where trends with a significance level greater than 95% were obtained. The blanks represent points where ENACW was scarcely detected. 33

2.8 a) Annual temperature trend (*°C per decade*) and b) Annual salinity trend (*psu per decade*), of ENACW mass in the North Atlantic area (0–20.5°W and 37.5–47.5°N) from 1975 to 2006. Black dots represent the grid points where trends with a significance level greater than 95% were obtained. The blanks represent points where ENACW was scarcely detected. 36

2.9 Annual temperature trend (*°C per decade*) corresponding to ENACW in the Bay of Biscay from 1975 to 2006. Black dots represent the grid points where trends with a significance level greater than 95% were obtained. The blanks represent points where ENACW was scarcely detected. 37

2.10 Annual salinity trend (*psu per decade*) corresponding to ENACW in the Bay of Biscay from 1975 to 2006. Black dots represent the grid points where trends with a significance level greater than 95% were obtained. The blanks represent points where ENACW was scarcely detected. 38

2.11 Mean depth of ENACW (*m*) in the Bay of Biscay for the period 1975–2006. Black dots represent the grid points where trends with a significance level greater than 95% were obtained. The blanks represent points where ENACW was scarcely detected. 39

LIST OF FIGURES

2.12 Depth trend of ENACW (*m per decade*) in the Bay of Biscay for the period 1975–2006. Black dots represent the grid points where trends with a significance level greater than 95% were obtained. The blanks represent points where ENACW was scarcely detected. 40

2.13 Time evolution of temperature (*thin black line*), salinity of ENACW (*solid gray line*) and NAO index (*thick black line*) in the Bay of Biscay from 1975 to 2006. The NAO index was calculated for the extended winter (DJFM). Signals were normalized to be represented together. A running average of ± 1 year was applied to smooth signals. 41

3.1 Study area. SST points (+) are placed on $1^\circ \times 1^\circ$ from $9.5^\circ W$ to $21.5^\circ W$ and from $42.5^\circ N$ to $37.5^\circ N$. Circles (*o*) represent coastal ($9.5^\circ W$) an oceanic ($17.5^\circ W$) reference SST points. Crosses (*x*) represent the location of wind data (located at $10.0^\circ W$, $37.5^\circ N$, $40.0^\circ N$ and $42.5^\circ N$). 47

3.2 a) Spatial and temporal distribution of SST along the study area for the period 1900–2008, (the x-axis corresponds with the eastern latitudes) . b) Inter-annual variation of the meridional average of coastal (*solid line*) and oceanic (*dashed line*) SST ($^\circ C$). 49

3.3 Inter-annual evolution of the meridional average of ΔSST ($^\circ C$) from 1900 to 2008. ΔSST was defined as ocean SST minus coastal SST as described in *equation(3.1)*. A running average of ± 5 years was considered to smooth the signal. Straight lines were used to highlight the increasing and decreasing periods of ΔSST 52

LIST OF FIGURES

3.4 Evolution of AMO index (*gray solid line*) compared with the mean SST anomaly (SST^a) (*black solid line*) calculated at the SST points depicted in Fig.3.1. Dashed lines correspond to $SST^a \pm 2\sigma(SST^a)$. Once again, a running average of ± 5 years was considered. The signal was filtered with a running average (± 5 years) prior to the calculation of correlation coefficients. Correlation is significant at 99% for all longitudes. 53

3.5 Correlation coefficient between the annual AMO index and the annual meridional average of SST at different longitudes calculated for the period 1900–2008. The signal was filtered with a running average (± 5 years) prior to the calculation of correlation coefficients. Correlation is significant at 99% for all longitudes. 54

3.6 Correlation coefficients were calculated between seasonal (April–Sept) meridional wind stress (τ_y) and *AMJJAS* SST at different longitudes for the period 1948–2008. Once again, signals were filtered with a running average (± 5 years) prior to the calculation of correlation coefficients. Only the three first locations (until $12^\circ W$) are statistically significant at 90%. 55

3.7 Time evolution of seasonal (April–September) UI (*full bars*), EA index (*empty bars*) and ΔSST (*dark line*) anomalies relatives to the period 1948–2008. The signals were filtered by means of a running average (± 5 years). In addition, the UI anomaly was multiplied by a factor $0.75/(max(UI) - min(UI))$ to allow a better visual comparison between signals. UI showed to be correlated with ΔSST ($R = 0.67$, significant at 90%) and negatively correlated with EA ($R = -0.62$, significant at 90%). 56

LIST OF FIGURES

3.8 a) Mean sea temperature ($^{\circ}C$) at surface layer (upper 5 m) from the SODA, b) mean SST from Pathfinder and c) mean SST from HadISST1.1. Data were averaged over the period 1982–2006. d) SST trend ($^{\circ}C$ per decade) calculated at $41.75^{\circ}N$ from 1982 to 2006 using the three data bases mentioned above. SST data were previously re-meshed to a common spatial resolution of $0.5^{\circ} \times 0.5^{\circ}$. Legend in the figure P: Pathfinder; S: SODA; H: HadISST. 58

3.9 Mixed layer depth (MLD) at two transects located at $41.75^{\circ}N$ (*black line*) and $39.75^{\circ}N$ (*gray line*). The MLD was calculated following the temperature criterion $SST - ST(z) = 0.2^{\circ}C$, where $ST(z)$ is the water temperature at depth (z). This criterion identifies the MLD as the depth at which the temperature is $0.2^{\circ}C$ lower than the SST. 60

3.10 Near surface water temperature ($^{\circ}C$) averaged for the mixed layer (from 5.0 to 46.6 m) over the period 1975–2006. . . . 61

3.11 Horizontal map of the temperature trend ($^{\circ}C$ per decade) calculated at different depths over the period 1975–2006: a) mixed layer (from 0 to 46.6 m deep), b) thermocline base (from 58 to 197 m deep) and c) intermediate water (from 229.5 to 729.4 m deep). 62

3.12 Temperature trend ($^{\circ}C$ per decade) for the period 1975–2006 calculated at two latitudes: a) $41.75^{\circ}N$ and b) $39.75^{\circ}N$ 63

3.13 Vertical profiles of temperature trends ($^{\circ}C$ per decade) meridionally averaged for the three longitudes nearest to the coast (*solid line*) and for the three longitudes farthest the coast (*dashed line*). 64

LIST OF FIGURES

3.14 Heat content anomaly, $Q(J)$, meridionally averaged from 38.25 to 43.25°N over the period 1975-2006. Error bars were calculated using the standard deviation of monthly data, $\sigma(Q)$, divided by the square root of the number of data. All trends are significant with $p < 0.05$ 65

3.15 Time evolution of the heat content anomaly ($Q(J)$) meridionally averaged from 38.25 to 43.25°N over the period 1975–2006. The *black solid line* is the mean of the three nearest locations to the coast and the *grey dashed line* is the mean of the three most oceanward locations. A running average of ± 2 years was considered to smooth the signal. 66

3.16 Area under study. Colors represent mean SST(°C) averaged from 1982 to 2011. The upwelling imprint is reflected by a land-ocean SST gradient on the order of 0.5°C. *Circles (dots)* correspond to coastal (ocean) pixels. Crosses represent the locations where upwelling index was calculated. 71

3.17 SST trends (°C per decade) over the period 1982–2011. (a) Map of trends. Dots mark trends with significance higher than 95%; (b) Trends at the control points shown in Fig.3.16, oceanic (coastal) points represent by *gray line (black line)*. Error bars were calculated using the standard deviation over the square root of the number of data. 73

3.18 Annual trends in the frequency of extreme hot days over the period 1982–2011. (a) Map of trends. Dots mark trends with significance higher than 95%; (b) Trends at coastal (dark line) and ocean (light line) locations. 74

LIST OF FIGURES

3.19 Seasonal trends in the frequency of extreme hot days over the period 1982–2011. Frames as in Fig.3.18 (a,b) Winter; (c,d) Spring; (e,f) Summer; (g,h) Autumn. Dots mark trends with significance higher than 95% 76

3.20 Seasonal trends in the frequency of extreme hot days over the period 1982–2011. Frames as in Fig.3.18 (a,b) Winter; (c,d) Spring; (e,f) Summer; (g,h) Autumn. Dots mark trends with significance higher than 95% 77

3.21 Trend in summer upwelling calculated over the period 1982–2011 using CFSR data. Circles mark trends with significance higher than 95%. 79

4.1 Mean $SST(^{\circ}C)$ averaged from 1982 to 2010. Polygons represent coastal and ocean locations along the area under study. *White* points represent the control points where Ekman transport was calculated. 83

4.2 Mean Ekman transport ($m^3s^{-1}km^{-1}$) averaged from 1982 to 2010 calculated at the six points described in Fig.4.1. 85

4.3 SST trend ($^{\circ}C$ per decade) calculated from monthly SST anomalies over the period 1982–2010. A running average (72 pixels) was applied to smooth the signal. Negative (ΔSST^{trend}) values are only observed for coastal locations located opposite the Canary archipelago ($28-31^{\circ}N$). 86

4.4 Difference between SST warming at ocean and coastal locations for the same latitude ($\Delta SST^{trend} = SST_{ocean}^{trend} - SST_{coast}^{trend}$). A running average (± 2 pixels) was applied to smooth the signal. Negative ΔSST^{trend} values are only observed for coastal locations located opposite the Canary archipelago ($28-31^{\circ}N$). 87

LIST OF FIGURES

4.5 Air temperature trend ($^{\circ}C$ per decade) calculated from 1982 to 2010. The *black line* marks the coast line. Air temperature was considered at 1,000 *HPa* to avoid topographic effects on atmospheric circulation. 88

4.6 Annual cycle calculated by averaging $UI(m^3s^{-1}km^{-1})$ in latitude ($22-32^{\circ}N$) and time (1982–2010). The error bars were calculated as $(UI)/\sqrt{N}$, where $\sigma(UI)$ is the standard deviation of monthly data and $N = 29$ is the number of monthly values over the period 1982–2010. 89

4.7 Inter-annual evolution of $UI(\textit{black line})$ averaged from May to September and $(\Delta SST^{trend} = SST_{ocean}^{trend} - SST_{coast}^{trend})$ (*gray line*) averaged from August to December (3 months lag) over the period 1982–2010. Both variables were normalized to be compared. A ± 1 year running average was considered to smooth both signals. 90

4.8 Correlation between extended winter (from December to March) EA and ΔSST grouped in months. A positive correlation was observed between both signals. In particular, the best correlation was found for ΔSST^{MJJAS} . *Dots* mark the correlations significant at 95%. 91

4.9 Inter-annual evolution of EA^{DJFM} index (*black line*) and $\Delta SST^{MJJAS}(t)$ (*gray line*) over the period 1982–2010. Both variables were normalized to be compared. A ± 1 year running average was considered to smooth both signals. 92

LIST OF FIGURES

4.10 SST ($^{\circ}C$) annual average for the area under study from 1970 to 2009. *Black empty circles* represent the locations where SST data were extracted. Two transects of 16 points each were considered in front of the Namibia coast and the western coast of South Africa (from 18° to $35^{\circ}S$). The coastal transect was located at 1 degree from the coast and the oceanic one 15° seaward. *White crosses* represent a 6-points transect parallel to the shore line where Ekman transport was calculated. 94

4.11 a) Inter-annual variation of SST($^{\circ}C$) meridionally averaged from $18^{\circ}S$ to $35^{\circ}S$ at different distances from the coast for the period 1900–2009. *Bottom line* represents transect located at 1° from the coast and the *top line* represents transect located 15° from the coast. A running average of ± 5 years was used to smooth high frequency variations in temperature. The shadow area between vertical lines marks the break point between periods with significantly different coastal SST trends (1970). b) SST trends calculated from 1970 to 2009. *X* axis represents the transect distance (in degrees) from the coast. *Dots* represent SST trends, *small circles* correspond to trends with $0.01 < P < 0.1$ and *large circles* correspond to trends with $P < 0.01$ 96

4.12 a) Annual SST trend($^{\circ}C$ per decade) for the area under study from 1970 to 2009. b) Seasonal SST trend ($^{\circ}C$ per decade) for the area under study from 1970 to 2009. (1) January–March (JFM); (2) April–June (AMJ); (3) July–September (JAS) and (4) October–December (OND). 98

LIST OF FIGURES

4.13 Inter-annual variation of $\Delta SST = SST_{coast} - SST_{ocean}$ ($^{\circ}C$) from 1970 to 2009. A running average of ± 5 years was used to smooth high frequency variations in temperature. The *solid line* represents a linear trend of $-0.18^{\circ}C$ per decade ($P < 0.01$). 99

4.14 a) Ekman transport field ($m^3 s^{-1} km^{-1}$) averaged using PFEL data for the area under scope from 1981 to 2009. b) Annual cycle of UI ($m^3 s^{-1} km^{-1}$) for the six points along the BUES (crosses in Fig.4.10) calculated using NCEP/NCAR data for the period 1970 to 2009. c) Annual UI cycle ($m^3 s^{-1} km^{-1}$) meridionally averaged from $20^{\circ}S$ to $32^{\circ}S$ for the period 1970 to 2009. *Error bars* were calculated using the standard deviation of the monthly data, $\sigma(UI)$, divided by the square root of the number of data. 100

4.15 UI variability from 1970 to 2009. UI was spatially averaged for the 6 points parallel to the BUES (crosses in Fig.4.1). A running average of ± 5 year was used to smooth high frequency variations in UI. The straight line represents the linear trend with a slope of $87 m^3 s^{-1} km^{-1}$ per decade, ($P < 0.01$). 101

4.16 Monthly Southern Annular Mode (SAM) index from 1970 to 2009 (*gray bars*). The *solid black line* represents a linear trend of 0.37 per decade ($P < 0.01$). 103

4.17 Evolution of the South Atlantic High from 1970 to 2009. Mean SLP (in $10^5 Pa$). The SLP maximum (SLP^{max}) is located at mid latitudes ($30.6^{\circ}S$, $5.4^{\circ}W$) with a value of $102,246 Pa$ 104

LIST OF FIGURES

4.18 Evolution of the South Atlantic High from 1970 to 2009.
 (a) Evolution of SLP^{max} anomaly (*bars*). The *dark line* represents the linear tendency ($14Pa$ per decade, $P = 0.06$).
 (b) Displacement in the latitude of the SLP^{max} relative to the mean position (*bars*). The *dark line* represents the trend (-0.19° per decade, $P = 0.07$). (c) Displacement in the longitude of the SLP^{max} relative to the mean position (*bars*). The *dark line* represents the trend (0.27° per decade without statistical significance). 105

A.1 Trends in upwelling index (UI) along the western coast of the Iberian Peninsula (WIP) for the period 1958–1999. Data were grouped in intervals of 21 *yr* prior to linear fitting. The *dashed line* corresponds to the raw trends, and the *solid line* to the trends smoothed with a running average (± 1 *yr*) . . . 112

A.2 Comparison between the upwelling index signal that was filtered and averaged in space (\tilde{UI} ; *solid line*) and the different fitting functions. Linear (*dashed line*); linear and sinusoidal (*open circles*); Linear and double sinusoid (*closed circles*) . . . 113

LIST OF FIGURES

DATABASE

1.1 *Ocean database*

1.1.1 HadleyISST

HadISST1.1 is a data set combination of monthly globally fields of Sea Surface Temperature (SST) and sea Ice concentration, Fig.1.1.

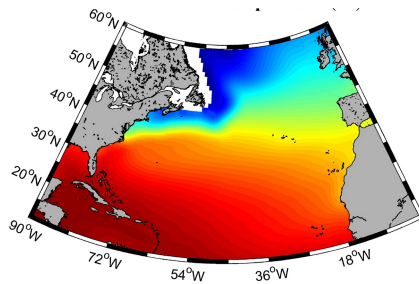


Figure 1.1: Mean SST calculated with the HadISST1.1 database for the North Atlantic for the period 1900–2000

1. DATABASE

This database can be obtained from the UK Meteorological office, Hadley Center HadISST1.1–Global sea–Ice coverage and SST (<http://badc.nerc.ac.uk/data/hadisst>). Data are available from 1870 to nowadays, with a monthly periodicity of $1^\circ \times 1^\circ$ [Rayner 2003]. They utilize both in situ SSTs from ships and buoys, and bias-adjusted SSTs from the satellite-borne advanced very high resolution radiometer (AVHRR, as does HadISST1), but it only starts in late 1981 when AVHRR began. The best known non interpolated gridded in situ–only historical SST data set is included within the Comprehensive Ocean–Atmosphere Data Set (COADS). Other interpolated historical data sets [Kaplan 1997] are at most quasi–global, do not contain varying sea ice and have lower spatial resolution because of the relative lack of data before the satellite era. These historical data sets all use data reconstruction techniques based on empirical orthogonal functions (EOFs), which are used to capture the major modes of SST variability and are then projected onto the available gridded SST observations to form quasi–globally complete fields.

1.1.2 Pathfinder

Pathfinder 5.2

Daily SST data can be obtained from day time measurements carried out by the Advanced Very–High Resolution Radiometer (AVHRR) on board of NOAA series satellites. Data can be retrieved from Pathfinder version 5.2 with an approximate spatial resolution of $0.04^\circ \times 0.04^\circ$ for the entire World and extending from 1982 to nowadays, (<ftp://ftp.nodc.noaa.gov/pub/data.nodc/pathfinder/Version5.2/>) Fig.1.2a.

Quality flag ranging from 0 to 7 was assigned to each pixel, with 7 being the highest quality and 0 the lowest. The SST grid contained voids in the data caused by adverse weather conditions or satellite malfunctions.

1.1. Ocean database

The presence of voids, whose position depends on the month, is especially evident for winter months, where the existence of clouds can mask large areas, ([Kilpatrick 2001];[Relvas 2009]).

Voids were covered using an iterative procedure:

- 1) Land points were detected, corresponding to land or to pixels where temperature values were not valid in more than 10% of the samples.
- 2) Land points were discarded and not used to interpolate nearby points.
- 3) Data voids were then detected.
- 4) A SST value was assigned to each void using values from its close vicinity (temporal and spatial), using *Equation 1.2*.
- 5) Steps 3 and 4 were iterated till the number of corrected voids in a step was zero. This method is different to those used by [Gesteira 2008a] and by [Relvas 2009], although it generates similar SST patterns.

$$SST_{i,j}^n = \frac{1}{N} \sum (SST_{i,j}^{n-1} + SST_{i,j}^n + SST_{i,j}^{n+1}) \quad (1.1)$$

$$\left[M_{i,j}^n \right] = \begin{bmatrix} \frac{\theta_{i-1,j+1}^n T_{i-1,j+1}^n}{\sqrt{2}} & \theta_{i,j+1}^n T_{i,j+1}^n & \frac{\theta_{i+1,j+1}^n T_{i+1,j+1}^n}{\sqrt{2}} \\ \theta_{i-1,j}^n T_{i-1,j}^n & 0 & \theta_{i+1,j}^n T_{i+1,j}^n \\ \frac{\theta_{i-1,j-1}^n T_{i-1,j-1}^n}{\sqrt{2}} & \theta_{i,j-1}^n T_{i,j-1}^n & \frac{\theta_{i+1,j-1}^n T_{i+1,j-1}^n}{\sqrt{2}} \end{bmatrix} \quad (1.2)$$

$$\left[M_{i,j}^{n\pm 1} \right] = \begin{bmatrix} \frac{\theta_{i-1,j+1}^{n\pm 1} T_{i-1,j+1}^{n\pm 1}}{\sqrt{3}} & \frac{\theta_{i,j+1}^{n\pm 1} T_{i,j+1}^{n\pm 1}}{\sqrt{2}} & \frac{\theta_{i+1,j+1}^{n\pm 1} T_{i+1,j+1}^{n\pm 1}}{\sqrt{3}} \\ \frac{\theta_{i-1,j}^{n\pm 1} T_{i-1,j}^{n\pm 1}}{\sqrt{2}} & \theta_{i,j}^{n\pm 1} T_{i,j}^{n\pm 1} & \frac{\theta_{i+1,j}^{n\pm 1} T_{i+1,j}^{n\pm 1}}{\sqrt{2}} \\ \frac{\theta_{i-1,j-1}^{n\pm 1} T_{i-1,j-1}^{n\pm 1}}{\sqrt{3}} & \frac{\theta_{i,j-1}^{n\pm 1} T_{i,j-1}^{n\pm 1}}{\sqrt{2}} & \frac{\theta_{i+1,j-1}^{n\pm 1} T_{i+1,j-1}^{n\pm 1}}{\sqrt{3}} \end{bmatrix} \quad (1.3)$$

1. DATABASE

The summation in *Equation 1.1* refers to all the elements of matrices M , T is the SST obtained from satellite measurements, y is a function of position (i, j) and time (n) that can take either of two values :

- 0– When the point corresponds to avoid.
- 1– When there is a valid value at the point.

Neighboring points were weighted as a function of distance in pixels (this weighting is higher for space than time). The normalization value N is the summation of all terms of the form θ/\sqrt{m} , with $m=1,2,3$ or ∞ , depending on the assigned weighting.

Pathfinder OI 1.4

New high resolution SST analysis products have been developed using optimum interpolation (OI) Fig.1.2b.

Two new high resolution sea surface temperature (SST) analysis products have been developed using optimum interpolation (OI). The analyses have a spatial grid resolution of 0.25° and temporal resolution of 1 day. One product uses Advanced Very High Resolution Radiometer (AVHRR) infrared satellite SST data. The other uses AVHRR and Advanced Microwave Scanning Radiometer (AMSR) on the NASA Earth Observing System satellite SST data. Both products also use in situ data from ships and buoys and include a large-scale adjustment of satellite biases with respect to the in situ data. Two products are needed because there is an increase in signal variance when AMSR became available in June 2002 due to its near all-weather coverage. The AVHRR is only used because allows a long analysis. For both products, the results show improved spatial and temporal resolution compared to previous version, that used weekly time resolution for the period 1982–2012. In the

1.1. Ocean database

present work, the AVHRR product was used because allowing a long analysis (<http://www.ncdc.noaa.gov/oa/climate/research/sst/description.php>) .

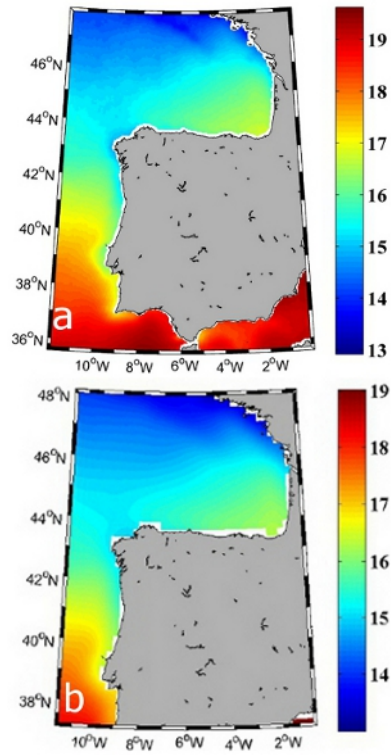


Figure 1.2: Mean SST for the period from 1982–2010 for the Arc Atlantic, calculated with: a) Advanced Very-high Resolution Radiometer (AVHRR) database Pathfinder 5.2, b) Advanced Very-High Resolution Radiometer (AVHRR) database Pathfinder OI 1.4

1. DATABASE

1.1.3 SODA

Simple Ocean Data Assimilation (*SODA*) is a reanalysis data. For this purpose a Geophysical Fluid Dynamics Laboratory Modular Ocean Model *2.b* code was used to analyzed the general circulation ocean model. This database covers the period 1958–2010 and it is available at monthly scale with a horizontal resolution of $0.5^\circ \times 0.5^\circ$ and a vertical resolution of 40 levels from 5 m to 5375 m Fig.1.3 (<http://www.atmos.umd.edu/ocean/>).

The detailed information about vertical resolution can be found at [Carton 2000a] and [Carton 2000b]. The temperature and salinity data records were obtained from World Ocean Atlas–94 [Levitus 1994], (*WOA–94*) as well as additional hydrography, sea surface temperature [Reynolds 1994], and altimeter sea level from the Geosat, ERS-1, and TOPEX / Poseidon satellites, and also for different instrument types: mechanical bathythermograph MBTs, expendable bathythermograph XBTs, conductivity temperature depth CTDs, and salinity Temperature depth probes and station data.

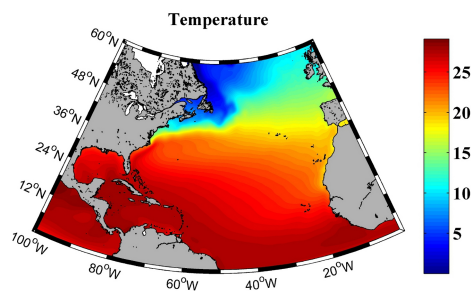


Figure 1.3: Mean SST calculated with Simple Ocean Data Assimilation (SODA) database for the North Atlantic, for the period from 1960–2005

1.1. Ocean database

A summary of the oceanic Database used and their main characteristics can be found in *Table 2.1*.

Base	Variable Used	Espatial resol	Temporal resol
HadleyISST	SST	$1^{\circ} \times 1^{\circ}$	1870–2012
Pathfinder 5.2	SST	$0.04^{\circ} \times 0.04^{\circ}$	1982–2012
Pathfinder O.I 1.4	SST	$0.25^{\circ} \times 0.25^{\circ}$	1982–2012
SODA	SST & Salinty	$0.25^{\circ} \times 0.25^{\circ}$	1958–2010

Table 1.1: Oceanic Database. SODA database also has a vertical resolution of 40 levels from 5–5372 *m*.

1.2 *Oceanographic Modes*

1.2.1 Atlantic Multidecadal Oscillation (AMO)

AMO is a coherent pattern of multidecadal variability in SST centered on the North Atlantic Ocean with a cycle ranging from 35 to 80 years depending on the author ([Delworth 1993];[Timmermann 1998];[Kerr 2000]; [Dima 2001]). Following [Trenberth 2006], the magnitude of the AMO signal is modest; the range is less than $0.4^{\circ}C$.

The AMO has been linked with the variability in Northeast Brazilian rainfall [Folland 1990], North American climate [Sutton 2005] and *U.S.* rain fall and river flows [Enfield 2001]. In addition, the AMO also affects the number of Atlantic hurricanes and the tropical storms ([Goldenberng 2001]; [Trenberth 2006]);[Delworth 1993], suggested a link between the AMO and the variability of the *Thermohaline Circulation* (THC) as the mean THC transports sufficient heat northward [Ganachaud 2000], to warm the Northern Hemisphere by several degrees [Vellinga 2002]. More recently, [Knight 2005] by means of a 1,400 year simulation with the HADCM3 climate model [Gordon 2000], were able to simulated the observed AMO pattern and amplitude from measurements dating back to the nineteenth century. The results imply that the AMO is a genuine quasi-periodic cycle of internal climate variability persisting for many centuries, and is related to variability in the oceanic THC.

1.3. Atmospheric database

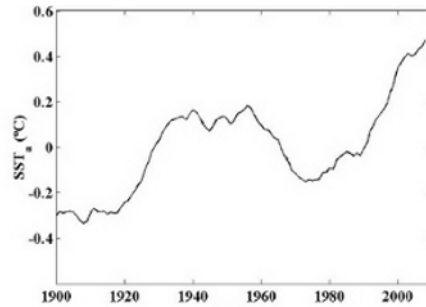


Figure 1.4: Atlantic multidecadal Oscillation index has been traditionally calculated as the average of SST anomaly for the North Atlantic north of the equator [Enfield 2001]

1.3 Atmospheric database

1.3.1 National Center of Atmospheric Research/National Center for Environmental Prediction(NCEP/NCAR)

Wind

Wind components at 10 m above the sea surface can be obtained from the National Center of Atmospheric Research/National Center for Environmental Prediction (NCEP/NCAR). Reanalysis data are supplied on a T62 Gaussian grid, corresponding to $\sim 1.91^\circ$ both in longitude and in latitude. They are available at: 4-times daily, daily and monthly scale from 1948 on wards (www.cdc.noaa.gov/)

From wind data **Ekman transport** can be calculated as follows:

$$Q_x = \frac{\rho_a C_d}{\rho f} (W_x^2 + W_y^2)^{1/2} W_y \quad (1.4)$$

1. DATABASE

$$Q_{y-} = \frac{\rho_a C_d}{\rho f} (W_x^2 + W_y^2)^{1/2} W_x \quad (1.5)$$

where W is the wind speed near surface, ρ is the sea water density (1025 kg m^{-3}), C_d is a dimensionless drag coefficient (1.4×10^{-3}), ρ_a is the air density (1.22 kg m^{-3}) and f is the *Coriolis* parameter defined as twice the vertical component of the Earth's angular velocity, Ω about the local vertical given by $f = 2\Omega \sin(\theta)$ at latitude θ . Finally, x subscript corresponds to the zonal component and y subscript to the meridional one, [Nykjaer 1994].

Upwelling Index (UI) can be defined as the Ekman transport component in the direction perpendicular to the shore line [Nykjaer 1994] pointing seaward. UI was calculated as follows:

$$UI = -\sin(\phi)Q_x + \cos(\phi)Q_y \quad (1.6)$$

where ϕ is the angle between the shoreline and the equator. Using this definition, positive (negative) upwelling indices correspond to upwelling favorable (unfavorable) conditions.

Sea level Pressure

The sea level Pressure (*SLP*) can be obtained from the National Center of Atmospheric Research/National Center for Environmental Prediction (NCEP/NCAR), Fig.1.5a. Reanalysis data are supplied on a *T62* Gaussian grid, corresponding to $\sim 1.91^\circ$ both in longitude and in latitude. As happens with wind, SLP are available 4-times daily, daily and monthly values from 1948 onwards (www.cdc.noaa.gov/).

Monthly air Temperature

Monthly air temperature (T^{air}) data can be obtained from reanalysis data from NCEP/NCAR project, from 1948 to present. Air temperature

1.3. Atmospheric database

was considered at $1,000\text{HPa}$ to avoid topographic effects on atmospheric circulation Fig.1.5b.

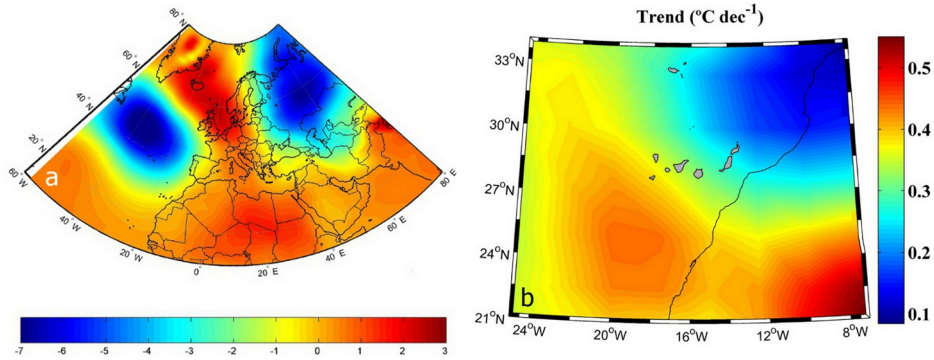


Figure 1.5: National Center of Atmospheric Research/National Center for Environmental Prediction (NCEP/NCAR). a) Mean SLP T (in 10^5 Pa) for the period 1970 to 2009. b) Air temperature trend ($^{\circ}\text{C per decade}$) for the Canary region, calculated from 1982 to 2010

1. DATABASE

1.3.2 Pacific Fisheries Enviromental Laboratory (PFEL)

Wind data were also provided by the Pacific Fisheries Enviromental Laboratory (PFEL) (<http://www.pfeg.noaa.gov>). Data are 6 hours available approximately, on $1^\circ \times 1^\circ$ of spatial resolution, from 1981 to nowadays, Fig.1.6.

1.3.3 Climate Forecast System Reanalysis (CFSR)

NCEP Climate Forecast System Reanalysis (CFSR). The CFSR wind product has a spatial resolution of $0.5 \times 0.5^\circ$ and a 6-hourly time resolution from January 1979 to December 2011, covering the atmosphere, ocean, sea ice and land. The CFSR data was developed by NOAA's National Centers for Environmental Prediction (NCEP) (<http://rda.ucar.edu/pub/cfsr.html>). The data for this study are from NOAA's National Operational Model Archive and Distribution System (NOMADS) which is maintained at NOAA's National Climatic Data Center (NCDC) [Saha 2010]. The reference height of wind data is 10 m.

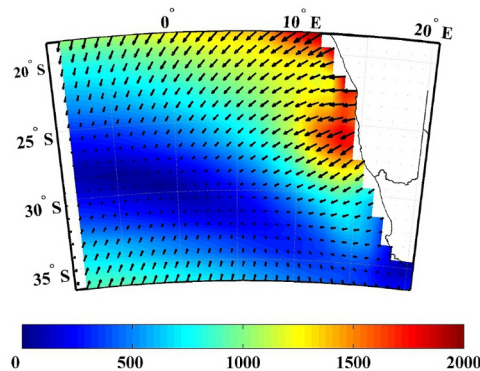


Figure 1.6: Ekman trasport field ($m^3 s^{-1} km^{-1}$) averaged using PFEL data for the period 1981 to 2009

1.3. Atmospheric database

A summary of the atmospheric database used and their main characteristics can be found in *Table 2.2*.

Base	Variable Used	Espatial resol	Tempral resol
NCEP/NCAR	Wind	$1.91^\circ \times 1.91^\circ$	1948–2012
NCEP/NCAR	SLP	$1.91^\circ \times 1.91^\circ$	1948–2012
NCEP/NCAR	T^{air}	$1.91^\circ \times 1.91^\circ$	1948–2012
PFEL	Wind	$1^\circ \times 1^\circ$	1981–2012
CFSR	Wind	$0.5^\circ \times 0.5^\circ$	1979–2012

Table 1.2: Atmospheric Database.

1.4 *Atmospheric Modes*

Teleconnection patterns reflect large-scale changes in the atmospheric wave and jet stream patterns, which can influence temperature, rainfall, storm tracks, and/or jet stream location/intensity over vast areas. The atmospheric circulation patterns are indicators of large-scale decadal changes and play a key role in long-term variability of winds across the North Atlantic affecting, for example, coastal upwelling intensity. Several studies have indicated the influence of the main atmospheric circulation modes on the interannual precipitation variability and drought occurrence in Spain ([Rodo 1997];[RodriguezPuebla 1988];[PozoVázquez 2005];[deCastro 2008a]). In particular, many authors have pointed out that several atmospheric circulation patterns influence precipitation in the northwest part of the IP, but that no pattern describes the bulk of the variability in precipitation over the region [RodriguezPuebla 2001]. The most representative regional patterns of atmospheric variation in the Northern Hemisphere, with some influence on the eastern North Atlantic region, are:

- North Atlantic Multidecadal Oscillation (NAO)
- East Atlantic pattern (EA)
- Scandinavia pattern (SCA)
- East Atlantic/Western Russia pattern (EA/WR)
- Polar/Eurasia pattern (POL)
- Southern Hemisphere Annular Mode (SAM)

1.4.1 North Atlantic Multidecadal Oscillation (NAO)

The NAO consists of a north–south dipole of geopotential anomalies with one centre located over Greenland and the other one spanning between 35 and 40°N in the central North Atlantic. There are two phases of NAO.

A **positive phase** in the NAO index represents an increase in the pressure differences, resulting in an increase in frequency and strength of winter storms crossing the Atlantic Ocean that typically take a more northerly track. This causes warm and wet winters in the northern part of Europe and drier than normal winters in the south.

The **negative phase** represents a reduced pressure gradient resulting in fewer and weaker winter storms crossing Europe, which travel on a more west–east pathway. This brings moist air into the Mediterranean and causes drier winters in the northern part of Europe. Research has identified the NAO index as the local manifestation of the more global pattern of the Arctic Oscillation (AO) during the winter (December–February (DJF)) [Thompson 2000]. It has been found that the NAO can be predicted with reasonable skill from North Atlantic SST anomalies (SSTa) averaged over several prior months ([Czaja 2002];[Bojariu 2003]). The relationship between the NAO index and winter surface temperatures, especially over Europe, has been extensively recorded [Kapala 1998]. [Slonosky 2002] analyzed the degree to which the NAO index reflects the zonal and meridional flow and its influence on SST by means of a near sea surface data set for the years from 1856 to 2000. Although the NAO index has been the most commonly studied mode in the IP ([RodriguezPuebla 1988]; [Trigo 2004];[SantosA 2005]), recent studies ([deCastro 2006];[Lorenzo 2008]) have shown the need to consider additional modes to explain the variable structure of winter rainfall, river flow and upwelling in Iberian Peninsula (IP).

1. DATABASE

1.4.2 East Atlantic pattern (EA)

The EA pattern consists of a north–south dipole that spans the entire North Atlantic Ocean with centres near $55^{\circ}N$, 20 to $35^{\circ}W$ and 25 to $35^{\circ}N$, 0 to $10^{\circ}W$. It is the second prominent mode of low–frequency variability over the North Atlantic, and appears to be the leading mode in all months. The EA pattern is structurally similar to the NAO, but with the anomaly centres displaced south-eastward to the approximate nodal lines of the NAO pattern. For this reason, the EA pattern is often interpreted as a southward shifted NAO pattern. However, the lower-latitude centre contains a strong subtropical link in association with modulations in the subtropical ridge intensity and location. This subtropical link makes the EA pattern distinct from its NAO counterpart. The positive phase of the EA is associated with above-average precipitation over northern Europe and Scandinavia and with below-average precipitation across southern Europe ([RodriguezPuebla 1988];[RodriguezPuebla 2001]). On the other hand, the positive phase of the EA pattern is associated with above average surface temperatures in Europe. In particular in the northern part of the IP, the EA pattern is the most important variation explaining temperature variability [Saenz 2001].

1.4.3 Scandinavia pattern (SCA)

The SCA pattern [Barnston 1987] consists of a primary circulation centre over Scandinavia, with a weaker centre with the opposite sign over Western Europe. The positive phase of this pattern is associated with positive height anomalies, sometimes reflecting major blocking anticyclones over Scandinavia and western Russia.

1.4.4 East Atlantic/Western Russia pattern (EA/WR)

The EA/WR pattern [Barnston 1987] is 1 of 3 prominent teleconnection patterns that affect Eurasia throughout the year. This pattern consists of 4 main anomaly centres. The positive phase is associated with positive height anomalies located over Europe and northern China and negative height anomalies located over the central North Atlantic and north of the Caspian Sea. The main precipitation departures associated with the positive phase of the EA/WR pattern reflect generally above-average precipitation in eastern China and below-average precipitation across central Europe.

1.4.5 Polar/Eurasia pattern (POL)

The POL [Barnston 1987] consists of one centre over the polar region and centres of the opposite sign over Europe and north-eastern China. The positive phase of this pattern is associated with the presence of anomalies over western Europe blocking the passage of low pressure fronts to the north-western coast of the IP and causing drier than normal winters.

1.4.6 Southern Hemisphere Annular Mode (SAM)

The principal mode of atmospheric variability in the Southern Hemisphere extratropics and high latitudes is the Southern Hemisphere Annular Mode (SAM). The SAM index is defined as the difference in the normalized monthly zonal mean of SLP between 40 and 70°S [Nan 2003]. This index is a modification of the Antarctic Oscillation (AAO) index defined as the difference in the normalized monthly zonal mean of SLP between 40 and 65°S [Gong 1999]. The SAM index shows a stronger negative correlation in the zonal mean SLP anomalies than that between 40 and 65°S [Nan 2003].

1. DATABASE

Evolution of water masses along the Atlantic Arc

2.1 *Water Masses*

Here we will present a brief overview of the main water masses observed close to the Atlantic and Cantabrian coast of the Iberian Peninsula. For a more complete description the reader is referred to ([Ambar 1979a]; [Ambar 1979b];[Ambar 1983];[Emery 1986];[Acken 1996];[Pollard 1996]; [OSPAR2000]). Table 2.1 summarizes the different water masses observed in the area.

2.1.1 **Surface waters**

Different layers can be considered, the subsurface water and the near surface water. In particular, subsurface water has attracted the interest of scientist during the last decades since it is placed at the shelf and pumped to the surface in the coast of the western Iberian Peninsula under favorable conditions. This process, usually called coastal upwelling.

Eastern North Atlantic Central Water (ENACW) [Pollard 1996] consti-

2. EVOLUTION OF WATER MASSES ALONG THE ATLANTIC ARC

Water mass	Depth(m)	$\theta(^{\circ}C)$	Salinity (<i>psu</i>)
ENACW			
Subtropical	< 300	13.13–18.50	35.80–36.75
Subpolar	< 400	10.00–12.20	35.40–35.66
Mediterranean Water	400–1500	9.5–13.50	35.8–37.5
Labrador sea Water	1500–3000	3.4	34.89
NA Deep Water	< 3500	2.2	34.91

Table 2.1: Summary of water masses close to the Atlantic and Cantabrian coast of the Iberian Peninsula. (Where θ is the Potential Temperature)

tutes the main subsurface water near the Western Iberian Peninsula shelf. Its lower limit is located below 300–400 *m*, depending on the branch, and its upper limit depends on position, season and meteorological forcing. This water is not represented by a single point in the Salinity-Temperature diagram but it covers a wide range both in salinity and temperature (see Fig.2.1).

ENACW is formed in two main areas; a *subpolar branch* ($ENACW^{sp}$) (10.5–12.5 $^{\circ}C$ and 35.55–35.70 *psu*) which is formed to the south of the North Atlantic Current and spreads southwards or south–eastwards [Pollard 1996], and a *subtropical branch* ($ENACW^{st}$) (temperature and salinity values greater than 12.5 $^{\circ}C$ and 35.75 *psu*, respectively) formed at the northern margin of the Azores Current which moves northeastwards towards the Iberian coast [Pingree 1997]. Some authors [Fraga 1982] have identified a local mode water within the Bay of Biscay.

According to [Rios 1992] the two main branches of the ENACW converge off the north-west corner of the IP. There the subpolar branch sinks and spreads southwards under the subtropical branch. On the other hand, the subtropical branch tends to lose its identity to the north of the convergence

2.1. Water Masses

zone. This convergence is especially remarkable near Cape Finisterre, where a stationary maximum in coastal upwelling and the presence of an upwelling filament have been observed ([Blanton 1984];[Castro1994];[Haynes 1993]). Fig.2.1 shows an example of water masses observed at $3.25^{\circ}W$ and $44.75^{\circ}N$. In particular, ENACW has been highlighted in gray color. This $T-S$ diagram is similar to the one described by [GonzalezPola 2005] near Santander (south of Bay of Biscay) from 1991 to 2003.

The properties of near surface water depend on local meteorological conditions especially in the first 20–30 m . In the lower part (30–50 m) there is a seasonal thermocline that only disappears in winter, when the solar irradiance attains a minimum. This water is also locally affected by the presence of river plumes.

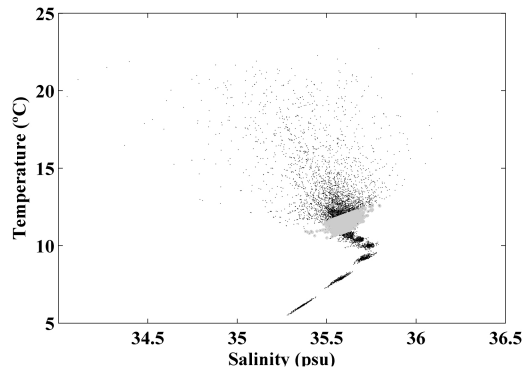


Figure 2.1: $T-S$ diagram of the water masses present in the Bay of Biscay at $3.25^{\circ}W$ and $44.75^{\circ}N$ from 1975 to 2006 till a depth of 700 m . ENACW is highlighted by means of gray dots. This water mass was identified by salinity and temperature values which generate a density ranging from 27.0 to 27.2 kg m^{-3} .

2.1.2 Intermediate waters

The **Mediterranean Water (MW)** is an intermediate water, which attains the Western Iberian Peninsula coast with low dilution. This water is formed in the Mediterranean Sea and splits into two veins after leaving the Gibraltar Strait. The lower one flows northward along the coast of the Iberian Peninsula, at 1,200 *m* depth [DiazdelRio 1998]. At the equilibrium depth, its temperature ranges from 9.5 to 12.5°C and its salinity ranges from 35.8 to 37.5 *psu*. The upper core flows at a depth of 800 *m* with temperature ranging from 10.5 to 13.5°C and a salinity ranging from 35.8 to 36.8 *psu*.

The so called **Labrador Sea Water (LSW)**, is located between North Atlantic Deep Water (NADW) and MW and flows in the opposite direction. This water constitutes a layer of minimum salinity and maximum oxygen concentration. It's main properties in the formation zone are $T = 3.4^{\circ}C$ and $S = 34.89$ *psu*.

2.1.3 Deep waters

North Atlantic Deep Water (NADW) can be observed below 3,500 *m* depth. This water mass is characterized by a temperature of 2.2°C and a salinity of 34.91 *psu* (Table 2.1). The NADW observed in the western Iberian Peninsula coast comprises two different water masses, namely; Antarctic Bottom Water (AABW) and North-West Atlantic Bottom water (NWABW).

2.2 *Changes in Water masses*

Water masses surrounding the Atlantic and Cantabrian coast of the Iberian Peninsula (see bathymetry in Fig.2.2) have changed over the last decades. Note that the French continental shelf is much wider than the Spanish and Portuguese one. Here we will try to introduce some of the main changes observed for the most relevant water masses ENACW and MW.

In general, changes can be assumed for any water mass but here we will only focus on ENACW and MW for several reasons:

- 1) They are the water masses more commonly sampled.
- 2) They can be sampled at near shore areas, that are precisely the areas where most of the present memory is focused.
- 3) The most important changes in ocean heat content occur along the first 2,000 *m* of the water column where these masses are sampled [Levitus 2012]. In fact, most of the authors simply consider that the highest percentage of change can be observed along the first 700 *m* [Levitus 2001].

An example of these changes can be seen in Fig.2.3 with data corresponding to the Atlantic coast over the period 1975–2008 and in Fig.2.4 with data corresponding to the Bay of Biscay over the period 1975–2006. Fig.2.3 shows an intense warming for those depths characterized by ENACW (from 5 *m* to 728 *m*, *black solid line*) and for those depths characterized by MW (from 728 *m* to 3,125 *m*, *gray solid line*). Mean warming is 0.11 °C *per decade* at ENACW layer and 0.06 °C *per decade* at MW layer. The evolution of salinity follows a similar pattern to the temperature one. Similar warming trend (0.2–0.3 °C *per decade*) were widely detected at surface layer from 1974 on along IP ([Gesteira 2008a];[Gesteira 2011];[Santos 2011b]).

Fig.2.4a shows a significant (95%) warming till 600 *m* deep. The warm-

2. EVOLUTION OF WATER MASSES ALONG THE ATLANTIC ARC

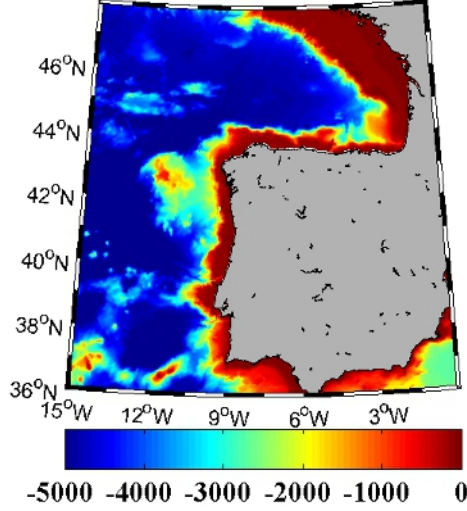


Figure 2.2: Bathymetry of 0–20.5°W and 36.5–48.5°N

ing rates range from values close to 0.25°C near surface to $0.03^{\circ}\text{C per decade}$ at 700 m deep. Warming decreases quickly along the upper 100 m reaching values on the order of $0.15^{\circ}\text{C per decade}$, then it increases slightly between 100 and 200 m deep and, finally, it decreases quasi-linearly till 700 m deep. The surface warming trend is on the same order of magnitude as observed in previous studies carried out in the area (eg.[Koutsikopoulos 1998]): $0.64^{\circ}\text{C per decade}$ for the period 1972–1993 with a grid based on vessels and buoys; [Planque 2003]: $0.6^{\circ}\text{C per decade}$ in the southeastern corner using SST data from Meteo–France; [Llope 2006]: $0.5^{\circ}\text{C per decade}$ over the period 1993–2003 using the coefficients of an empirical model; [Goikoetxea 2009]: $0.23^{\circ}\text{C per decade}$ over the period 1977–2007 with data from the Aquarium of San Sebastian; [Gesteira 2008a]: $0.35^{\circ}\text{C per decade}$ from 1985 to 2005 using satellite SST data and [deCastro 2009]: $0.22^{\circ}\text{C per decade}$ over the period 1974–2007 by means of extended reconstructed SST data). In addition, [Michel 2009], who used simulations and in situ (WOD) measurements,

2.2. Changes in Water masses

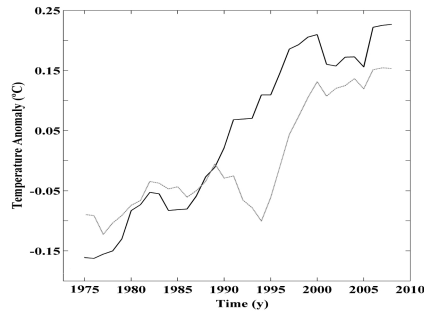


Figure 2.3: Time evolution of the temperature anomaly ($^{\circ}C$) along the Atlantic Coast of the Iberian Peninsula over the period 1975–2008. *Black line* represents the temperature average to those depths characterized by ENACW (from 5 m to 700 m) and *gray line* represents the temperature average to those depths characterized by MW (from 728 m to 3,125 m)

observed a similar vertical profile of temperature trends with warming rates ranging from $0.23^{\circ}C$ per decade near surface to $-0.04^{\circ}C$ per decade at 600 m over the period 1965–2003. Similar trends can be observed for salinity Fig.2.4b. The warming and salinification trends observed throughout the water column suggest that changes are not constrained at the surface by the air-sea interaction but also linked to changes in water masses.

2. EVOLUTION OF WATER MASSES ALONG THE ATLANTIC ARC

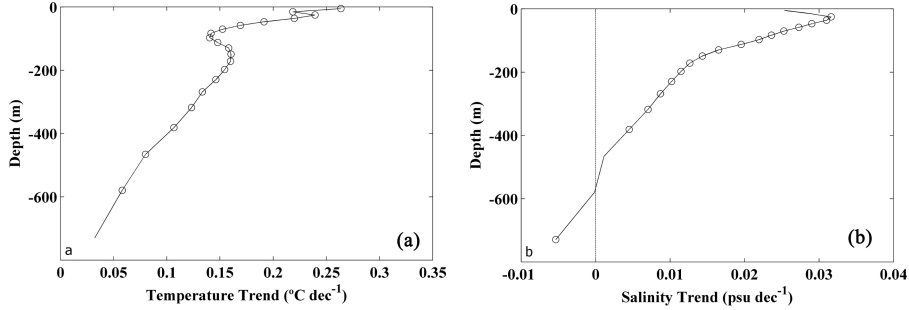


Figure 2.4: Vertical profile of a) temperature trends ($^{\circ}C$ per decade), b) salinity trends (psu per decade) for the entire Bay of Biscay from 1975 to 2006. Circles represent trends with a significance level greater than 95%.

2.3 Changes in ENACW and MW along the Atlantic coast of the Iberian Peninsula

2.3.1 Motivation

The aim of this subsection is the long-term analysis of salinity and temperature changes in ENACW and MW along the western continental shelf of the IP from 1975–2008. This analysis will know the influence of these water masses changes in trends of the Atlantic water vertical profiles. In addition, this study will provide us information about regions where long-term variations in salinity and temperature were more intense.

2.3.2 Methods

Ocean temperature and salinity data were obtained from SODA. The time period ranges from 1975 to 2008 which corresponds to the strongest warming period detected in the North Atlantic Area ([Koutsikopoulos 1998]; [IPCC2007]; [GarciaSoto 2002]; [Gesteira 2008a]; [deCastro 2009]; [Gesteira 2011]).

The following steps had been done to identify the ENACW and MW

2.3. Changes in ENACW and MW along the Atlantic coast of the Iberian Peninsula

by means of the salinity and temperature values.

First of all, the grid points where ENACW or MW was rarely sampled (less than 800 valid samples) were discarded.

Considering the vertical layers and the monthly scale, the number of samples varies between 8,000 and 12,000. The threshold imposed (800 ENACW samples) only represents between 10%–7% of the samples. In addition, results showed to be almost insensitive to changes in this threshold.

Salinity and temperature data corresponding to each grid point were averaged to convert them into annual values.

All salinity and temperature data corresponding to the density interval 27.0–27.2 $kg\ m^{-3}$ for a certain year were averaged, no matter their layer, in order to obtain the value of the mean ENACW salinity and temperature for that year.

All salinity and temperature data corresponding to the density interval 27.4–27.65 (27.7–27.85) $kg\ m^{-3}$ for a certain year were averaged, no matter their layer, in order to obtain the value of the mean upper (lower) MW salinity and temperature for that year.

The mean ENACW or MW depth was calculated in the same way.

Long-term processes like warming–cooling or salinification–freshening and their implications in the water column stratification were analyzed by means of annual trends which were assumed to be linear. All trends were calculated on raw data, without using any filter or running mean.

The Spearman rank correlation coefficient was used to analyze the significance of trends due to its robustness to deviations from linearity and its resistance to the influence of outliers [Saunders 2008].

2.3.3 Trends in the vertical profiles of the Atlantic water

Trends in temperature and salinity of AW were calculated for each degree in latitude along the IP (Fig.2.5 and Fig.2.6). Top subplots correspond to $42.75^{\circ}N$ and bottom subplots to $37.75^{\circ}N$.

Temperature trends along the entire IP show lower values near shore (*black line*) than in the ocean (*gray line*) at surface layers and there is not warming in deep Atlantic water (depths higher than 2,500 m). Temperature trends at latitudes north of $40.75^{\circ}N$ share some common features (Fig.2.5(a-l)). Warming occurs from surface to 2,500 m depth both near coast and in the ocean. A practically homogeneous warming rate was observed near coast (between 0 and $0.1^{\circ}C$ per decade). On the other hand, warming was not homogeneous in the ocean with two peaks of around $\sim 0.25^{\circ}C$ per decade near surface and at MW layers. The surface warming peak occurs at a depth of ~ 50 m where water is not affected by winds [Michel 2009]. South of $40.75^{\circ}N$ (Fig.2.5(g-l)), coastal warming occurs at MW layers ($\sim 0.15^{\circ}C$ per decade) and only some of these latitudes show a cooling ($\sim -0.05^{\circ}C$ per decade) near surface (Fig.2.5(g-j)). On the contrary, ocean warming was only detected near surface and at ENACW layers ($0.25^{\circ}C$ per decade).

Salinity trends at latitudes north of $41.75^{\circ}N$ share some common features (Fig.2.6(a-d)). Coastal freshening is observed only near surface ($\sim -0.01^{\circ}C$ per decade) and ocean salinification at ENACW layers (~ 0.04 psu per decade). On the contrary, MW layers show an increase in salinity both in the ocean (0.05 – 0.07 psu per decade) and near coast (~ 0.04 psu per decade). The Atlantic Water vertical profile of salinity changes at $40.75^{\circ}N$ (Fig.2.6(e, f)) showing a salinity increase both at ENACW and at MW layers in the whole region. Salinification is higher in ocean (~ 0.04 psu per decade at ENACW layers and ~ 0.05 psu per decade at MW layers)

2.3. Changes in ENACW and MW along the Atlantic coast of the Iberian Peninsula

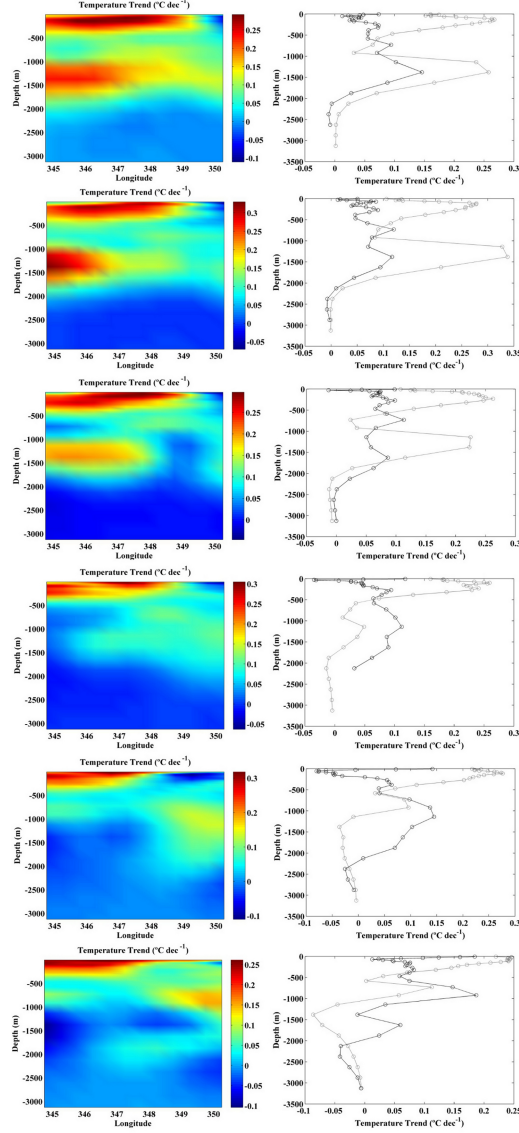


Figure 2.5: Vertical profiles of temperature trends ($^{\circ}C$ per decade) along the Atlantic coast (from 37.75 to $42.75^{\circ}N$) of the IP over the period 1975–2008 (*left pannels*). Vertical profiles of temperature ($^{\circ}C$ per decade) along the Atlantic coast of the IP at coastal (*black line*) and oceanic (*gray line*) location (*right pannels*). Temperature trend at coastal (oceanic) locations was calculated averaging temperature values at the three latitudes nearest (farthest).

2. EVOLUTION OF WATER MASSES ALONG THE ATLANTIC ARC

than near coast (~ 0.02 *psu per decade* at ENACW layers and ~ 0.025 *psu per decade* at MW layers) throughout the water column. A similar coastal freshening near surface to that observed north is obtained south of $40.75^\circ N$ (Fig.2.6(g-1)). In addition, salinification is observed in ocean only at ENACW layers (0.02 – 0.03 *psu per decade*) while near coast salinification occurs both at ENACW layers (~ 0.02 *per decade*) and at MW layers (0.25 – 0.35 *psu per decade*). In this case, salinity trends are higher near coast than in ocean at MW layers. No salinity trends were detected in deep Atlantic Water.

Salinity and temperature trends for ENACW and MW masses were correlated. These water masses were delimited following the procedure described in methods section. Changes in temperature and salinity are highly correlated both for ENACW ($r = 0.99$, $p < 0.01$) and MW ($r = 91$, $p < 0.01$ for upper MW and $r = 99$, $p < 0.01$ for lower MW). These correlations indicate that long-term salinity and temperature changes are density compensated.

2.3. Changes in ENACW and MW along the Atlantic coast of the Iberian Peninsula

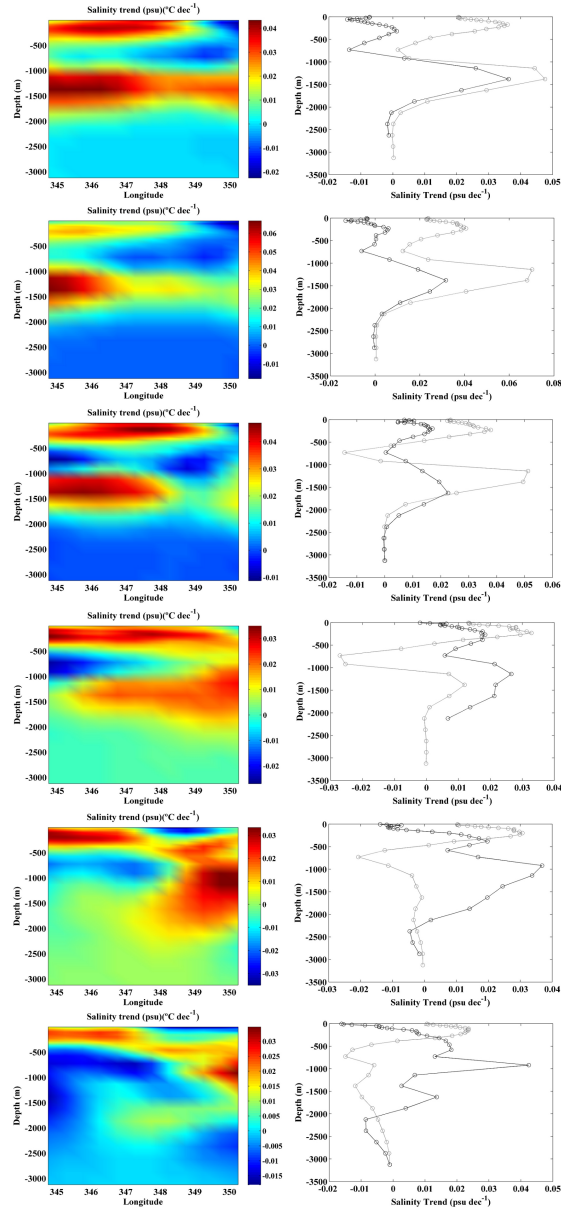


Figure 2.6: Vertical profiles of salinity trends (*psu per decade*) along the Atlantic coast (from 37.75 to $42.75^\circ N$) of the IP over the period 1975–2008 (*left pannels*). Vertical profiles of salinity (*psu per decade*) along the Atlantic coast of the IP at coastal (*black line*) and oceanic (*gray line*) location (*right pannels*). Salinity trend at coastal (oceanic) locations was calculated averaging salinity values at the three latitudes nearest (farthest).

2.3.4 Trends in ENACW and MW

The temperature and salinity trends corresponding to ENACW and MW masses over the period 1975–2008 were depicted in Fig.2.7(a- f). Left (right) panels correspond to temperature (salinity) trends. From top to bottom, ENACW mass, upper MW mass and lower MW mass were considered. Black dots represent the grid points with a significance level greater than 95%. The blanks correspond to points where the water masses were scarcely detected for the period under study following the protocol described above.

Temperature trend of ENACW mass (Fig.2.7(a)) shows an inhomogeneous spatial pattern along the IP with a significant warming in ocean and cooling near coast. Maximum warming (cooling) observed is $0.08^{\circ}\text{C per decade}$ ($-0.08^{\circ}\text{C per decade}$). This water mass tendency explains the ocean warming peak and the coastal cooling observed at ENACW layers in Fig.2.5(a- d). The temperature trend of upper MW mass (Fig.2.76(c)) is positive for the entire area with a significant warming near coast and at some ocean points. Maximum warming ($0.15^{\circ}\text{C per decade}$) is detected at the southern coastal area and ocean warming is negligible from 13°W for most of latitudes. Note that the upper MW warming is higher than the ENACW warming. This water mass trend explains coastal warming detected at MW layers in Fig.2.5 which is more pronounced south of 39.75°N . Temperature trend for lower MW (Fig.2.7(e)) shows significant warming both in ocean and near coast for latitudes northern than 40.75°N . The warming rate detected for the lower MW is higher than the one detected for ENACW and upper MW. The maximum warming of lower MW is $0.5^{\circ}\text{C per decade}$. This water mass trend explains the ocean warming observed in the Atlantic Water (Fig.2.5) at MW layers northern than 40.75°N and the coastal warming at MW layers at 42.75°N .

Salinity trend of ENACW, upper and lower MW masses show a similar

2.3. Changes in ENACW and MW along the Atlantic coast of the Iberian Peninsula

pattern to the temperature one (Fig.2.7, right panels). As for temperature, all water masses show salinification with the exception of ENACW near coast. Salinification is higher for the lower MW than for the other water masses. The salinity trend observed in these water masses explains the salinity trends observed in the Atlantic Water column (Fig.2.5).

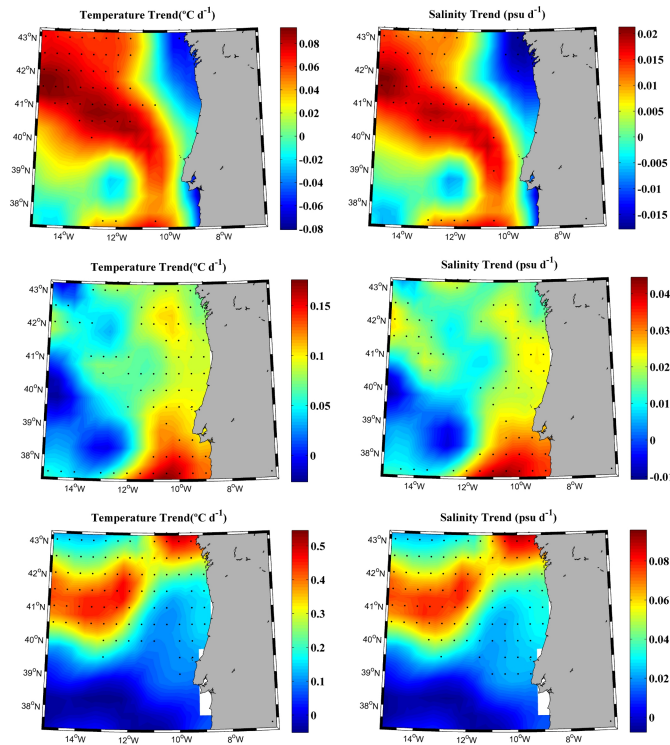


Figure 2.7: Annual temperature (*left panels*) and salinity (*right panels*) trends ($^{\circ}\text{C per decade}$ and psu per decade) corresponding from top to bottom to ENACW, upper MW and lower MC along the Atlantic coast of the IP from 1975 to 2008. Black dots represent the grid points where trends with a significance level greater than 95% were obtained. The blanks represent points where ENACW was scarcely detected.

2.4 *Changes in ENACW along the Bay of Biscay*

2.4.1 Motivation

The aim of this sub-section is to analyze the changes observed in ENACW during the last three decades (1975–2006) in the North-Atlantic area surrounding the Iberian Peninsula. Trends in salinity and temperature corresponding to the isopycnals ranging from 27.0 to 27.2 kg m^{-3} will be calculated to determine the rate of change of ENACW during that period.

2.4.2 Methods

Only the first 21 vertical levels, which correspond to a water depth of 729 m were considered because the present study is focused on the upper layer: from near surface (5 m) to the upper permanent thermocline depth (700 m). The time period ranges from 1975 to 2006, which corresponds to the strongest warming period detected in the North Atlantic area ([Koutsikopoulos 1998];[IPCC2007]; [GarciaSoto 2002]; [Gesteira 2008a];[deCastro 2009];[Gesteira 2011]).

The steps to identify ENACW was described in the previous section 2.3.2

Results will be correlated with atmospheric forcing. Thus, the NAO teleconnection index was obtained from the Climate Prediction Center (CPC) at the National Center of Environmental Prediction (NCEP). Data are available at a monthly time scale with a global coverage from 1950 to nowadays. Rotated Principal Component Analysis (RPCA) was used to identify the Northern Hemisphere teleconnection patterns and indices [Barnston 1987]. In this point 2.3 of this chapter the extended winter of the NAO index (from December to March) was considered from 1975 to 2006.

2.4.3 Trends in ENACW

Salinity and temperature trends were calculated for the North Atlantic area surrounding the Iberian Peninsula (Fig.2.8). Black dots represent the grid points where trends with a significance level greater than 95% were obtained and the blanks represent the grid points where ENACW was scarcely detected. The maximum positive trends were detected both in temperature ($0.3^{\circ}\text{C per decade}$; Fig.2.8a) and in salinity ($\approx 0.045 \text{ psu per decade}$; Fig.2.8b) on the North Atlantic area where $ENACW^{sp}$ develops. Trends are negative in wide areas located in front of the Iberian Peninsula, which are mainly affected by the subtropical mode. These preliminary results show that the changes in ENACW are moderate along the Atlantic coast of the Iberian Peninsula both for salinity and temperature.

The most important changes can be observed in the area stretching from the Celtic Sea to the Cantabrian Coast. In particular, we will analyze in more detail the so called Bay of Biscay. The temperature and salinity trends corresponding to ENACW over the period 1975–2006 are depicted in Fig.2.9 and Fig.2.10. Once again, black dots represent the grid points where trends with a significance level greater than 95% were obtained. The blanks observed on the French continental shelf, correspond to points where ENACW was scarcely detected for the period under study following the protocol described above.

The temperature trend (Fig.2.9) is positive for the entire area with maximum values close to $0.12^{\circ}\text{C per decade}$ in the northeastern part. In fact, the ENACW warming is negligible at the southwestern corner (values lower than $0.04^{\circ}\text{C per decade}$) and small (around $0.08^{\circ}\text{C per decade}$) along the southern coast of the Bay. A similar pattern was observed for salinity (Fig.2.10) with positive values in the entire area and with maximum values close to $0.018 \text{ psu per decade}$ in the eastern part of the Bay. The

2. EVOLUTION OF WATER MASSES ALONG THE ATLANTIC ARC

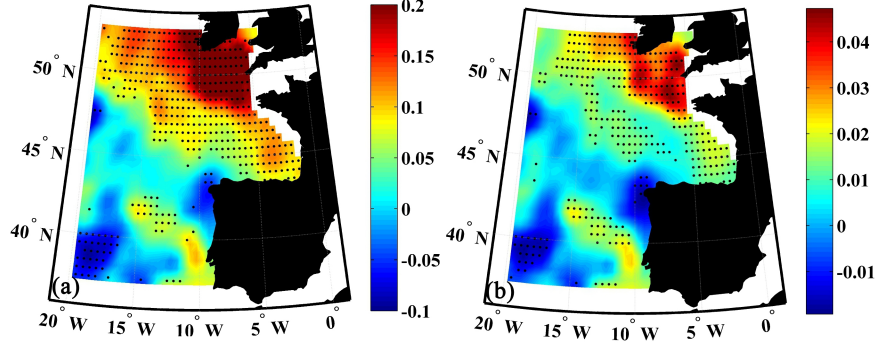


Figure 2.8: a) Annual temperature trend ($^{\circ}C$ per decade) and b) Annual salinity trend (psu per decade), of ENACW mass in the North Atlantic area ($0-20.5^{\circ}W$ and $37.5-47.5^{\circ}N$) from 1975 to 2006. Black dots represent the grid points where trends with a significance level greater than 95% were obtained. The blanks represent points where ENACW was scarcely detected.

ENACW salinification is negligible (values ranging from 0.003 to 0.006 psu per decade) at the western part of the Bay (from $4^{\circ}W$ to $7.5^{\circ}W$). Both temperature and salinity trends show warming and salinification of ENACW from 1975 to 2006. These tendencies are not homogeneous in space, being more pronounced at the north-eastern part of the bay and almost negligible at the western part.

2.4. Changes in ENACW along the Bay of Biscay

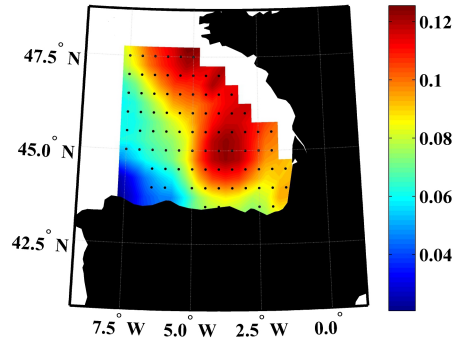


Figure 2.9: Annual temperature trend ($^{\circ}C$ per decade) corresponding to ENACW in the Bay of Biscay from 1975 to 2006. Black dots represent the grid points where trends with a significance level greater than 95% were obtained. The blanks represent points where ENACW was scarcely detected.

Results can be compared to the local analysis carried out by [GonzalezPola 2005], who observed an intense ENACW warming ranging from 0.2 to 0.4 $^{\circ}C$ per decade from 1992 to 2003 at 200–500 *db* using *in situ* data. They also indicate a moderate decrease in ENACW salinity at 200–500 *db*, which ranged from 0.01 to 0.02 *psu per decade*. Although there is a qualitative agreement in temperature, the salinity trends are opposite. This is possibly due to the different extent of both intervals. In fact, the salinity series shown by [Llope 2006] in the area close to Cape Peñas, about 150 *km* away from the area described by [GonzalezPola 2005], shows a clear oscillatory behavior, which cannot be accurately described by a linear fitting. There, small changes in the extent of the interval can lead to opposite trends.

The mean ENACW depth calculated at the Bay of Biscay from 1975 to 2006 (Fig.2.11) ranges from 230 to 290 *m*. The maximum depth (~ 290 *m*) was observed at the southeastern part of the basin and at the western part at latitudes close to 45°N. The minimum depth (~ 230 *m*) was observed

2. EVOLUTION OF WATER MASSES ALONG THE ATLANTIC ARC

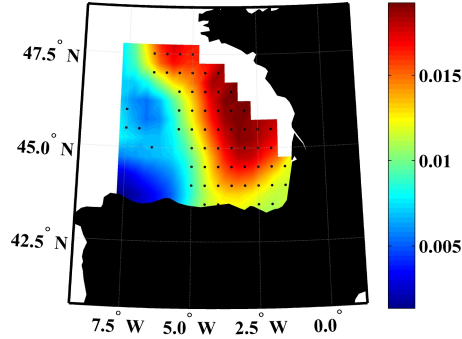


Figure 2.10: Annual salinity trend (*psu per decade*) corresponding to ENACW in the Bay of Biscay from 1975 to 2006. Black dots represent the grid points where trends with a significance level greater than 95% were obtained. The blanks represent points where ENACW was scarcely detected.

at the northern part. This result is similar to the ones measured by other authors. Thus, for example, a depth on the order of 325–350 *m* can be inferred from [GonzalezPola 2005], analyzing their 27.1 and 27.2 $kg\ m^{-3}$ isopycnals. This value is comparable to the one observed in our study for that area (280–290 *m*). Note that neither the time interval nor the ENACW range was exactly the same in both studies.

The warming and salinification of ENACW is accompanied by a sinking of the water mass in the entire area from 1975 to 2006 (Fig.2.12). The deepening of ENACW ranges from 10–15 *m per decade* (near coast and at the open ocean) to 40 *m per decade* in the central part of the Bay. [GonzalezPola 2005] also observed the sinking of upper ENACW (bounded by 27.1 and 27.2 isopycnals) from 1992 to 2003. They linked this fact to a greater input of lighter water at the upper layers associated to a temperature increase and a progressive salinity reduction from 1998 on. In our case the sinking of ENACW is related to the unbalance between the rates of warming and salinification. Actually, the deepening is less intense in the areas where salinification and warming are more intense. Examining the trends in salinity and temperature calculated in the Bay of Biscay, one can

2.4. Changes in ENACW along the Bay of Biscay

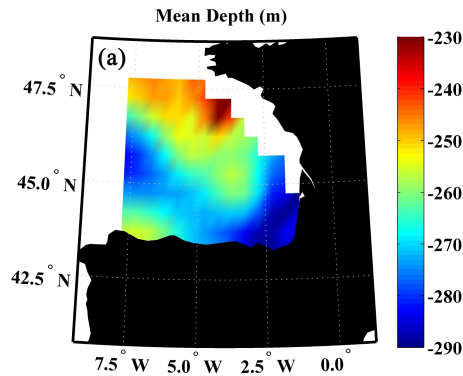


Figure 2.11: Mean depth of ENACW (m) in the Bay of Biscay for the period 1975–2006. Black dots represent the grid points where trends with a significance level greater than 95% were obtained. The blanks represent points where ENACW was scarcely detected.

wonder about the origin of the observed changes. Inside the domain, the most intense trends in salinity and temperature are found in the middle part of the Bay although they are not exactly located at the same place. On the other hand, it is rather clear that the trends are negligible at the western boundary since the values have not statistical significance. In addition, the maximum trends are observed at the northeastern boundary. In addition, patterns shown in Fig.2.8 show that the highest increase in salinity and temperature occur at the Celtic Sea area

Authors as, [Johnson 2007], have described decadal water mass variations in the Northern hemisphere along $20^{\circ}W$. They related the observed changes to the 1995–1996 shift of the NAO [Halpert 1997], which is the leading mode of variability in the area. Following this shift, the subpolar gyre retreated to the northwest, which gave rise to changes in the SubPolar Mode Water, which became saltier and warmer. This fact was also mentioned by [GonzalezPola 2005] to put into context the warming observed in

2. EVOLUTION OF WATER MASSES ALONG THE ATLANTIC ARC

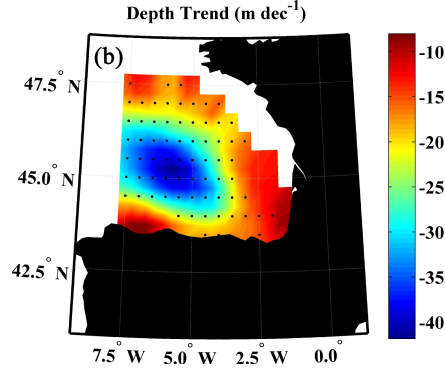


Figure 2.12: Depth trend of ENACW (*m per decade*) in the Bay of Biscay for the period 1975–2006. Black dots represent the grid points where trends with a significance level greater than 95% were obtained. The blanks represent points where ENACW was scarcely detected.

ENACW near Santander.

In this chapter we have compared the salinity and temperature series with the extended winter index of NAO. The spatial mean of temperature (salinity) in the Bay of Biscay was calculated by averaging the grid points with trends significant at the 95%. (see Fig.2.9 and Fig.2.10). Fig.2.13 shows the time evolution of the three series (NAO *thick black line*, temperature *thin black line* and salinity *solid gray line*) which were normalized to be represented together. The correlations between salinity and temperature with NAO were carried out considering a 1 *year* lag between NAO and the oceanographic variables. The correlations obtained are rather surprising, since the same correlation is not keep all over the period. Thus, the series are positively correlated ($R = 0.90$, $p < 0.01$ for temperature and $R = 0.83$, $p < 0.01$ for salinity) over the period 1975–1995, which mostly coincides with the positive phase of NAO. However, the series are negatively correlated ($R = -0.78$, $p < 0.01$ for temperature and $R = -0.67$, $p < 0.05$

2.4. Changes in ENACW along the Bay of Biscay

for salinity) over the period 1996–2006, which corresponds to the negative phase of NAO. This shift in tendency is possibly due to the displacement of NAO dipole between positive and negative phase [Halpert 1997]. Thus, during the positive phase, the high was located at central latitudes of the North Atlantic but it is displaced toward the Iberian Peninsula during the negative phase.

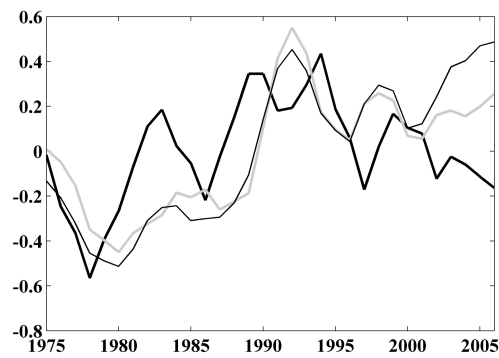


Figure 2.13: Time evolution of temperature (*thin black line*), salinity of ENACW (*solid gray line*) and NAO index (*thick black line*) in the Bay of Biscay from 1975 to 2006. The NAO index was calculated for the extended winter (DJFM). Signals were normalized to be represented together. A running average of ± 1 year was applied to smooth signals.

2.4.4 Conclusions

ENACW mas shows a significant warming along the Atlantic ocean of the IP and a cooling near coast from 1975 to 2008. This water mass trends explain the ocean warming peak and the coastal cooling shown in the Atlantic water column at those layers characterized by the presence of ENACW.

Upper MW mas warms in the whole area being significant near coast and at some ocean points. The uppwe MW warming is higher than the ENACW one. This water mass warming explain the coastal warming shown by the Atlantic Water at those layers characterized by the presence of upper MW, specially southern than $40.75^{\circ}N$.

Lower MW mas shows a significant warming both in ocean and near coast for latitudes northern than $40.75^{\circ}N$. This water mas warming explain the coastal warming at $42.75^{\circ}N$ and the ocean warming northern than $40.75^{\circ}N$ at those layers characterized by the presence of this water mass.

All water masses show salinification along the Atlantic coast of the IP with the exception of ENACW near coast. Salinification is higher for the lower MW than for the other water masses.

Changes in ENACW have been observed in the Bay of Biscay over the period 1975–2006, coinciding with the last warming period in the North Atlantic.

This water mass has been observed to warm and salinificate in most of the area at a maximum rate of $0.12^{\circ}C$ *per decade* and 0.018 *psu per decade* respectively. The trends were more intense in the middle part of the Bay and at the northeastern boundary.

The origin of the observed changes in ENACW seems to be related to changes in the *ENACW^{sp}* formation area where the trends have been observed to reach a maximum on the order of $0.3^{\circ}C$ *per decade* and 0.045

2.4. Changes in ENACW along the Bay of Biscay

psu per decade respectively.

The ENACW changes in the Bay of Biscay are well correlated with the NAO index being positively correlated during the positive phase of the NAO (from 1975 to 1995) and negatively correlated during its negative phase (from 1996 to 2006).

2. EVOLUTION OF WATER MASSES ALONG THE ATLANTIC ARC

Differences between ocean and coastal SST along Western Iberian Peninsula (WIP)

3.1 *Differences between ocean and coastal SST*

3.1.1 Motivation

The aim is to describe the differences in SST evolution during the last century at coastal and oceanic locations along western Iberian Peninsula. The SST variability will be analyzed in terms of upwelling and THC intensity.

3.1.2 Methods

In the present case, 78 data points in front of the western Iberian Peninsula (WIP) coast were considered from 1900 to 2008. These points range from $9^{\circ}W$ to $21.5^{\circ}W$ and from $37.5^{\circ}N$ to $42.5^{\circ}N$, (see, Fig.3.1) where obtained from HadISST. Monthly SST data were seasonally and annually

3. DIFFERENCES BETWEEN OCEAN AND COASTAL SST

averaged. The SST difference between coast and ocean was calculated as:

$$\Delta SST = SST_{ocean} - SST_{coast} \quad (3.1)$$

Twelve points were considered for this purpose. Points located at $9.5^\circ W$ ($17.5^\circ W$) are representative of coastal (oceanic) conditions (Fig.3.1, *circles O*). Differences were calculated between each pair of points located at the same latitude and then meridionally averaged.

Wind data were obtained from NCEP/NCAR at points located at $10^\circ W$ and $42.5^\circ N$, $40^\circ N$ and $37.5^\circ N$, from 1948 to 2008 (Fig.3.1, *crosses x*). Time series obtained at the different points showed to be well correlated ($R > 0.8$) allowing a meridional average. The upwelling index (UI) can be defined as minus the zonal component of Ekman transport. Note that the shore line is macroscopically perpendicular to the Equator along the WIP:

$$UI = -Q_x = \frac{-\tau_y}{\rho_w f} \quad (3.2)$$

where

$$\tau_y = \rho_a C_d (W_x^2 + W_y^2)^{1/2} W_y \quad (3.3)$$

being τ_y the meridional wind stress, W the wind speed near surface, ρ_w the sea water density (1025 kg m^{-3}), C_d a dimensionless drag coefficient, (1.4×10^{-3}), ρ_a the air density (1.22 kg m^{-3}) and f is the Coriolis parameter defined as twice the vertical component of the Earth's angular velocity, Ω , about the local vertical given by $f = 2\Omega \sin(\Theta)$ at latitude Θ . Finally, x subscript corresponds to the zonal component and the y subscript to the meridional one. Negative (positive) τ_y values result in positive (negative) UI values, which correspond to upwelling favorable (unfavorable) conditions.

According to previous research [deCastro 2008a], the EA mode shows a significant negative correlation with upwelling along the entire western coast

3.1. Differences between ocean and coastal SST

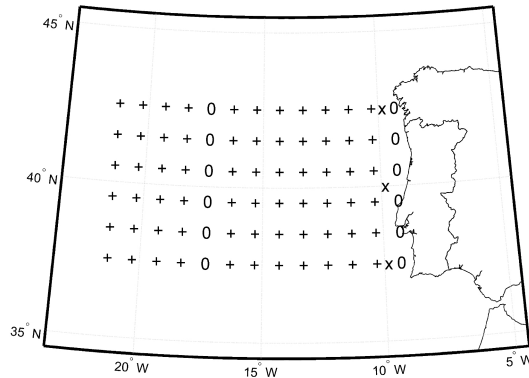


Figure 3.1: Study area. SST points (+) are placed on $1^\circ \times 1^\circ$ from $9.5^\circ W$ to $21.5^\circ W$ and from $42.5^\circ N$ to $37.5^\circ N$. Circles (o) represent coastal ($9.5^\circ W$) and oceanic ($17.5^\circ W$) reference SST points. Crosses (x) represent the location of wind data (located at $10.0^\circ W$, $37.5^\circ N$, $40.0^\circ N$ and $42.5^\circ N$).

of the Iberian Peninsula. The NAO, which is the first prominent mode over the North Atlantic, just has influence on the upwelling index between 38° and 41° . Thus, EA will be the only mode considered in this point. The teleconnection indices were obtained from the Climate Prediction Center (CPC) at the NCEP at monthly time scales from 1950 to 2009. Rotated principal component analysis (RPCA) was used to identify the Northern Hemisphere teleconnection patterns and indices [Barnston 1987]. This procedure isolates the primary teleconnection patterns for all months and allows time series of the patterns to be constructed.

3.1.3 Results and Discussion

The spatial and temporal distribution of SST along the study area is depicted in Fig.3.2a. A running average of ± 5 years was used to smooth high frequency variations in temperature. A SST gradient on the order of 1°C can be observed from coast ($\sim 9.5^{\circ}\text{W}$) to ocean, with lower values near coast. In addition, several warming cooling cycles can be observed at all longitudes during the period 1900–2008. Maximum values were observed around 1950 and at present and minimum values around 1900 and 1975.

The inter-annual evolution of the meridional average of coastal (at 9.5°W) and oceanic (at 17.5°W) SST are represented in Fig.3.2b (*solid* and *dashed lines*, respectively). A running average of ± 5 years was also considered. Macroscopically, there is an overall increase of SST at both longitudes during this period (approximately 1.1°C both at coastal and ocean locations).

This increase is comparable to the one obtained at adjacent areas ([GarciaSoto 2002];[deCastro 2009];[Gesteira 2011]), and also to the values provided by the IPCC for the whole Atlantic Basin [IPCC2007]. In addition, coastal water(*solid line*) is cooler than the oceanic one (*dashed line*) as mentioned above. According to previous research, this temperature gradient is mainly due to coastal upwelling in spring–summer ([Nykjaer 1994]; [Santos 2011c];[Álvarez 2008a]) and to water cooling developed in shallow waters at the end of autumn due to net heat loss from surface ([Fiuza 1983]; [desChamps 1984]). As mentioned above, three different warming-cooling periods can be observed in both signals, a warming period from 1920 to 1950, a cooling period from 1950 to 1974 and another warming period from 1974 to 2008. In the first warming period, oceanic (coastal) SST shows an increase of 0.26 (0.18) $^{\circ}\text{C per decade}$ and in the second one shows an increase of 0.30 (0.28) $^{\circ}\text{C per decade}$.

3.1. Differences between ocean and coastal SST

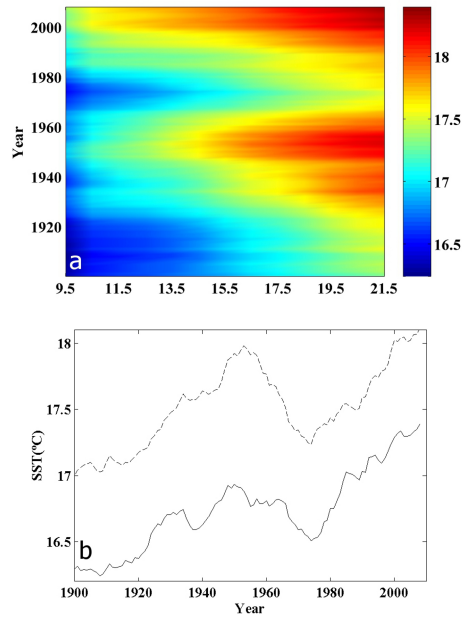


Figure 3.2: a) Spatial and temporal distribution of SST along the study area for the period 1900–2008, (the x-axis corresponds with the eastern latitudes). b) Inter-annual variation of the meridional average of coastal (*solid line*) and oceanic (*dashed line*) SST ($^{\circ}C$).

The last warming period is more intense than the previous one both near coast and in the ocean. In addition, the cooling period shows a decrease of -0.33 (-0.21) $^{\circ}C$ per decade. Similar warming-cooling cycles had been observed at regional seas in the North Atlantic area as described [GarciaSoto 2002] in the Celtic shelf, [deCastro 2009] in the Bay of Biscay and [Gesteira 2008a] in the area close to the North western corner of the Iberian Peninsula. It is worth noting that both cooling and warming tend to be more intense at open ocean locations than near coast. This effect is better depicted by means of the inter-annual variability of the meridional

3. DIFFERENCES BETWEEN OCEAN AND COASTAL SST

average of the $\Delta SST(^{\circ}C)$ described in *Equation (3.1)* (Fig.3.3).

The ΔSST parameter shows three different periods that were highlighted with a straight line: two increasing periods (from 1925 to 1956 and from 1987 to 2008) and one decreasing period (from 1956 to 1987). The increase and decrease rates for the different periods are shown in *Tabel 3.1*. A running average of ± 5 years was also applied to smooth the signal.

Note that the intervals where the thermal gradient ocean–coast is more (less) intense do not exactly coincide with the warming (cooling) cycles shown in Fig.3.2a. Actually, they are delayed in about 5–10 years. Although this effect can be partially due to the use of a running average of ± 5 years, the different time scales of the involved phenomena, global changes in temperature and coastal upwelling, can also play a non negligible role.

As we mentioned in previous chapters, AMO index is a good indicator of SST changes in the North Atlantic mainly related to THC. Fig.3.4 shows the inter–annual variability of AMO (*solid gray line*) and SST anomaly SST^a (*black solid line*) averaged at the 78 locations shown in Fig.3.1. The dashed lines correspond to $SST^a \pm 2\sigma(SST^a)$.

Both signals, which were previously smoothed by means of a ± 5 year running average, show a similar pattern with comparable warming–cooling cycles. Overall, the AMO warming for the period 1900–2008 is on the order of $0.8^{\circ}C$, which is slightly lower than observed along the WIP ($1.1^{\circ}C$ as mentioned above). The apparent similarity between AMO and SST^a can be shown to be dependent on longitude (Fig.3.5). In spite of the correlation is significant at 99% for all longitudes, the correlation coefficient decreases rapidly from values close to 0.96 at open ocean locations ($21.5^{\circ}W$) to 0.88 near coast ($9.5^{\circ}W$).

The decrease of the correlation coefficient is observed to be more sharply near coast, which seems to indicate the existence of a local mechanism affecting SST, apart from the global warming–cooling of the ocean due to changes

3.1. Differences between ocean and coastal SST

Period	Slope
1925–1956	-0.13
1956–1987	0.16
1987–2008	-0.1

Table 3.1: Annual ΔSST ($^{\circ}C$ per decade) from 1900 to 2008. ΔSST was meridionally averaged along the WIP. All values have a significance level of 99% in the t-test

in the THC. As we mentioned above, changes in wind patterns can be related to changes in SST. According to previous research carried out along the WIP ([Nykjaer 1994];[Álvarez 2008a];[Gesteira 2006];[Álvarez 2008b]) there is clear prevalence of northerly (southerly) wind along the dry (wet) season. During the wet season (*ONDJFM*) wind tends to drive air from southern latitudes, which is warmer than local air. Thus, the meridional component of wind stress (τ_y) tends to be positively correlated with SST both near coast and at open sea locations. Actually, the correlation coefficient between τ_y calculated at $10^{\circ}W$ and SST for every longitude from $9.5^{\circ}W$ to $21.5^{\circ}W$ is approximately equal to 0.75 (significant at 95%) with a negligible dependence on longitude. On the contrary, during the dry season (*AMJJAS*), northerly winds tend to generate coastal upwelling. Fig.3.6 shows the correlation coefficient between τ_y calculated at $10^{\circ}W$ and SST for longitudes ranging from $9.5^{\circ}W$ to $21.5^{\circ}W$ for the period 1949–2008. Significant correlation ($R^2 \sim 0.55$) at a 90% level in the t-test is only observed near coast with a sharp decrease seaward, reaching values below 0.3 for longitudes over $15.5^{\circ}W$. τ_y and near shore SST are positively correlated since when τ_y becomes more negative (more intense northerly winds) coastal SST decreases due to the enhancement of coastal upwelling, which replaces surface water with cooler water. A similar conclusion was attained

3. DIFFERENCES BETWEEN OCEAN AND COASTAL SST

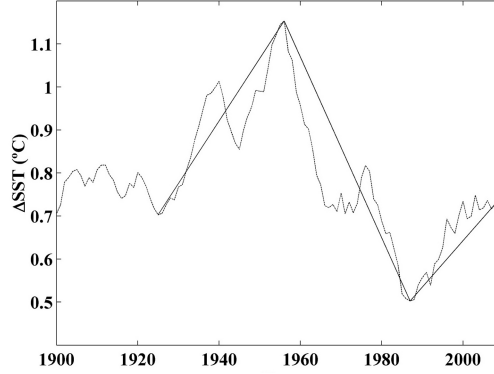


Figure 3.3: Inter-annual evolution of the meridional average of $\Delta SST(^{\circ}C)$ from 1900 to 2008. ΔSST was defined as ocean SST minus coastal SST as described in *equation(3.1)*. A running average of ± 5 years was considered to smooth the signal. Straight lines were used to highlight the increasing and decreasing periods of ΔSST

by [Schwing 1997] who compared SST and wind stress in the California Current System.

The time evolution of upwelling and ΔSST signals during the dry season can be observed in Fig.3.7. The anomaly of both signals relative to the period 1948–2008 was previously calculated to allow visual comparison. In addition, the high frequency was filtered by means of a running average (± 5 years). Macroscopically, periods with *UI* values (*full bars*) over the mean tend to coincide with periods with ΔSST over the mean (*black line*). Note that high ΔSST values correspond to large temperature differences between ocean and coastal water. Actually, the correlation coefficient between both signals ($R = 0.67$) is significant at 90%. According to [deCastro 2008a], changes in upwelling intensity are related to changes in the teleconnection patterns, in particular in EA pattern. The empty bars in Fig.3.7 represent the time evolution of EA, which showed to be negatively correlated with UI ($R = -0.62$, significant at 90%). Thus the observed changes in UI are not an isolated coastal fact, but they can be related to changes in EA pattern,

3.1. Differences between ocean and coastal SST

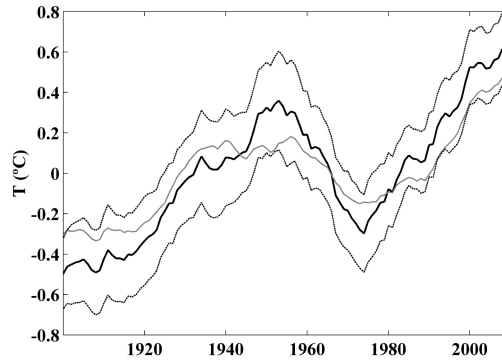


Figure 3.4: Evolution of AMO index (*gray solid line*) compared with the mean SST anomaly (SST^a) (*black solid line*) calculated at the SST points depicted in Fig.3.1. Dashed lines correspond to $SST^a \pm 2\sigma(SST^a)$. Once again, a running average of ± 5 years was considered. The signal was filtered with a running average (± 5 years) prior to the calculation of correlation coefficients. Correlation is significant at 99% for all longitudes.

which explain most of the upwelling variability.

[Schwing 1997] found upwelling intensification coinciding with warmer SST in the California Current System. There the long-term SST trend masks the cooling effect due to upwelling increase. Remarkable differences have been found between that manuscript and the present analysis. First, ΔSST was used in order to remove the global component from the signal. Thus, the warming-cooling cycles affecting the North Atlantic are considered to affect in a similar way to both coastal and ocean locations. Then, the temperature gradient (ΔSST) is assumed to be mainly due to local forcing. Second, the observed trends do not indicate increase in seasonal upwelling as suggested by [Bakun 1990] who hypothesized the existence of near coast SST cooling via increased coastal upwelling generated by the different warming rates over land and sea ([Jones 2001];[Sutton 2007]). No evidence of such a mechanism was found in the present study. Actually, most of the

3. DIFFERENCES BETWEEN OCEAN AND COASTAL SST

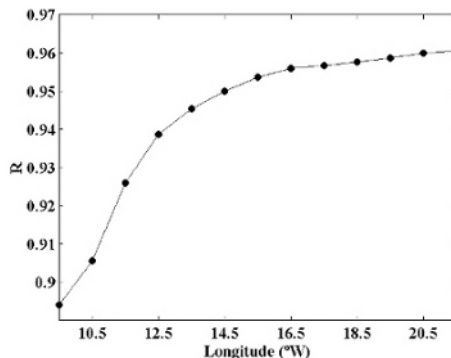


Figure 3.5: Correlation coefficient between the annual AMO index and the annual meridional average of SST at different longitudes calculated for the period 1900–2008. The signal was filtered with a running average (± 5 years) prior to the calculation of correlation coefficients. Correlation is significant at 99% for all longitudes.

studies carried out during the last decades have shown a decreasing trend in upwelling intensity. Thus, [Lemos 2004] found evidence of a progressive weakening of the upwelling regime for the period 1941–2000, [Álvarez 2008a] did not observe a clear trend at monthly scale, although, in average, upwelling tended to decrease for the period 1967–2006. A remarkable decrease in upwelling index was also described by [Pérez 2010] at the north–western corner of the Iberian Peninsula for the period 1965–2007. The same authors [Pardo 2011] extended their analysis to the period 1948–2009 with similar conclusions. [Gesteira 2011] found a significant decrease in upwelling index for the region Galicia–North Portugal over the period 1975–2008. Only [Santos 2011a] hypothesized the existence of different periodicities in upwelling evolution without a clear increasing or decreasing trend.

Finally, it is unclear if the correlation between SST and wind stress is due to a causal physical process or simply they covary with other processes at a global scale, since the observed commonality in trends does not neces-

3.1. Differences between ocean and coastal SST

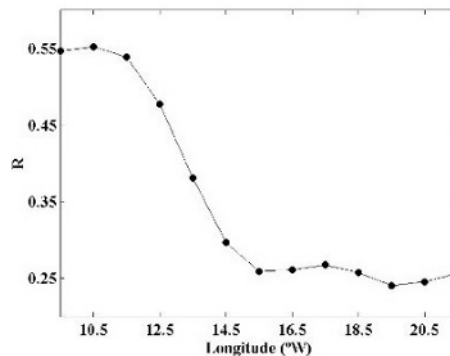


Figure 3.6: Correlation coefficients were calculated between seasonal (April–September) meridional wind stress (τ_y) and *AMJJAS* SST at different longitudes for the period 1948–2008. Once again, signals were filtered with a running average (± 5 years) prior to the calculation of correlation coefficients. Only the three first locations (until $12^\circ W$) are statistically significant at 90%.

sarily imply the existence of an underlying dynamical link as pointed out by [Mendelsohn 2002]. Possibly, a non linear interaction between changes in ocean temperature and atmospheric patterns is behind the observed evolution of SST and UI, although new research should be conducted to elucidate the underlying mechanism.

3.1.4 Conclusions

Different warming–cooling cycles in SST had been observed in the North Atlantic region during the last century, although the different response of ocean and coastal waters had not been described so far. New findings about the differences in coastal and ocean SST trends along the WIP can be with drawn from the present research:

- Ocean and coastal SST evolve at different rates. Actually, the difference in SST (ocean minus coast) tends to increase (decrease) during

3. DIFFERENCES BETWEEN OCEAN AND COASTAL SST

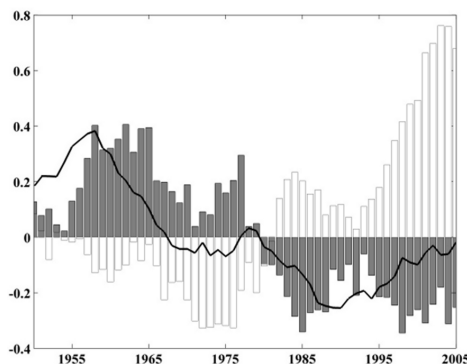


Figure 3.7: Time evolution of seasonal (April–September) UI (*full bars*), EA index (*empty bars*) and ΔSST (*dark line*) anomalies relative to the period 1948–2008. The signals were filtered by means of a running average (± 5 years). In addition, the UI anomaly was multiplied by a factor $0.75 / (\max(UI) - \min(UI))$ to allow a better visual comparison between signals. UI showed to be correlated with ΔSST ($R = 0.67$, significant at 90%) and negatively correlated with EA ($R = -0.62$, significant at 90%).

warming (cooling) periods.

- Both coastal and oceanic SST is highly correlated with the Atlantic Multidecadal Oscillation (AMO), although the correlation was observed to decrease coastward.
- Near coast SST is also correlated with meridional wind stress (τ_y) during the dry season. This τ_y characterizes coastal upwelling, which is the main feature of the western Iberian Peninsula coast during spring and summer.

3.2 Variability of coastal and ocean water temperature in the upper 700 m.

3.2.1 Motivation

The aim is to describe the differences in the variability of temperature and heat content between coastal and ocean locations along the WIP from 1975 to 2006. This analysis will be carried out by means of data obtained from SODA reanalysis. Which provide information about the vertical structure of temperature.

3.2.2 Methods

Only the first 21 vertical levels of the SODA database (from 5.0 *m* to 729.35 *m*) were considered in this point of the chapter. According to ([Levitus 2005] and [Levitus 2001]), the most important changes in heat content observed for the world ocean during the last decades correspond to the upper 700 *m*. Trends were calculated over the period 1975 to 2006, which corresponds to the last warming cycle in the North Atlantic.

Other data bases were considered for comparison purposes, as Pathfinder 5.2 and HadISST1.1.

The mean temperature provided by SODA at surface layer (upper 5 *m*, Fig.3.8a) can be compared to the mean of SST obtained from Pathfinder (Fig.3.8b) and HadISST (Fig.3.8c). Macroscopically, similar qualitative and quantitative behaviour can be observed in the three frames corresponding to the period 1982–2006, which is common to the three databases. Actually, the biggest differences are observed between HADISST and the rest of the databases at coastal areas due to its coarser grid. The comparison among temperature trends (T^{trend}) was calculated for a transect located at 41.75°N (Fig.3.8d). Sea temperature data were first re-meshed on the same spatial

3. DIFFERENCES BETWEEN OCEAN AND COASTAL SST

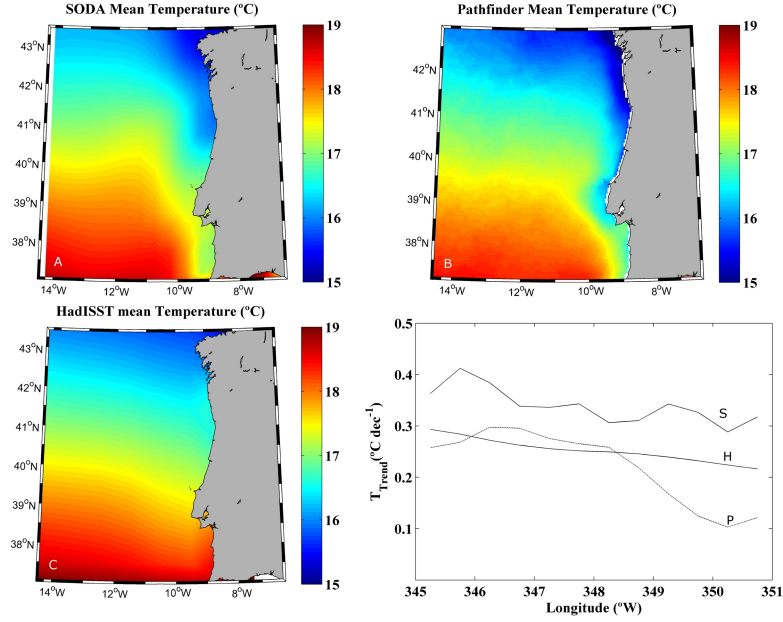


Figure 3.8: a) Mean sea temperature ($^{\circ}C$) at surface layer (upper 5 m) from the SODA, b) mean SST from Pathfinder and c) mean SST from HadISST1.1. Data were averaged over the period 1982–2006. d) SST trend ($^{\circ}C$ per decade) calculated at $41.75^{\circ}N$ from 1982 to 2006 using the three data bases mentioned above. SST data were previously re-meshed to a common spatial resolution of $0.5^{\circ} \times 0.5^{\circ}$. Legend in the figure P: Pathfinder; S: SODA; H: HadISST.

scale ($0.5^{\circ} \times 0.5^{\circ}$) and calculated for the same period (1982–2006). The trend provided by the three databases is always positive and on the same order of magnitude. The trend was also observed to decrease landward in the three cases.

Following [Bakun 1990], three different layers will be considered in the further analysis for the ocean vertical profile of SODA: the mixed layer (from 5.0 to 46.6 m deep), the thermocline base (from 58 to 197 m deep) and the intermediate water (from 229.5 to 729.4 m deep). The mixed layer depth (MLD) was calculated following the temperature criterion, $SST - ST(z) =$

3.2. Variability of coastal and ocean water temperature in the upper 700 m.

0.2°C, described in *Table 1* in [Kara 2000], where $ST(z)$ is the temperature at depth (z). This criterion indicates that the layer depth is defined as the depth where the temperature is 0.2°C less than the SST. The mean annual mixed layer depth was averaged over the period 1975–2006 for two transects perpendicular to the shore line (*transect 1* at 41.75°N and *transect 2* at 39.75°N, see Fig.3.9). The mean MLD obtained for both transect is –44.5 m and –43.5 m respectively, in good agreement with the value shown above. Note that the layers in SODA are not equally spaced and the closest ones are located at –35.8, –46.6 and –58.0 m respectively.

Heat content anomaly was calculated at each grid point over the period 1975–2006 in terms of temperature anomaly, following the expression:

$$Q = m_w c_w \Delta T_w \quad (3.4)$$

where $c_w = 3.981 \times 10^3 J (^\circ C kg)^{-1}$ is the specific heat of seawater at constant pressure at the sea surface, $m_w = \rho_w V_w$ is the mass of the seawater block, where $\rho_w = 1.02767 \times 10^3 kg m^{-3}$ is the density and $V_w = (0.5 \times 111120)(0.5 \times 111120 \cos((2\pi/180)lat)) \times \Delta h$ the volume, being lat the latitude of the water parcel and Δh the water column height from surface to 729.35 m. c_w and ρ_w values were taken from [Gill 1982]. Finally, temperature anomaly was calculated following $\Delta T_w = dT \Delta t (^\circ C)$, where dT is the temperature trend (*°C per year*) and Δt the period under study (in *years*).

3.2.3 Results and Discussion

The area located in front of the WIP (from 37.25 to 43.25°N and from 9.75 to 14.75°W) has been considered. This region is characterized by a shoreline perpendicular to the equator, being coastal upwelling the main driving mechanism (see [Gesteira 2011] and the references herein). The cho-

3. DIFFERENCES BETWEEN OCEAN AND COASTAL SST

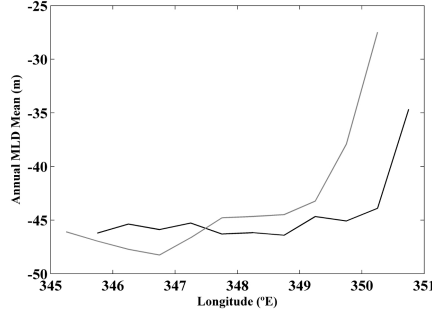


Figure 3.9: Mixed layer depth (MLD) at two transects located at $41.75^{\circ}N$ (*black line*) and $39.75^{\circ}N$ (*gray line*). The MLD was calculated following the temperature criterion $SST - ST(z) = 0.2^{\circ}C$, where $ST(z)$ is the water temperature at depth (z). This criterion identifies the MLD as the depth at which the temperature is $0.2^{\circ}C$ lower than the SST.

sen period, 1975–2006, corresponds to the last warming period both in the North Atlantic and in the area under study ([deCastro 2009];[Gesteira 2011]; [Gesteira 2008a];[Santos 2011b]). Near surface water temperature averaged for the mixed layer (5.0 to 46.6 m) from 1975 to 2006 is shown in Fig.3.10. The criterion followed to calculate the mixed layer is described in Data and Methods section. Coastal water is observed to be considerably colder than ocean water at the same latitude, showing the imprint of coastal upwelling.

Fig.3.11 shows the temperature trend calculated at different depths over the period 1975–2006. Fig.3.11a shows the temperature trend for the mixed layer. The warming trend observed near coast (~ 0.10 – $0.15^{\circ}C$ *per decade*), is considerably lower than in the ocean (0.25 – $0.35^{\circ}C$ *per decade*). Temperature trends were also calculated for the thermocline base (Fig.3.11b), which ranges approximately from 50 to 200 m . There, coastal temperature trends are on the order of 0 – $0.1^{\circ}C$ *per decade* and ocean trends on the order of 0.15 – $0.25^{\circ}C$ *per decade*. Finally, trends were also calculated for

3.2. Variability of coastal and ocean water temperature in the upper 700 m.

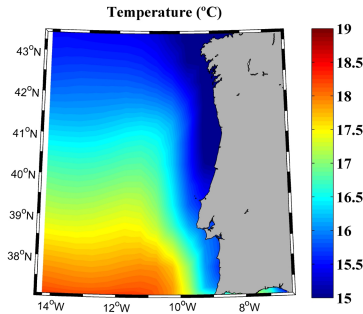


Figure 3.10: Near surface water temperature ($^{\circ}C$) averaged for the mixed layer (from 5.0 to 46.6 m) over the period 1975–2006.

the intermediate water which ranges approximately from 200 to 700 m (Fig.3.11c). The pattern observed from $43.25^{\circ}N$ to approximately $38.25^{\circ}N$ is similar to the previous ones. Coastal trends on the order of $0-0.05^{\circ}C$ per decade and ocean trends on the order of $0.10-0.15^{\circ}C$ per decade can be observed for these latitudes. This pattern is not observed further South due to the input of Mediterranean Water. Due to the identifiable presence of this water mass in the southernmost part of the study area, only the region ranging from 38.25 to $43.25^{\circ}N$ will be considered from now on.

Vertical profiles of temperature trends were used to analyze the water column (Fig.3.12). Profiles were calculated at two different latitudes $41.75^{\circ}N$ (Fig.3.12a) and $39.75^{\circ}N$ (Fig.3.12b). Some common features can be observed in both plots. The ocean warming (10.75 to $14.75^{\circ}W$) is considerably higher than the coastal one (9.75 to $10.75^{\circ}W$). The highest warming ($0.2-0.4^{\circ}C$ per decade), is found at ocean locations covering the upper 300 m. On the contrary, the warming hardly attains $0.2^{\circ}C$ per decade near shore and only affects the upper 20 m, being practically negligible ($< 0.1^{\circ}C$ per decade) below 50 m. These common features can also be observed at the rest of latitudes from 38.25 to $43.25^{\circ}N$ (not shown).

The vertical profile of coastal temperature trends (Fig.3.13, *solid line*)

3. DIFFERENCES BETWEEN OCEAN AND COASTAL SST

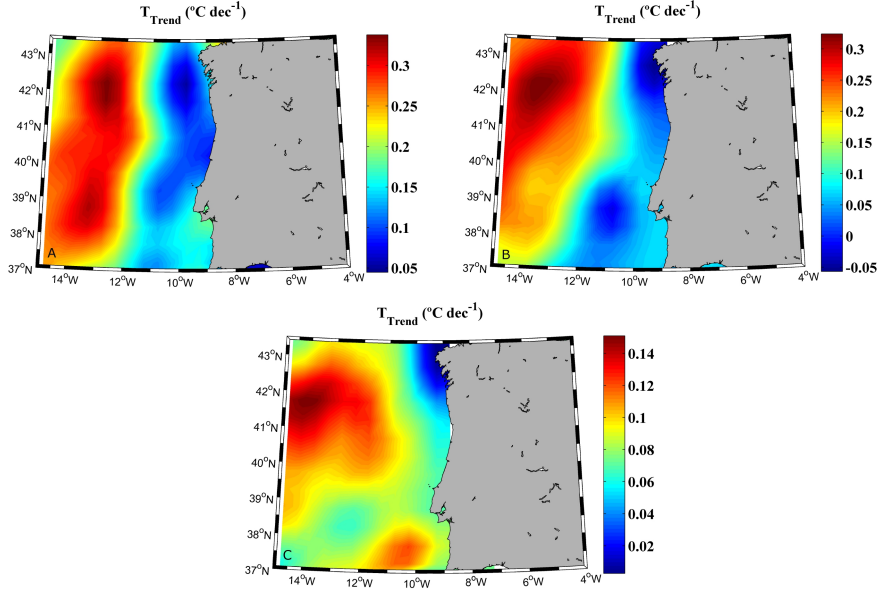


Figure 3.11: Horizontal map of the temperature trend ($^{\circ}C$ per decade) calculated at different depths over the period 1975–2006: a) mixed layer (from 0 to 46.6 m deep), b) thermocline base (from 58 to 197 m deep) and c) intermediate water (from 229.5 to 729.4 m deep).

was calculated by averaging the temperature trends considering the three longitudes closest to coast and all latitudes from 38.25 to $43.25^{\circ}N$. The coastal vertical profile allows characterizing trends in the zone influenced by upwelling processes. Previous studies carried out on the WIP [Santos 2011b] have shown that zone influenced by coastal upwelling is mainly constrained to the first degree from coast. The ocean profile (Fig.3.13, *dashed line*) was calculated in the same way but considering the three longitudes farthest from coast. In this way, the oceanic trend is not influenced by coastal processes. The ocean warming is higher than the coastal one as mentioned in Fig.3.12. In particular, values on the order of $0.3^{\circ}C$ per decade are observed near surface at the ocean decreasing with depth till reaching values below

3.2. Variability of coastal and ocean water temperature in the upper 700 m.

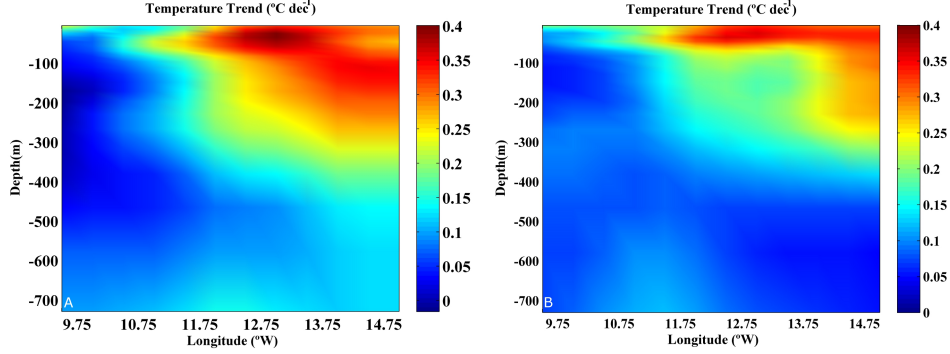


Figure 3.12: Temperature trend ($^{\circ}C$ per decade) for the period 1975–2006 calculated at two latitudes: a) $41.75^{\circ}N$ and b) $39.75^{\circ}N$.

$0.1^{\circ}C$ per decade at 500 m. The coastal warming is much smaller, reaching values close to $0.2^{\circ}C$ per decade near surface and decreasing rapidly at values below $0.1^{\circ}C$ per decade for depths on the order of 50 m.

Once the difference between coastal and ocean warming has been analyzed, we will quantify the changes observed in heat anomaly (Q), which was calculated from temperature anomaly following Equation (3.4) in methods section. The heat content anomaly was meridionally averaged from 38.25 to $43.25^{\circ}N$ over the period 1975–2006 (Fig.3.14). Q shows a sharp increase from coast, $1.1 \times 10^{18} J$ ($0.46 W m^{-2}$), to ocean, $3.7 \times 10^{18} J$ ($1.59 W m^{-2}$). Error bars were calculated using the standard deviation of the monthly data, $\sigma(Q)$, divided by the square root of the number of data.

The time evolution of heat anomaly (Fig.3.15) is also different for coastal (*solid line*) and ocean (*dashed line*) locations. Coastal (ocean) heat anomaly was calculated by averaging heat anomaly at the three most landward (seaward) points. A running average (± 2 years) was applied to smooth the signal. Heat content anomaly shows a sharp increase ($\sim 1.1 \times 10^{18} J$ per decade) at ocean locations and a smoother one ($\sim 0.6 \times 10^{18} J$ per decade) at coastal locations.

3. DIFFERENCES BETWEEN OCEAN AND COASTAL SST

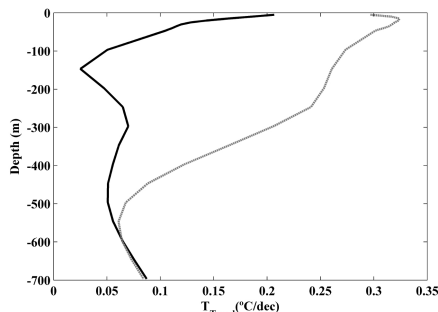


Figure 3.13: Vertical profiles of temperature trends ($^{\circ}C$ per decade) meridionally averaged for the three longitudes nearest to the coast (*solid line*) and for the three longitudes farthest the coast (*dashed line*).

The difference in SST warming rates between near coast and at ocean locations had been previously described for the WIP [Santos 2011b] and for other areas like the CUES [Santos 2012c] and the BUES [Santos 2012b] (see *Chapter 5*). Nevertheless, the extent of this difference with depth had not been analyzed in detail due to the lack of data along the water column. The use of a tridimensional data obtained from SODA has allowed a more in-depth analysis over the period 1975–2006. The warming trend (Fig.3.11a) observed for the mixed layer (from 0 to 46 m deep) near coast is considerably lower (~ 0.10 – $0.15^{\circ}C$ per decade) than at the ocean (0.25 – $0.35^{\circ}C$ per decade). These values are similar to SST trends observed for the same area near shore ($0.14 \pm 0.01^{\circ}C$ per decade) over the period 1985–2005 [Gesteira 2008a]. Similar SST trends ($0.27 \pm 0.04^{\circ}C$ per decade near shore and $0.38 \pm 0.04^{\circ}C$ per decade at open sea locations) were found over the period 1974–2008 [Santos 2011a]. Finally, a similar warming trend was measured near coast ($0.24^{\circ}C$ per decade) over the period 1974–2007 for the NW corner of the Iberian Peninsula [Gesteira 2011]. In spite of slight differences in the observed trends, which are mostly due to differences among databases and to the extent of the areas and periods under

3.2. Variability of coastal and ocean water temperature in the upper 700 m.

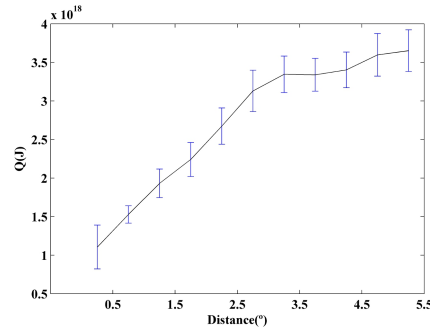


Figure 3.14: Heat content anomaly, $Q(J)$, meridionally averaged from 38.25 to $43.25^{\circ}N$ over the period 1975-2006. Error bars were calculated using the standard deviation of monthly data, $\sigma(Q)$, divided by the square root of the number of data. All trends are significant with $p < 0.05$.

study, these previous studies highlight the existence of different SST warming rates at coastal and ocean locations. However, little was known about temperature changes along the water column. Fig.3.11b shows that the differences between coast and ocean previously described for the mixed layer are kept for the thermocline base (from 58 to 197 m deep). This situation is not maintained for the whole area when analyzing intermediate water (from 229.5 to 729.4 m deep) as it can be observed in Fig.3.11c. At these depths the warming pattern changes south of $38.25^{\circ}N$ due to the intrusion of the Mediterranean Water, which flows approximately between 400 and 1500 m (for a brief summary about the different water masses in the zone the reader is referred to ([Ambar 2002];[OSPAR2000] and to the references therein).

The meridional average of trends was calculated for coastal and ocean locations considering all latitudes ranging from 38.25 to $43.25^{\circ}N$ (Fig.3.13). The coastal vertical profile shows a slight warming ($\sim 0.2^{\circ}C$ per decade) near surface (upper 20 m), which decreases rapidly and becomes negligible below 50 m. On the contrary, the ocean vertical profile shows a stronger

3. DIFFERENCES BETWEEN OCEAN AND COASTAL SST

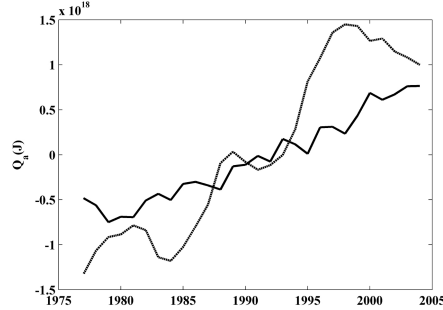


Figure 3.15: Time evolution of the heat content anomaly ($Q(J)$) meridionally averaged from 38.25 to $43.25^\circ N$ over the period 1975–2006. The *black solid line* is the mean of the three nearest locations to the coast and the *grey dashed line* is the mean of the three most oceanward locations. A running average of ± 2 years was considered to smooth the signal.

surface warming ($0.2\text{--}0.4^\circ C$ per decade), which penetrates down to 300 m . That ocean vertical profile of temperature trend is similar to the warming decrease with depth described for the Bay of Biscay along the upper 400 m [Michel 2009] using the World Ocean Database. There, the authors obtained a maximum trend ($\sim 0.25^\circ C$ per decade) at subsurface layer, which is similar to the one observed in the present study ($\sim 0.32^\circ C$ per decade) for ocean locations. In addition, their trend does not decrease abruptly during the first tens of meters but it remains positive till approximately 500 m . The same was observed in our study, where trends on the order of $0.05^\circ C$ per decade are observed at 600 m . Note that study described in [Michel 2009] averages the whole Bay of Biscay, in such a way that the mean values clearly resemble the oceanic behavior since the coastal points are only a small percentage of the total set.

It should be noted that the area has suffered a noticeable warming from 1975 on. Actually, according to [Gesteira 2011], the land temperature in the area has increased at an approximate rate of $0.5^\circ C$ per decade.

3.2. Variability of coastal and ocean water temperature in the upper 700 m.

At ocean locations, the upper layers of the ocean are also affected by the warming observed for air temperature. There, heat is mainly transported down from surface to lower layers by thermal diffusion. Near shore, coastal upwelling is the most important forcing mechanism, in such a way that cold water is pumped intermittently from below to near surface layers. Thus, diffusion is offset by advection, which mixes deeper colder water with warmer surface water. Thus, diffusive atmospheric heating is constrained to near surface layers, resulting in a weaker coastal warming. This difference in coastal and ocean warming rates is not necessarily correlated with changes in upwelling intensity. In fact, the mechanism proposed in [Bakun 1990] by which global warming would result in increased upwelling intensity is the subject of wide controversy in the area under study ([Lemos 2004];[Santos 2011b];[Pérez 2010];[Pardo 2011];[Santos 2011c]). Even some authors found that upwelling intensification coincided with warmer SST in the CUES, proving that other factors like long-term SST warming can mask the cooling effect associated to upwelling [Schwing 1997]. Thus, the mere presence of upwelling may be sufficient to constrain the warming to the upper layers. However, the difference between coastal and ocean trends are more marked in those regions that have experienced changes in upwelling intensity during the last decades as shown in recent studies carried out in the BUES [Santos 2012b] and the CUES [Santos 2012c] (see *Chapter 5*).

The heat content anomaly meridionally averaged from 38.25 to 43.25°N increases from coast ($0.46W m^{-2}$) to ocean ($1.59W m^{-2}$). The increment for the ocean is considerably higher than that obtained for the world ocean ($0.20W m^{-2}$) and for the Atlantic Ocean ($0.52W m^{-2}$) [Levitus 2005]. Note that, the period considered in that study was 1955–1998, which contains a cooling part from the mid-fifties to the mid-seventies and a warming part from the mid-seventies on. Later, these results were corrected increasing

3. DIFFERENCES BETWEEN OCEAN AND COASTAL SST

to $0.25W m^{-2}$ for the world ocean over the period 1969–2008 considering the upper 700 m [Levitus 2001]. More recently, an increase of $0.64W m^{-2}$ was detected for the world ocean over the period 1993–2008 considering the upper 700 m [Lyman 2010]. In addition, an increase on the order of $0.8W m^{-2}$ can be estimated for the upper North Atlantic (0–700 m) over the period 1968–2003 [Levitus 2005]. Even, more recently, [Levitus 2012] calculated the ocean heat content over the period 1955–2010. Values of $0.27W m^{-2}$ ($0.39W m^{-2}$) were obtained for the world ocean considering the upper 700 and 2000 m respectively. In the particular case of the Atlantic Ocean, the increase is on the order of $0.54W m^{-2}$ ($0.81W m^{-2}$) for the upper 700 m (2000 m). Finally, different studies shows that the heat content anomaly calculated using SODA for the band 15° – $60^{\circ}N$ over the 1961–2001 period [Carton 2008] is about 50% higher than obtained by [Levitus 2005] for the same years and band. Even, considering that there are significant differences among heat content anomalies calculated using different databases, the present study shows that the rate between heat content increase at coastal and ocean locations along the WIP is on the order of one third. This is in good agreement with previous studies carried out by the authors in different upwelling areas ([Santos 2011b];[Santos 2012b];[Santos 2012c]), which show that SST warming at coastal locations is less intense than at adjacent ocean locations.

3.2.4 Conclusions

The differences in water temperature and heat content were analyzed by means of the SODA package over the upper 700 m along the WIP a from 1975 to 2006.

Warming is considerably higher at ocean locations than at the coastal ones at the same latitude. This behavior is observed throughout the water

3.3. *Changes in the frequency of extreme sea temperatures events from 1982 to 2011*

column. In particular, ocean warming ($0.2\text{--}0.4^\circ\text{C per decade}$) penetrates down to 300 m whilst coastal warming ($\sim 0.10^\circ\text{C per decade}$) only affects the upper 20 m . Actually, coastal warming is practically negligible under 50 m . The heat content anomaly was hence increased from coastal (0.42 W m^{-2} at 9.75°W) to ocean locations (1.59 W m^{-2} at 12.25°W).

Coastal upwelling, which is the most importing forcing mechanism along the western coast of the Iberian Peninsula, seems to be responsible of the weaker coastal warming compared with the ocean warming at the same latitude.

3.3 *Changes in the frequency of extreme sea temperatures events from 1982 to 2011*

3.3.1 Motivation

The question addressed is to analyze the existence of trends in the frequency of extreme hot days along the WIP over the period 1982 to 2011. More specifically, the difference between ocean and coastal trends will be analyzed both at seasonal and annual scale.

3.3.2 Methods

The area under study covers the region $37\text{--}43^\circ\text{N}$ and $349\text{--}352^\circ\text{E}$ which corresponds to the WIP coast and its adjacent shelf (Fig.3.16). The WIP coast maintains an almost constant S-N orientation without any island, large peninsula or semienclosed basin. The region may be regarded as the northern boundary of the CUES. Previous studies ([SantosA 2005];[Álvarez 2008a]) have shown that seasonal (April-October) coastal upwelling is the most important forcing factor at the region. SST was retrieved from Pathfinder

3. DIFFERENCES BETWEEN OCEAN AND COASTAL SST

O.I. 1.4 Degree Daily SST data provided by NOAA's National Climatic data Center.

The analysis of coastal SST requires the consideration of very close land pixels. In order to avoid that these pixels were land contaminated, coastal pixels were only those with less than 50% of land contamination following the procedure described by [Lima 2012]. Twenty three ocean points (*dots* in Fig.3.16) were considered at the same latitude that coastal ones (*circles* in Fig.3.16) but displaced one degree seaward.

SST trends

Daily SST values were monthly averaged at every point and then the monthly anomalies were calculated by subtracting to the temperature of a certain month (e.g. January 1982) the mean temperature of that month (January) over the period 1982–2011. Trends were calculated at each pixel as the slope of the linear regression of the SST anomalies versus time. The Spearman rank correlation coefficient was used to analyze the significance of trends due to its robustness to deviations from linearity and its resistance to the influence of outliers. This procedure generates a matrix of annual trends ($Trend_{i,j}$) calculated from $SST_{i,j}^m$ anomalies, where i and j correspond to the longitude and latitude of the pixel and m represents the month. Trends at coastal and ocean points shown in Fig.3.16 were calculated by spatially averaging the ($Trend_{i,j}$) matrix in the closest neighbourhood (± 1) of every pixel i, j . The standard deviation was calculated considering the same neighbourhood. Note that both the mean and the standard deviation are calculated by using around 9 pixels (some of them can be land and then discarded), which reduces the effect of spatial inhomogeneities. The same procedure was also applied at seasonal scale: winter (January-March); spring (April-June); summer (July-September); and autumn (October-December).

3.3. Changes in the frequency of extreme sea temperatures events from 1982 to 2011

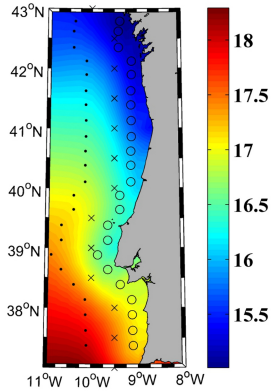


Figure 3.16: Area under study. Colors represent mean SST ($^{\circ}\text{C}$) averaged from 1982 to 2011. The upwelling imprint is reflected by a land-ocean SST gradient on the order of 0.5°C . Circles (dots) correspond to coastal (ocean) pixels. Crosses represent the locations where upwelling index was calculated.

Extreme SST

The 95th percentile of the local SST was also considered to characterize extreme events, days with extremely hot SST. The analysis of trends in the frequency of extreme days per decade was carried out for each pixel following several steps:

- 1) SST anomaly was calculated for each day over the period 1982 to 2011. Anomalies were calculated by subtracting to the temperature of a certain day (e.g. January first, 1982) the mean temperature of that day (January first) over the period 1982–2011.
- 2) The number of days with SST anomaly over the 95 percentile was calculated yearly and seasonally.
- 3) Annual and seasonal trends were calculated as the slope of the linear regression of the frequency of extreme SST versus time. This proce-

3. DIFFERENCES BETWEEN OCEAN AND COASTAL SST

ture generates a matrix of trends in extreme hot events ($Trend_{i,j}^{95}$) similar to the one describe above for temperature. The mean and the standard deviation at the coastal and ocean control points were also calculated following the method described above for temperature.

Upwelling Index

Data for this point of the chapter were retrieved from NOAA's National Operational Model Archive and Distribution System (NOMADS) which is maintained at NOAA's National Climatic Data Center (NCDC) [Saha 2010]. Ekman transport was calculated following the *Equations 1.4 and 1.5* described in the previous chapter.

UI can be defined as the Ekman transport component in the direction perpendicular to the shoreline [Nykjaer 1994] following the *Equation 1.6*.

3.3.3 Results and Discussion

The existence of different warming rates at coast and ocean is depicted in Fig.3.17a. Ocean warms ($0.25\text{--}0.3^\circ\text{C per decade}$, *gray line*) faster than coast ($0.20\text{--}0.24^\circ\text{C per decade}$, *black line*) at all latitudes (Fig.3.17b).

Warming rates on the same order were obtained both near coast and at ocean by other authors. [Gesteira 2008a] detected a coastal warming of $0.14 \pm 0.01^\circ\text{C per decade}$ over the period 1985–2005 . [Santos 2011a] obtain similar ocean and coastal warming trends (0.38 ± 0.04 and $0.27 \pm 0.04^\circ\text{C per decade}$, respectively) over the period 1974–2008. [Relvas 2009] found similar ocean and coastal warming trends (0.33 and $0.22^\circ\text{C per decade}$, respectively) over the period 1985–2008. Differences between ocean and coastal warming were also detected in other parts of the world, in particular along the BUES and CUES (see *Chapter 5*). In the BUES, [Santos 2012b] detected an ocean warming of $0.06^\circ\text{C per decade}$ and a coastal warming

3.3. Changes in the frequency of extreme sea temperatures events from 1982 to 2011

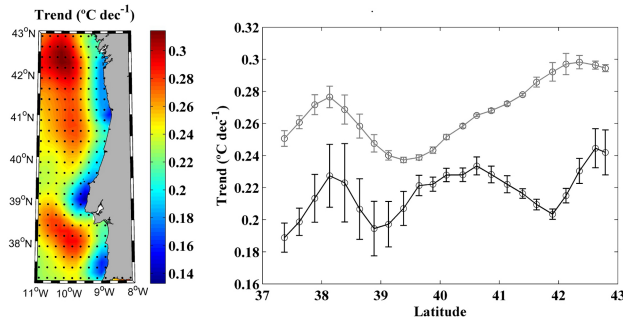


Figure 3.17: SST trends ($^{\circ}C$ per decade) over the period 1982–2011. (a) Map of trends. Dots mark trends with significance higher than 95%; (b) Trends at the control points shown in Fig.3.16, oceanic (coastal) points represent by *gray line* (*black line*). Error bars were calculated using the standard deviation over the square root of the number of data.

of $-0.13^{\circ}C$ per decade associated to the strengthening of coastal upwelling over the period 1970–2009. In the CUES, [Santos 2012c] detected an ocean warming of $0.40^{\circ}C$ per decade and a coastal warming of $0.35^{\circ}C$ per decade that was also linked to the strengthening of coastal upwelling over the period 1982–2010. In a broader context, [Lima 2012] detected a mean coastal warming rate of $0.27 \pm 0.13^{\circ}C$ per decade along the Eastern Atlantic coast with a particularly rapid increase along the margins of both Norwegian and North Seas. In the particular case of the WIP coast, coastal warming ranged from 0.2 to $0.3^{\circ}C$ per decade, especially during spring and summer as previously described in [Gesteira 2011].

Annual trends in the frequency of extreme hot days were calculated along the WIP coast from 1982 to 2011 (Fig.3.18a). The number of extreme hot days has increased during this period with values ranging from 6 and 15 days per decade. The increase is not spatially homogeneous (Fig.3.18b). The lowest increase was detected near coast south of $39^{\circ}N$ and the highest one at ocean locations for the same latitudes. In short, this area shows the highest differences between coast and ocean at annual scale. North of $39^{\circ}N$

3. DIFFERENCES BETWEEN OCEAN AND COASTAL SST

the differences between coast and ocean are practically negligible, although the increase in the number of hot days tends to be slightly bigger for ocean locations. Only north of $42^{\circ}N$ the difference increases again, although at a much lesser extent than observed south of $39^{\circ}N$.

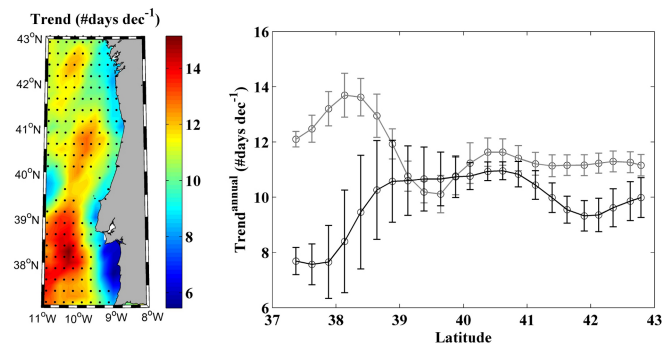


Figure 3.18: Annual trends in the frequency of extreme hot days over the period 1982–2011. (a) Map of trends. Dots mark trends with significance higher than 95%; (b) Trends at coastal (dark line) and ocean (light line) locations.

3.3. Changes in the frequency of extreme sea temperatures events from 1982 to 2011

The existence of a remarkable seasonal component in warming pattern shown in previous research ([Gesteira 2008a];[Relvas 2009];[Gesteira 2011]; [Lima 2012]) has motivated the seasonal analysis shown in Fig.3.19a-h. First of all, the number of extreme hot days is practically constant during winter (Fig.3.19a,b) both at ocean and coastal locations. On the contrary, the highest number of additional extreme hot days occurs during spring, although the behavior is similar both at ocean and near coast (Fig.3.19c,d). The number of days decreases with latitude from *6.5 days per decade* at $37^{\circ}N$ to close *3 days per decade* at $43^{\circ}N$. It can also be observed that, only during this season, the increase in the frequency of hot days is slightly higher at coastal locations than at ocean ones (at least for the area ranging from $38^{\circ}N$ to $41^{\circ}N$). The highest differences between coast and ocean locations are observed during summer (4e, 4f), when the increase of extreme hot days is higher at ocean locations than near coast. In particular, the highest differences can be observed south of $38.5^{\circ}N$. Even, close to $37^{\circ}N$ the trend is slightly negative. During this season the increment in the number of extreme hot days near shore ranges from *0 days per decade* at $37^{\circ}N$ to *3 days per decade* at $43^{\circ}N$. This contrasts with the behavior at ocean locations where the increment of extreme hot days ranges from 2 to 4 days per decade. Finally, during autumn (4g, 4h), the increase of extreme hot days is very similar at ocean and near coast, ranging from *1 day per decade* at $37^{\circ}N$ to *3–4 days per decade* at $43^{\circ}N$. This seasonal behavior in the frequency of extreme hot days reflects the seasonal behavior of ocean and coastal mean warming measured along the WIP coast from 1982 to 2011 as show Fig.3.20(a-h).

3. DIFFERENCES BETWEEN OCEAN AND COASTAL SST

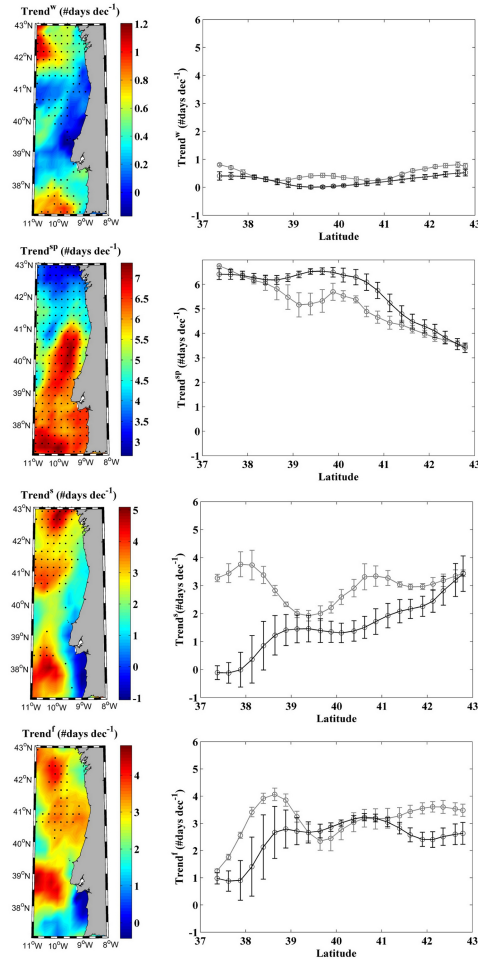


Figure 3.19: Seasonal trends in the frequency of extreme hot days over the period 1982–2011. Frames as in Fig.3.18 (a,b) Winter; (c,d) Spring; (e,f) Summer; (g,h) Autumn. Dots mark trends with significance higher than 95%

Spring shows to be the season that has experienced the highest increment in mean temperature during the last decades ([Gesteira 2008a]; [Gesteira 2011]) both at ocean and coastal locations as it was analyzed above.

3.3. Changes in the frequency of extreme sea temperatures events from 1982 to 2011

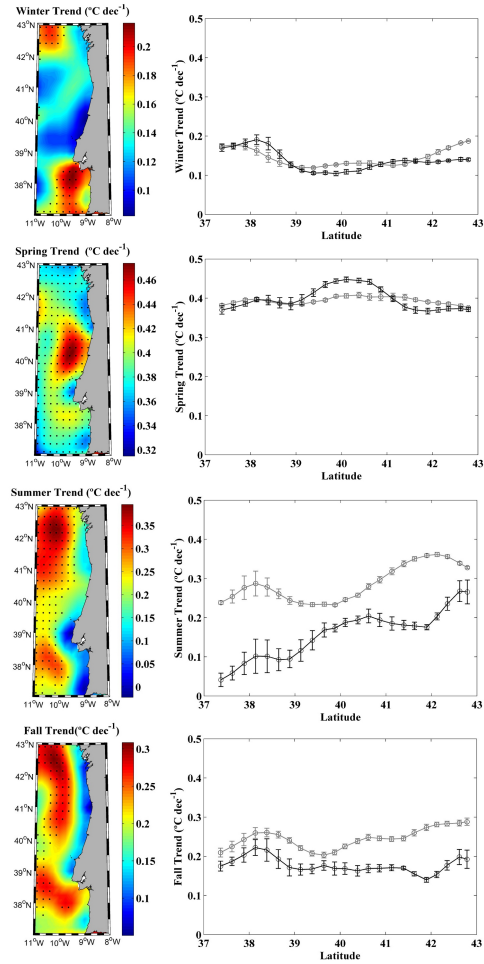


Figure 3.20: Seasonal trends in the frequency of extreme hot days over the period 1982–2011. Frames as in Fig.3.18 (a,b) Winter; (c,d) Spring; (e,f) Summer; (g,h) Autumn. Dots mark trends with significance higher than 95%

3. DIFFERENCES BETWEEN OCEAN AND COASTAL SST

In addition, coastal upwelling is quite limited during the season, since according to ([Álvarez 2008a];[Álvarez 2010]) permanent and intense upwelling events mainly occur during summer. On the other hand, the highest difference coast-ocean in the frequency of extreme hot days occurs during summer which is the most upwelling favorable season in the WIP area ([Álvarez 2008b];[Álvarez 2010]). Previous research ([Relvas 2009]; [Santos 2011b];[Santos 2012c]) has mentioned the different warming rates of WIP waters at coastal and ocean locations. Spring shows to be the season that has experienced the highest increment in mean temperature during the last decades ([Gesteira 2008a];[Gesteira 2011]) both at ocean and coastal locations as it was analyzed above. In addition, coastal upwelling is quite limited during the season, since according to ([Álvarez 2008a]; [Álvarez 2010]) permanent and intense upwelling events mainly occur during summer. These previous studies mention in a more or less explicit way the role played by coastal upwelling on coastal warming. Nevertheless, the role of upwelling was not examined in detail by means of wind fields of fine resolution and it is unclear whether the different warming rates are due to changes in upwelling intensity or merely to the presence of upwelling that enhances the advective mechanisms and prevents the diffusion of temperature from surface. Here, we have considered the summer evolution of UI over the period 1982–2011 using CFSR data with a resolution comparable to the one used for SST (Fig.3.21). The trend is observed to be positive (upwelling tends to increase) along the whole WIP coast, although it tends to decrease northward. In particular, the trend is practically negligible at northernmost part of the region. The observed trends are comparable to the ones observed at the BUES [Santos 2012a] and CUES [Santos 2012b] (see *Chapter 5*), which also result in a different warming rate at coastal locations.

3.3. Changes in the frequency of extreme sea temperatures events from 1982 to 2011

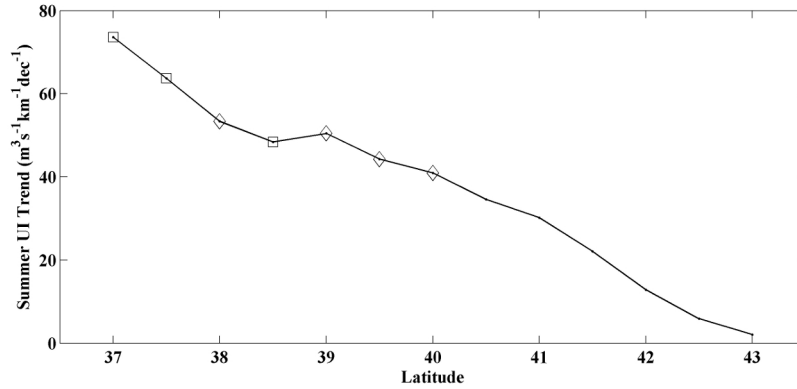


Figure 3.21: Trend in summer upwelling calculated over the period 1982–2011 using CFSR data. Circles mark trends with significance higher than 95%.

3.3.4 Conclusions

The WIP coast has warmed over the period 1982–2011. This warming showed remarkable seasonal and zonal differences with coastal regions warming slower than adjacent ocean areas. The main findings can be summarized as follows:

- The frequency of extreme hot days has increased both at ocean and coastal locations being the increase lower near coast than at adjacent ocean locations.
- Changes in the frequency of hot days were negligible in winter.
- Spring showed the highest increase in the number of extreme hot days being the increase similar at coast and ocean.
- The increase in the number of hot days was also important during summer. In addition, this season showed the highest differences between coast and ocean.

3. DIFFERENCES BETWEEN OCEAN AND COASTAL SST

- Autumn shows an intermediate situation between spring and summer. Trends show smaller differences between coast and ocean than during summer. In addition, the increase in the number of extreme hot days is similar to the one observed in summer.
- The differences between coast and ocean observed in summer are due to the increase of coastal upwelling observed during this season. In particular, the highest differences were observed at the southernmost part of the area, where upwelling increase was stronger.

The different behavior observed both in ocean warming and in the frequency of extreme hot days between ocean and coastal areas allows understanding how local and seasonal mechanisms like upwelling can influence a region making it less vulnerable to the effect of extreme events. The understanding of these changes should help to develop policies and procedures to preserve the ecological and economic richness of coastal regions.

Differences between ocean and coastal SST in other areas

4.1 *Differences between ocean and coastal SST in the Canary Upwelling Ecosystem*

4.1.1 Motivation

The aim is to describe the regional differences in the warming rates between coastal and oceanic locations for the same latitude in the Moroccan sub-region of the Canary Upwelling Ecosystem (CUE) from 1982 to 2010. The effect of local forcings like wind and air temperature and remote forcings like atmospheric circulation patterns will be analyzed.

4.1.2 Methods

In this study the area extending from $22^{\circ}N$ to $33^{\circ}N$ and from $6^{\circ}W$ to $22^{\circ}W$ Fig.4.1 was selected from 1982 to 2010 from the Pathfinder database. Only SST values with quality flags 6 or 7 were considered following ([Kilpatrick 2001] and [Relvas 2009]). Monthly values were calculated by

4. DIFFERENCES BETWEEN OCEAN AND COASTAL SST IN OTHER AREAS

averaging the daily data. Even using monthly data, the SST grid contained voids in the data caused by adverse weather conditions or satellite mal functions.

The polygon areas contoured by black solid lines in Fig.4.1 were used to calculate SST trends at ocean and coastal locations respectively. Each polygon contains, at least, 5000 pixels with valid SST values.

Local zonal differences between ocean and coastal warming trends

$$\Delta SST^{trend} = SST_{ocean}^{trend} - SST_{coast}^{trend} \quad (4.1)$$

were calculated as follows:

- First, considering a given latitude, the closest pixel to shore with valid SST values was detected.
- Then, SST trends corresponding to that latitude and placed at less than 1 degree from coast were spatially averaged to calculate SST_{coast}^{trend} .
- Similar spatial average was carried out for points located at a distance between 5 and 6 degrees from coast to calculate SST_{ocean}^{trend} .
- This procedure was carried out for all latitudes inside the study area.

Ekman transport was calculated from wind components at 10 *m* above the sea surface obtained from NCEP/NCAR, following expression shown in *Equations 1.4 and 1.5* in *Chapter 1*.

Upwelling Index (UI) can be defined as the Ekman transport component in the direction perpendicular to the shore line [Nyckjaer 1994] following the *Equation 1.6*.

Monthly air temperature (T^{air}) data were also obtained from reanalysis data from NCEP/NCAR project. In this point, the region 20–35°N and 5–25°W was cut from the global data set over the period 1982–2010.

4.1. Differences between ocean and coastal SST in the Canary Upwelling Ecosystem

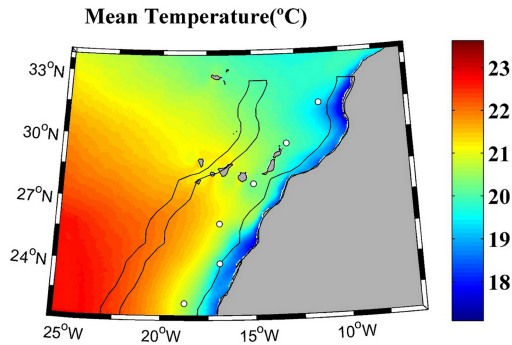


Figure 4.1: Mean $SST(^{\circ}C)$ averaged from 1982 to 2010. Polygons represent coastal and ocean locations along the area under study. *White* points represent the control points where Ekman transport was calculated.

The NAO and EA teleconnection indices were obtained from the CPC at the NCEP. Data area available at a monthly time scale with global coverage from 1950 onwards. Rotated Principal Component Analysis (RPCA) was used to identify the northern hemisphere teleconnection patterns and indices [Barnston 1987]. In the present study the extended winter mean of both indices (from December to March) was calculated from 1982 to 2010. The Spearman rank correlation coefficient was used to analyze the significance of trends due to its robustness to deviations from linearity and its resistance to the influence of outliers.

4.1.3 Results and Discussion

The mean $SST(^{\circ}C)$ calculated from 1982 to 2010 (see, Fig.4.1) shows gradients both in latitude and in longitude. SST increases southward with a latitudinal gradient around $2^{\circ}C$ at the oceanic part of the area. In contrast, the ocean–coast gradient at the same latitude reaches values close to $4^{\circ}C$ with SST increasing seaward. This ocean–coast gradient, which is characteristic of upwelling regions all over the world, had been previously shown for the same area by the other authors like [Barton 1998], covering the pe-

4. DIFFERENCES BETWEEN OCEAN AND COASTAL SST IN OTHER AREAS

riod 1981–1991, or [Gesteira 2008b] for the period 1985–2006. The presence of cooler surface water near coast reflects the existence of permanent upwelling ([Wooster 1976];[Nykjaer 1994];[Barton 1998];[SantosA 2005]). The existence of upwelling favorable conditions is also shown in terms of Ekman transport Fig.4.2 averaged from 1982 to 2010 at the control points described in (Fig.4.1 *circles*). Ekman transport is perpendicular to the shore line and decreases northward. This pattern is consistent with those described by the other authors for the same area ([VanCamp 1991];[Barton 1998]; [Gesteira 2008b];[Pardo 2011]).

SST trends were calculated from monthly SST anomalies for the period 1982–2010 (Fig.4.3). Warming trends ranging from $0^{\circ}\text{C per decade}$ to $0.65^{\circ}\text{C per decade}$ can be observed. At ocean locations, the SST warming shows a latitudinal increase from north, $0.35^{\circ}\text{C per decade}$, to south, $0.65^{\circ}\text{C per decade}$. In addition, differences between coastal and ocean trends can also be observed. Thus, considering the polygons described above, the ocean (coastal) warming trend is on the order of $0.40^{\circ}\text{C per decade}$ ($0.35^{\circ}\text{C per decade}$).

Warming trends have been macroscopically observed in the Atlantic over the period 1955–2003 [Levitus 2005]. Here we will compare our trends to other detected in the previous research for different Atlantic places. Obviously, each location has its own features, characterized by solar irradiance, prevailing winds, presence or absence of upwelling, tidal regime or currents among others. Nevertheless, some common facts are shared by most of them due to their Atlantic location. Thus, similar oceanic warming trends had been previously analyzed in other Atlantic regions, although with different warming rates depending on the region and the period under study. Thus, [Casey 2001] detected trends of $0.09 \pm 0.07^{\circ}\text{C per decade}$ in the south east Atlantic for the period 1960–1990. Other authors ([deCastro 2009];[Michel 2009]) detected trends on the order of $0.2\text{--}0.3^{\circ}\text{C}$

4.1. Differences between ocean and coastal SST in the Canary Upwelling Ecosystem

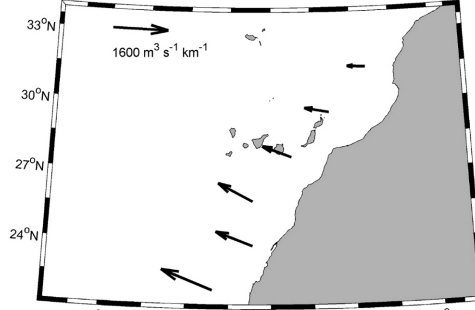


Figure 4.2: Mean Ekman transport ($m^3 s^{-1} km^{-1}$) averaged from 1982 to 2010 calculated at the six points described in Fig.4.1.

per decade in the Bay of Biscay for the last three decades of the 20th century. Similar trends were found by [Gesteira 2011] for the NW corner of the Iberian peninsula, by [Santos 2011b] along the WIP from 1974 to 2008 or by [Relvas 2009] along the same area from 1985 to 2008. Finally, [Santos 2012b] found trends of $0.06^\circ C$ *per decade* along the Benguela Upwelling System (BUE) from the 1970s onwards, (see *Section 5.2*).

As for the coastal SST, the observed warming rate is slightly higher than obtained at other north Atlantic locations. [Pardo 2011] estimated $0.21^\circ C$ *per decade* at the Moroccan sub-region from 1970 to 2009 and $0.3^\circ C$ *per decade* along the WIP for the same period; [Gesteira 2008a] obtained $0.23^\circ C$ *per decade* for the north Atlantic Arc from 1985 to 2005; [Goikoetxea 2009] calculated $0.26^\circ C$ *per decade* at $43^\circ 19N$, $21^\circ W$ from 1977 to 2007; [Santos 2011b] $0.28^\circ C$ *per decade* along the WIP from 1974 to 2008; and [Gesteira 2011] $0.17^\circ C$ *per decade* for the NW corner of the Iberian peninsula from 1985 to 2005. Nevertheless, it contrasts with the coastal SST cooling ($-0.13^\circ C$ *per decade*) measured in the BUE from the 1970s onwards [Santos 2012b], (see *Section 5.2*).

The local difference between ocean and coastal warming trends (ΔSST^{trend}),

4. DIFFERENCES BETWEEN OCEAN AND COASTAL SST IN OTHER AREAS

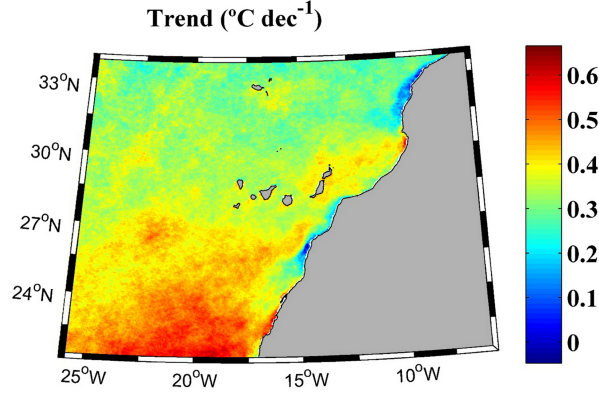


Figure 4.3: SST trend ($^{\circ}C$ per decade) calculated from monthly SST anomalies over the period 1982–2010. A running average (72 pixels) was applied to smooth the signal. Negative (ΔSST^{trend}) values are only observed for coastal locations located opposite the Canary archipelago ($28\text{--}31^{\circ}N$).

which was calculated as described above, is depicted in Fig.4.4. A spatial running average (± 2 pixels in latitude) was considered to smooth the signal. ΔSST^{trend} is positive for most latitudes indicating that the ocean warming rate is higher than the coastal one. A maximum value ($0.15^{\circ}C$ per decade) is observed at latitudes close to $32^{\circ}N$ and values around $0.12^{\circ}C$ per decade at latitudes around $25^{\circ}N$. ΔSST^{trend} is only negative for the coastal area placed opposite the Canary archipelago ($28\text{--}31^{\circ}N$) showing the modification of the SST patterns by the islands topography. These islands constitute a barrier to the equatorward flow of the Canary current and to the flow generated by the trade winds ([Aristegui 1994],[Aristegui 2009]).

Differences between coastal and ocean warming rates were previously detected both along the coast of the WIP ([Relvas 2009];[Santos 2012a]; [Santos 2011a];[Gesteira 2013]) and in the BUE [Santos 2012b]. These differences were attributed to an intensification of upwelling pattern off the southern part of the Iberian peninsula since 1985 [Relvas 2009] and to the

4.1. Differences between ocean and coastal SST in the Canary Upwelling Ecosystem

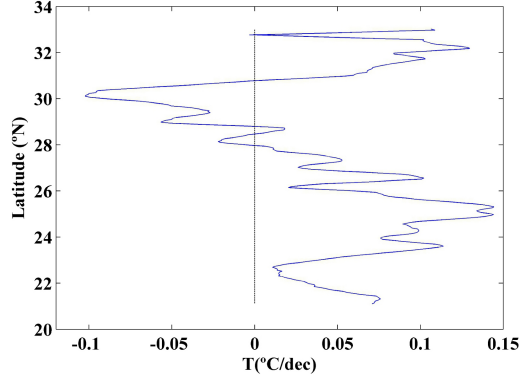


Figure 4.4: Difference between SST warming at ocean and coasta locations for the same latitude ($\Delta SST^{trend} = SST_{ocean}^{trend} - SST_{coast}^{trend}$). A running average (± 2 pixels) was applied to smooth the signal. Negative ΔSST^{trend} values are only observed for coastal locations located opposite the Canary archipelago ($28\text{--}31^\circ N$).

local wind regime which is itself a manifestation of the eastern Atlantic circulation pattern [Santos 2011b]. With respect to the BUE, the warming rates differences were attributed to coastal upwelling enhancement related to changes in the intensity and location of the south Atlantic high [Santos 2012b], (see *Chapter 5.2*).

In this point, the different SST warming rates detected both latitudinally and between coast and ocean can be attributed to several factors. Air temperature (T^{air} , Fig.4.5) trends calculated from 1982 to 2010 show how warming decreases northward. Considering the oceanic area near coast, T^{air} trends are significantly lower at $33^\circ N$ ($\sim 0.1^\circ C$ per decade) than at $21^\circ N$ ($\sim 0.4^\circ C$ per decade). This atmospheric pattern can explain the latitudinal gradient observed in the SST trends depicted in Fig.4.3, but not the differences between ocean and coastal warming trends, since T^{air} warming is similar at ocean and coastal locations.

The positive difference between trends (ΔSST^{trend} in Fig.4.4) can be

4. DIFFERENCES BETWEEN OCEAN AND COASTAL SST IN OTHER AREAS

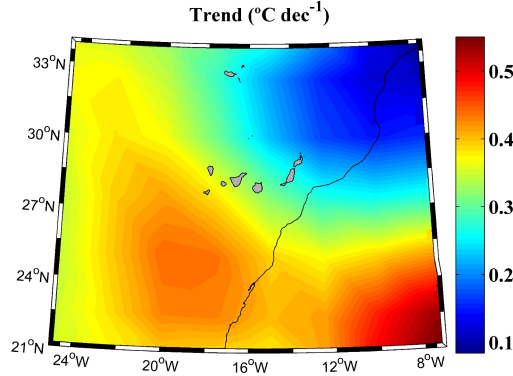


Figure 4.5: Air temperature trend ($^{\circ}C$ per decade) calculated from 1982 to 2010. The *black line* marks the coast line. Air temperature was considered at 1,000 *HPa* to avoid topographic effects on atmospheric circulation.

due to changes in coastal upwelling along the Canary region. The annual cycle of UI over the period 1982–2010 (Fig.4.6) shows positive values all over the year. The highest values are measured from May to September as pointed out in the previous research ([Gesteira 2008b];[Patti 2008];[Patti 2010]) being especially intense in August ($\sim 1,600 \text{ m}^3\text{s}^{-1}\text{km}^{-1}$). The error bars were calculated as $(UI)/\sqrt{N}$, where $\sigma(UI)$ is the standard deviation of the monthly data and $N = 29$ is the number of monthly values for the period 1982–2010. In general, the amplitude of error bars is negligible compared to the amplitude of the annual cycle.

Fig.4.7 shows the inter-annual evolution of UI over the period 1982–2010 (*black line*). Annual values were obtained by averaging monthly values from May to September (UI^{MJJAS}), which are the months with the highest upwelling values. UI^{MJJAS} is observed to increase at a rate of $9.5 \text{ m}^3\text{s}^{-1}\text{km}^{-1}$ per decade although without statistical significance. The analysis of upwelling trends along the Moroccan part of the CUE has been controversial since it is highly dependent on the selected area, the time interval and the period of the year. [Pardo 2011] calculated the upwelling trend during the

4.1. Differences between ocean and coastal SST in the Canary Upwelling Ecosystem

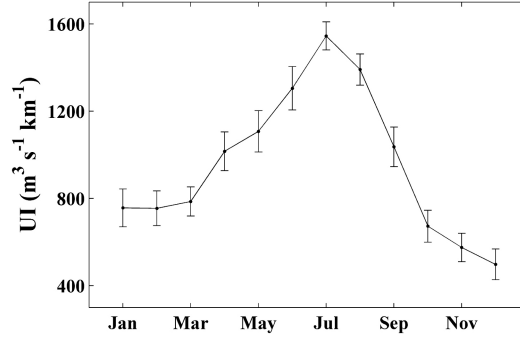


Figure 4.6: Annual cycle calculated by averaging $UI(m^3s^{-1}km^{-1})$ in latitude ($22-32^{\circ}N$) and time (1982–2010). The error bars were calculated as $(UI)/\sqrt{N}$, where $\sigma(UI)$ is the standard deviation of monthly data and $N = 29$ is the number of monthly values over the period 1982–2010.

last four decades, finding negative trends from 30 to $33^{\circ}N$, slightly positive trends from 27 to $30^{\circ}N$ and negative trends for the southernmost part of the area till $20^{\circ}N$. [Patti 2010] found an increase in wind stress for the area extending from 22 to $29^{\circ}N$, which should also result in upwelling reinforcement. Finally, [Gesteira 2008b] detected a significant negative trend over the period 1967–2006. $\Delta SST = SST^{ocean} - SST^{coast}$ averaged from August to December is also depicted in Fig.4.7 (*gray line*). According to the previous research ([Nykjaer 1994];[Gesteira 2008b]) the ΔSST signal is lagged some months from UI. Here, a *3-month* lag was considered since it provides the best correlation between both signals ($R = 0.44$; $p < 0.05$). On the other hand, ΔSST is smaller than calculated in the BUE [Santos 2012b], where the coast was observed to cool at a rate of $-0.13^{\circ}C$ per decade, linked to the strengthening of upwelling at a rate of $87 m^3s^{-1}km^{-1}$ per decade, (see *Section 5.2*).

The ΔSST^{trend} values shown in Fig.4.3 can also be related to atmospheric circulation patterns, especially to NAO and EA that are the most

4. DIFFERENCES BETWEEN OCEAN AND COASTAL SST IN OTHER AREAS

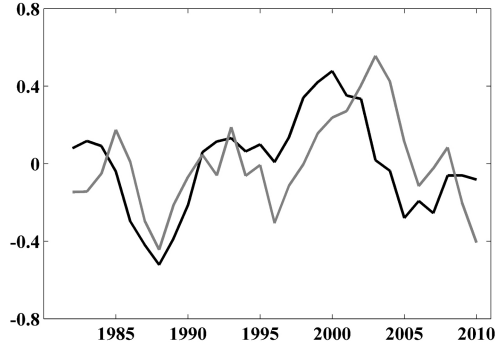


Figure 4.7: Inter-annual evolution of UI(*black line*) averaged from May to September and $(\Delta SST^{trend} = SST_{ocean}^{trend} - SST_{coast}^{trend})$ (*gray line*) averaged from August to December (3 months lag) over the period 1982–2010. Both variables were normalized to be compared. A ± 1 year running average was considered to smooth both signals.

prominent modes of variability over the north Atlantic Ocean. Extended winter (DJFM) indices were calculated over the period 1982–2010. Only EA index (Fig.4.8) showed a significant correlation with ΔSST . This mode had previously observed to have a remarkable influence on different oceanographic features around the Iberian peninsula ([deCastro 2008a]; [deCastro 2008b];[deCastro 2011]). Here, ΔSST values corresponding to different groups of months were considered. In spite of the correlation is always positive, no matter the chosen group, that correlation is only significant when including summer months. In particular, the best correlation was found for ΔSST^{MJJAS} both for raw ($R = 0.57; p < 0.01$) and detrended signals ($R = 0.58; p < 0.01$).

Note that the correlation was calculated considering a one-year lag between the atmospheric index and ΔSST . ΔSST^{MJJAS} and EA^{DJFM} index are depicted in (Fig.4.9). A good visual correlation can be observed between both signals, in agreement with the statistical comparison described

4.1. Differences between ocean and coastal SST in the Canary Upwelling Ecosystem

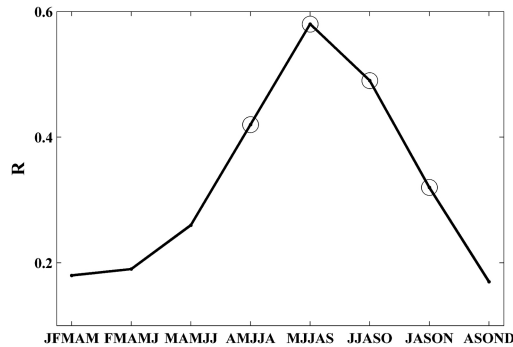


Figure 4.8: Correlation between extended winter (from December to March) EA and ΔSST grouped in months. A positive correlation was observed between both signals. In particular, the best correlation was found for ΔSST^{MJJAS} . Dots mark the correlations significant at 95%.

in Fig.4.8.

The observed warming rates at coastal and ocean locations described in the present study are obviously dependent on the selected period. These results can change when larger series are considered, which can not be analyzed here because not detailed data are available before the satellite era. Nevertheless, previous studies ([Santos 2011b];[Santos 2012b]) carried out in other areas with less complex coastal topography suggest that ocean water is more affected by the warming-cooling cycles than coastal water due to the presence of coastal upwelling. Thus, even in absence of marked changes in upwelling intensity, the presence of upwelling, which pumps colder water from below, can limit water warming in near shore areas.

4.1.4 Conclusions

SST warming rates have been analyzed along the region extending from 22 to 33°N over the period 1982–2010. This so called Moroccan sub-region is the part of the CUE characterized by permanent coastal upwelling. The

4. DIFFERENCES BETWEEN OCEAN AND COASTAL SST IN OTHER AREAS

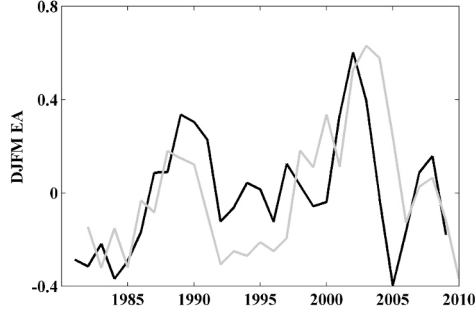


Figure 4.9: Inter-annual evolution of EA^{DJFM} index (*black line*) and $\Delta SST^{MJJAS}(t)$ (*gray line*) over the period 1982–2010. Both variables were normalized to be compared. A ± 1 year running average was considered to smooth both signals.

conclusions of the present study can be summarized as follows:

- The latitudinal gradient observed in the SST warming trends can be explained in terms of the T^{air} trends.
- ΔSST^{trend} is positive, indicating that the ocean warming rate is higher than the coastal one at most of latitudes.
- There is a significant positive correlation ($R = 0.44; p < 0.05$) between UI^{MJJAS} and ΔSST^{ASOND} , which relates the difference in temperature between coast and ocean to the strengthening of coastal upwelling.
- Extended winter EA index shows a positive correlation with ΔSST for the next year. This correlation is significant when considering summer months. In particular the best correlation was found for ΔSST^{MJJAS} ($R = 0.57; p < 0.01$).

4.2 Differences between ocean and coastal SST in the Benguela Upwelling Ecosystem (BUE)

4.2.1 Motivation

The aim is to characterize the differences in coastal and oceanic SST trends along the Benguela current system and the key role played by the persistent coastal upwelling observed in the region.

4.2.2 Methods

In the present study, two transects of 16 data points were considered in front of the Namibia coast and the western coast of South Africa (from 18 to 35°S): the coastal transect is located near shore and the oceanic transect is located 15° seaward (Fig.4.10, *empty circles*). Only HadISST data from 1900 on were considered due to data sparseness during the nineteenth century.

The amplitude of seasonal oscillations in temperature is on the order of 5°C for the region under study. Using unfiltered data would mask temperature trends, which are on the order of a few tenths of degree in most of the world ocean. Thus, data that were initially retrieved with a monthly periodicity were subsequently averaged at annual scale. This approach removes most of the seasonal variability.

The SST difference between coastal and oceanic transects will be highlighted by means of the SST increment, defined as: $\Delta SST = SST_{coast} - SST_{ocean}$, averaged at all coastal and oceanic locations.

For our purposes, monthly Ekman transport data obtained from PFEL were considered from 15 to 35°S and from 20°E to 10°W on an approximately 1° × 1° grid. Monthly SLP data from 1970 to 2009 were selected for this study on a grid covering from 0 to 60°S and from 25°W to 25°E.

4. DIFFERENCES BETWEEN OCEAN AND COASTAL SST IN OTHER AREAS

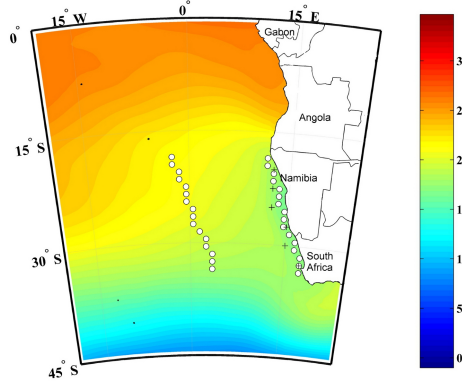


Figure 4.10: SST ($^{\circ}C$) annual average for the area under study from 1970 to 2009. *Black empty circles* represent the locations where SST data were extracted. Two transects of 16 points each were considered in front of the Namibia coast and the western coast of South Africa (from 18° to $35^{\circ}S$). The coastal transect was located at 1° from the coast and the oceanic one 15° seaward. *White crosses* represent a 6-points transect parallel to the shore line where Ekman transport was calculated.

With respect to wind data, 6-points located in front of the Namibia coast and the western coast of South Africa (from 18° to $35^{\circ}S$) were considered from 1970 to 2010 (Fig.4.10, *crosses*) from NCEP/NCAR database. These data lie on a spatial grid coarser than the previous ones, although with a longer temporal extent, which allows analyzing trends. UI can be defined as the Ekman transport component in the direction perpendicular to the shore line [Nykjaer 1994]. UI was calculated at the 6-point transect mentioned above (Fig.4.10, *crosses*) following [Gesteira 2006]:

$$U_i = -(\sin(\Theta - \pi/2)Q_x + \cos(\Theta - \pi/2)Q_y) \quad (4.2)$$

where Θ is the mean angle between the shore line and the Equator. $\Theta = 112.5^{\circ}$ was considered to be the mean coastal angle in this study and Q_x/Q_y are the same as were defined in the *Equation 4.2* in the chapter

4.2. Differences between ocean and coastal SST in the Benguela Upwelling Ecosystem (BUE)

4. Using this definition, positive (negative) upwelling indices correspond to upwelling–favorable (unfavorable) conditions.

4.2.3 Results and Discussion

The annual SST average in the area under study from 1970 to 2009 (Fig.4.10) highlights the interruption of the normal north–south SST gradient in the area by the intrusion of cooler water (around $16^{\circ}C$) near the Namibia coast. This representation shows the Benguela upwelling system stretching from the southern tip of Africa to about $15^{\circ}S$, where it is bounded by the Angola front. The inter–annual evolution of SST meridionally averaged from $18^{\circ}S$ to $35^{\circ}S$ was depicted for the period 1900–2009 (Fig.4.11a).

This analysis was carried out at different distances from the coast, from 1° (*bottom line*) till 15° (*top line*). A running average of ± 5 years was used to smooth out high frequency variations in temperature. In general, a mean increment in SST was obtained for the unfiltered signal at all distances from the coast for the period 1900–2009 ($0.07\text{--}0.08^{\circ}C$ per decade, $P < 0.01$).

This warming is similar to that described by [Rayner 2006] for the Southern Hemisphere, who found a temperature change of $0.68 \pm 0.18^{\circ}C$ from 1901 to 2004 using a linear trend. Other authors, [Folland 1990], found an increase of $0.38\text{--}0.58^{\circ}C$ for the Southern Hemisphere from 1861 to 1989.

Nevertheless, cooling can be observed at transects near the coast, (*lower lines*) during the last decades, whilst warming is still present at ocean all location (*upper lines*). Two procedures were considered in order to determine the break point between periods with significantly different trends. The first one, following the method described by [Tome 2004], shows a break point in 1972 for transects placed at 1 and 2° from the coast. The second method, which was also applied to the same transects, is based on the ab-

4. DIFFERENCES BETWEEN OCEAN AND COASTAL SST IN OTHER AREAS

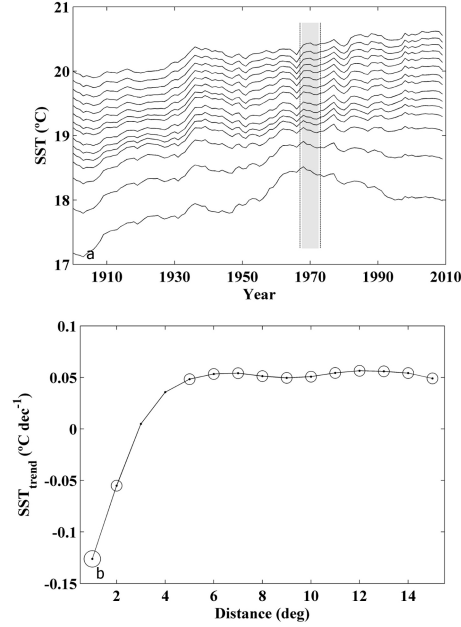


Figure 4.11: a) Inter-annual variation of SST($^{\circ}$ C) meridionally averaged from 18° S to 35° S at different distances from the coast for the period 1900–2009. *Bottom line* represents transect located at 1° from the coast and the *top line* represents transect located 15° from the coast. A running average of ± 5 years was used to smooth high frequency variations in temperature. The shadow area between vertical lines marks the break point between periods with significantly different coastal SST trends (1970). b) SST trends calculated from 1970 to 2009. *X* axis represents the transect distance (in degrees) from the coast. *Dots* represent SST trends, *small circles* correspond to trends with $0.01 < P < 0.1$ and *large circles* correspond to trends with $P < 0.01$

solute maximum calculation of the filtered SST signal for the whole period. In this case, the maximum appears in 1968. The mean between the values obtained from both procedures, 1970, was considered in this study.

SST trends were calculated from 1970 to 2009 (Fig.4.11b). *X* axis rep-

4.2. Differences between ocean and coastal SST in the Benguela Upwelling Ecosystem (BUE)

resents the distance (in degrees) from transect to shore. *Dots* represent SST trends, small circles correspond to trends with $0.01 < P < 0.1$ and large circles correspond to trends with $P < 0.01$. Near coast transects show significant negative trends. The most negative trend is obtained for the near-shore transect ($-0.13^{\circ}\text{C per decade}$, $P < 0.01$). The trend decreases for transect located at two degrees from the coast ($-0.06^{\circ}\text{C per decade}$, $P < 0.1$). No significant trends are observed for transects located at 3 and 4° from the coast. Significant positive trends are observed for rest of transects, where an early constant value is shown ($0.05\text{--}0.06^{\circ}\text{C per decade}$, $P < 0.1$). Note that the cooling observed near coast during the last decades is lower than the warming suffered from 1900 to 1970. Actually, the warming observed for that period was about $0.16^{\circ}\text{C per decade}$. Overall, the coastal region has warmed from 1900 to 2009 at a rate of $-0.13^{\circ}\text{C per decade}$.

The increase of oceanic SST from the seventies on had been reported in previous studies at global and regional scale ([IPCC2007];[deCastro 2009]; [Gesteira 2011];[Pardo 2011]). The ocean trend observed in BUES ($0.06^{\circ}\text{C per decade}$) is not far from the one calculated by [Casey 2001] for the South-east Atlantic using the COADS data set and a temperature class binning scheme and the period 1960–1990 ($0.09 \pm 0.07^{\circ}\text{C per decade}$). The BUES ocean warming is lower than observed in the North Atlantic ($0.2\text{--}0.3^{\circ}\text{C per decade}$) for the last three decades ([deCastro 2009];[Goikoetxea 2009]; [Michel 2009];[Gesteira 2011];[Santos 2011b];[Santos 2012a];[Gesteira 2013]). As for coastal SST, the observed cooling has not been detected in previous studies carried out in the same area [Pardo 2011], probably due to the coarseness of the SST grid used by those authors. The observed cooling in BUES ($-0.13^{\circ}\text{C per decade}$) contrasts with the warming reported in other coastal areas (e.g.[Gesteira 2008a] calculated a mean warming of $0.23^{\circ}\text{C per decade}$ in the North Atlantic Arc and [Gesteira 2013] who find a increment

4. DIFFERENCES BETWEEN OCEAN AND COASTAL SST IN OTHER AREAS

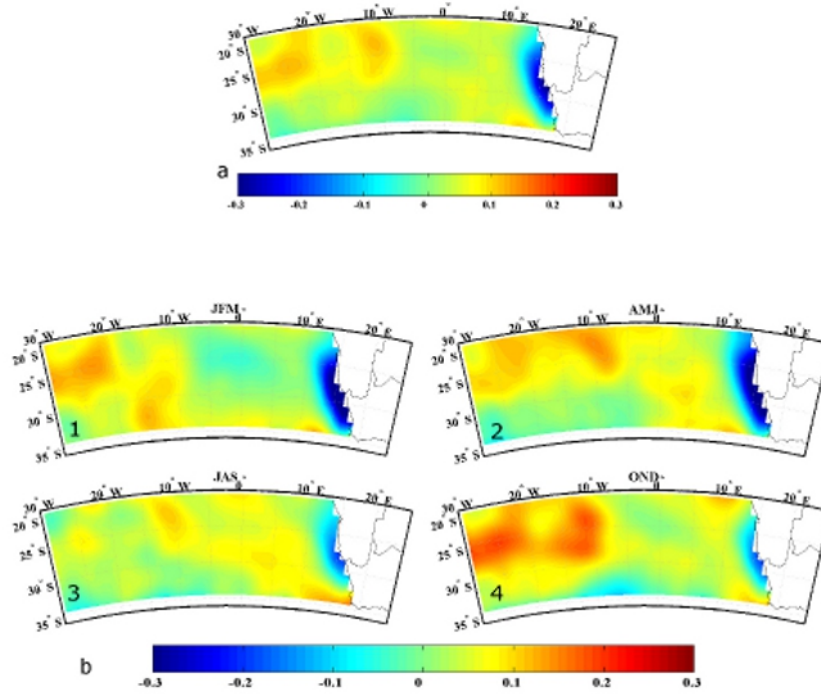


Figure 4.12: a) Annual SST trend ($^{\circ}\text{C per decade}$) for the area under study from 1970 to 2009. b) Seasonal SST trend ($^{\circ}\text{C per decade}$) for the area under study from 1970 to 2009. (1) January–March (JFM); (2) April–June (AMJ); (3) July–September (JAS) and (4) October–December (OND).

of 9.8 ± 0.3 days per decade near coast and 11.6 ± 0.2 days per decade, (see Chapter 4)).

Macroscopically, the annual SST tendency from 1970 to 2009 is also shown in Fig.4.12a. Negative values, ranging from 0 to $0.25^{\circ}\text{C per decade}$, are observed near to the coast and positive values, ranging from 0 to $0.15^{\circ}\text{C per decade}$, at the open ocean. The patterns detected at annual scale can also be reproduced at seasonal scale (Fig.4.12b 1–4).

Thus, the near shore area tends to cool and the ocean area to warm at all seasons. The coastal cooling is more intense during January–March

4.2. Differences between ocean and coastal SST in the Benguela Upwelling Ecosystem (BUE)

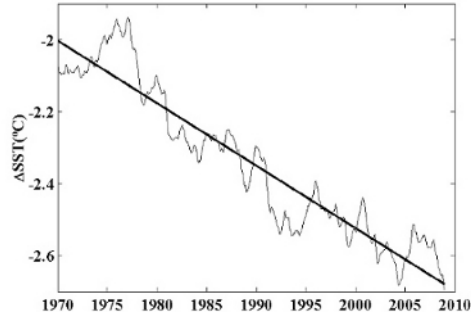


Figure 4.13: Inter-annual variation of $\Delta SST = SST_{coast} - SST_{ocean}$ ($^{\circ}C$) from 1970 to 2009. A running average of ± 5 years was used to smooth high frequency variations in temperature. The *solid line* represents a linear trend of $-0.18^{\circ}C$ per decade ($P < 0.01$).

(JFM) and April–June (AMJ) and the ocean warming is more intense during October–December (OND).

Fig.4.13 shows the different warming rate at coastal and oceanic locations. Note that ΔSST is always negative since coastal water is cooler than oceanic water due to the presence of persistent upwelling ([Nelson 1983]; [Fennel 1999]). A running average of ± 5 years was applied to smooth the signal only for representation purposes. A significant negative trend ($-0.18^{\circ}C$ per decade $^{-1}$, $P < 0.01$) was observed for the unfiltered signal. This trend is consistent with the warming (cooling) at ocean (coastal) areas described above.

The negative trend detected in the ΔSST from 1970 to 2009 is possibly related to the strengthening of persistent coastal upwelling in the Benguela region. To characterize this coastal upwelling system, the Ekman transport field averaged from 1981 to 2009 was analyzed in Fig.4.14a using data from the PFEL. Annual Ekman transport field shows the strongest values (between 1500 and 2000 $m^3 s^{-1} km^{-1}$) near the Namibia coast perpendicular to the shore line and pointing seaward. In addition, the annual cycle of

4. DIFFERENCES BETWEEN OCEAN AND COASTAL SST IN OTHER AREAS

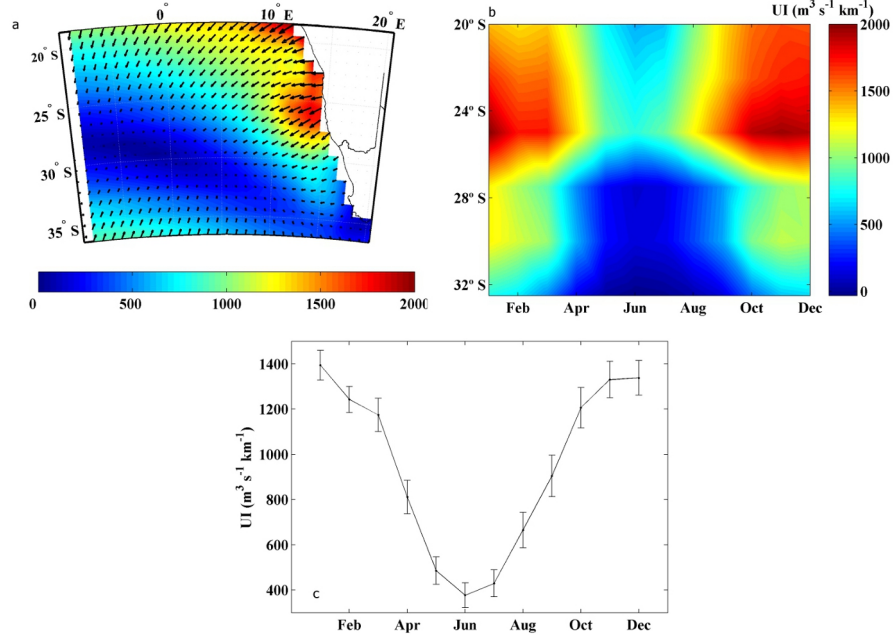


Figure 4.14: a) Ekman transport field ($m^3 s^{-1} km^{-1}$) averaged using PFEL data for the area under scope from 1981 to 2009. b) Annual cycle of UI ($m^3 s^{-1} km^{-1}$) for the six points along the BUES (crosses in Fig.4.10) calculated using NCEP/NCAR data for the period 1970 to 2009. c) Annual UI cycle ($m^3 s^{-1} km^{-1}$) meridionally averaged from $20^\circ S$ to $32^\circ S$ for the period 1970 to 2009. *Error bars* were calculated using the standard deviation of the monthly data, $\sigma(UI)$, divided by the square root of the number of data.

UI was calculated at the 6 points marked with crosses in Fig.4.10 using NCEP/NCAR data from 1970 to 2009 (Fig.4.14b).

The annual cycle is always positive (upwelling favorable conditions) showing its persistent character throughout the year. The maximum UI values were obtained at $25^\circ S$ during the austral spring and summer (values close to $2,000 m^3 s^{-1} km^{-1}$). Since the general behavior of UI is similar at

4.2. Differences between ocean and coastal SST in the Benguela Upwelling Ecosystem (BUE)

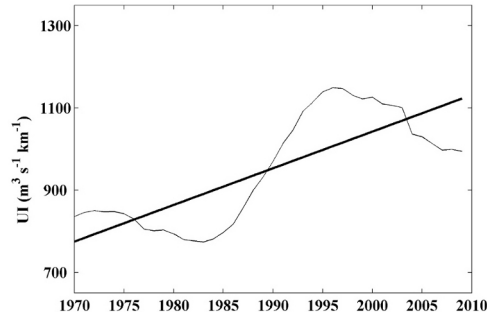


Figure 4.15: UI variability from 1970 to 2009. UI was spatially averaged for the 6 points parallel to the BUES (crosses in Fig.4.1). A running average of ± 5 year was used to smooth high frequency variations in UI. The straight line represents the linear trend with a slope of $87 \text{ m}^3 \text{ s}^{-1} \text{ km}^{-1}$ per decade, ($P < 0.01$).

all latitudes (positive and more intense during spring and summer), the UI annual cycle was meridionally averaged from 20 to 32°S (Fig.4.14c). The UI amplitude ranges from around $400 \text{ m}^3 \text{ s}^{-1} \text{ km}^{-1}$ during MJJ to around $1,300 \text{ m}^3 \text{ s}^{-1} \text{ km}^{-1}$ during NDJ. Error bars were calculated using the standard deviation of the monthly data, $\sigma(UI)$, divided by the square root of the number of data.

The UI trend was calculated from 1970 to 2009 (Fig.4.15). UI was spatially averaged for the 6 points along the BUES (*white crosses* in Fig.4.10). A running average of ± 5 year was applied to smooth the signal for representation. A clear positive trend can be observed for the unfiltered signal ($87 \text{ m}^3 \text{ s}^{-1} \text{ km}^{-1}$ per decade, $P < 0.01$). A similar general enhancement of the upwelling intensity in the BUES was detected by [Pardo 2011] with values ranging from 20 ± 3 to $100 \pm 4 \text{ m}^3 \text{ s}^{-1} \text{ km}^{-1}$ per decade for the last four decades. Trends in the rest of the mayor upwelling systems all over the world have been considered by other authors ([Schwing 1997];[Mendelssohn 2002];[Lemos 2004];[diLorenzo 2005]; [Lemos 2006];[Gesteira 2008b];[Patti 2010];[Pardo 2011]).

4. DIFFERENCES BETWEEN OCEAN AND COASTAL SST IN OTHER AREAS

<i>Month</i>	<i>UI(m³ s⁻¹ km⁻¹ yr⁻¹)</i>
Jan	16.5*
Feb	16.4*
Mar	12.5*
Apr	5.7*
May	3.1*
Jun	4.3*
Jul	2.5**
Aug	3.4**
Oct	11.8*
Nov	10.7*
Dec	14.4*

Table 4.1:
Monthly upwelling trends corresponding to the period 1970–2009

* $P < 0.01$

** $P < 0.05$

Trends in Benguela UI were also characterized at monthly scale from 1970 to 2009 (*Table 4.1*). All months show a significant positive trend, ranging from $25 \text{ m}^3\text{s}^{-1}\text{km}^{-1}$ *per decade* in July to $165 \text{ m}^3\text{s}^{-1}\text{km}^{-1}$ *per decade* in January. In general, the higher the upwelling intensity (ONDJFM in Fig.4.14c) the greater the trend.

The obtained UI trends can be explained in terms of a general atmospheric circulation pattern. In fact, several authors have reported the significant influence of the SAM index in the Southern Hemisphere climate variability ([Kidson 1999];[Baldwin 2001];[Nan 2003]) and in the large-scale variability of the Southern Ocean [Hall 2002]. In addition, several authors (see [Marshall 2003] and the references therein) have observed a trend in

4.2. Differences between ocean and coastal SST in the Benguela Upwelling Ecosystem (BUE)

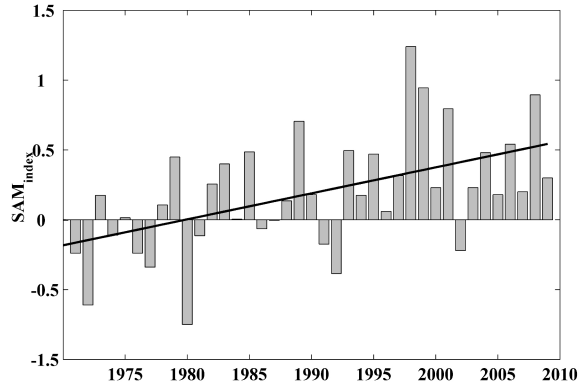


Figure 4.16: Monthly Southern Annular Mode (SAM) index from 1970 to 2009 (*gray bars*). The *solid black line* represents a linear trend of 0.37 *per decade* ($P < 0.01$).

the SAM index toward its positive phase and analyzed its influence on zonal winds. The inter-annual variability of the monthly SAM index from 1970 to 2009 shows a clear positive trend with a slope of 0.37 *per decade* and $P < 0.01$ (Fig.4.16). This trend represents an increase in the positive phase of the SAM index of approximately 20% during the period 1970–2009.

The positive phase of the SAM index represents relatively low pressures over Antarctic compared to those of mid latitudes. Thus, the evolution of the South Atlantic High can be analyzed for the period under study. The annual SLP averaged from 1970 to 2009 (Fig.4.17) shows a SLP maximum (SLP^{max}) of $102,246 Pa$ located at mid latitudes ($30.63^{\circ}S$ and $5.45^{\circ}W$). SLP anomalies were used to characterize the inter-annual evolution of the SLP^{max} from 1970 to 2009 (Fig.4.18a). A clear positive trend of $14 Pa$ *per decade*, ($P = 0.06$) is observed, reflecting the strengthening of the South Atlantic High from the seventies onward. In addition, the displacement of the High during the last four decades was also analyzed. A clear negative trend (-0.18° *per decade*, $P = 0.07$) is observed in latitude anomaly (Fig.4.18b) and a positive one (0.27° *per decade* without statistical significance) in lon-

4. DIFFERENCES BETWEEN OCEAN AND COASTAL SST IN OTHER AREAS

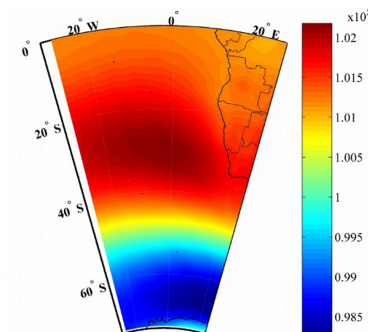


Figure 4.17: Evolution of the South Atlantic High from 1970 to 2009. Mean SLP (in $10^5 Pa$). The SLP maximum (SLP^{max}) is located at mid latitudes ($30.6^\circ S$, $5.4^\circ W$) with a value of $102,246 Pa$.

gitude anomaly (Fig.4.18c). This fact represents a southeastward drift of the South Atlantic High, approaching the BUES coast, which can also result in the strengthening of coastal winds.

4.2.4 Conclusions

The warming observed from the seventies onward at global scales might not be present or might even change sign in coastal areas due to the existence of some local forcing. Thus, in the Benguela upwelling ecosystem, the moderate ocean warming observed at the adjacent area ($0.06^\circ C$ per decade) was reversed by the strengthening in coastal upwelling, which resulted in water cooling near shore ($-0.13^\circ C$ per decade). This enhancement in coastal upwelling ($87 m^3 s^{-1} km^{-1}$ per decade) is in good agreement with the trend toward the positive phase (0.37 per decade) observed in the SAM index. Upwelling strengthening is also consistent with changes in the intensity and position of the South Atlantic High. The intensity was observed to increase in about $14 Pa$ per decade, and the position was observed to drift southeastward (-0.18° per decade in latitude and 0.27° per decade in longitude) approaching the coast and enhancing coastal winds.

4.2. Differences between ocean and coastal SST in the Benguela Upwelling Ecosystem (BUE)

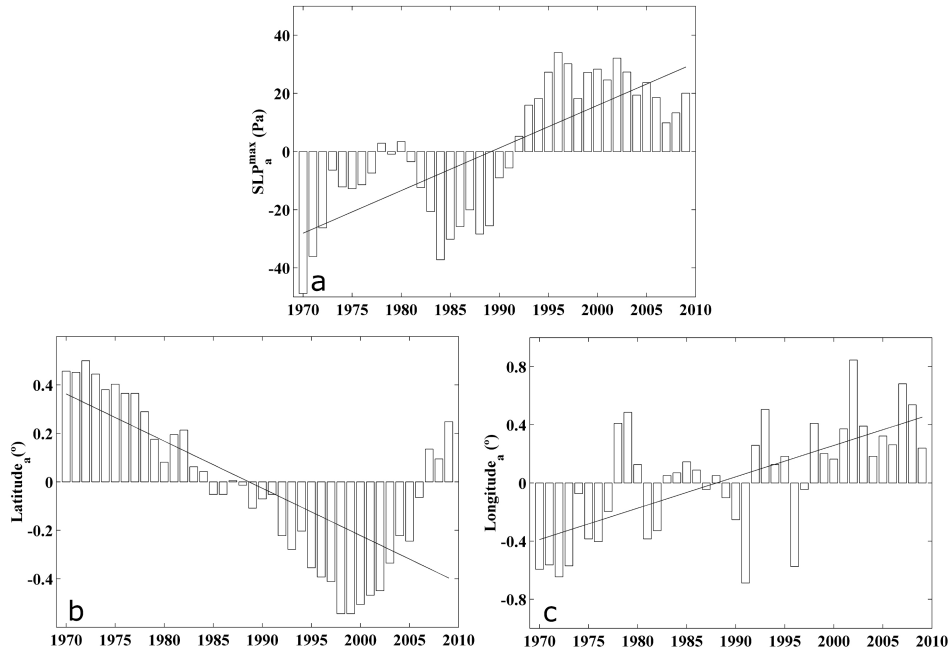


Figure 4.18: Evolution of the South Atlantic High from 1970 to 2009. (a) Evolution of SLP^{max} anomaly (bars). The dark line represents the linear tendency ($14 Pa$ per decade, $P = 0.06$). (b) Displacement in the latitude of the SLP^{max} relative to the mean position (bars). The dark line represents the trend (-0.19° per decade, $P = 0.07$). (c) Displacement in the longitude of the SLP^{max} relative to the mean position (bars). The dark line represents the trend (0.27° per decade without statistical significance).

4. DIFFERENCES BETWEEN OCEAN AND COASTAL SST IN OTHER AREAS

Upwelling along the western coast of the Iberian Peninsula

A.1 Motivation

In this appendix the goal is to describe the variability and trends in upwelling intensity from 1948–2009 along the WIP. Different fitting procedures, from the linear method to a model including a linear trend and several periodic modulations related to natural forcing, were considered.

A.2 Methods

Wind data were retrieved from the National Centers for Environmental Prediction/National Center for Atmospheric Research (NCEP/NCAR). Two points located in front of the WIP at $10^{\circ}W$ and 40.0 and $42.5^{\circ}N$, respectively, were considered in the present study, which covers the period 1948–2009. Although a third point is located along the WIP at $37.5^{\circ}N$, it is close to Cabo Sao Vicente, where the wind dynamics can change drastically due to topographical features. Thus, that point was discarded from the present analysis. Ekman transport was calculated from wind data following

expressions shown in *Equations 1.4 and 1.5* in chapter 1.

UI can be defined as the Ekman transport component in the direction perpendicular to the shoreline [Nykjaer 1994] following the *Equation 1.6*.

Wind fields must be correlated for the calculation of the mean UI. The correlation between UI at both points was $r = 0.85$, which allows considering a mean UI. Note that even though the points are located about 2.5° apart, the WIP coast is practically perpendicular to the equator in such a way that UI does not show important meridional differences. In the present study, we considered that the averaged values are more reliable than those calculated at single points, since the gridded data can present biases that vary from point to point (see [Josey 2002]).

The following methodology was applied:

- 1) UI was calculated from wind fields at the locations described
- 2) UI was meridionally and seasonally averaged using monthly values corresponding to the extended summer (April through September, following [Nykjaer 1994] and [Álvarez 2008a]).
- 3) Seasonal data were smoothed with a (± 2) running average filter centered in the year under study; this running average filter filters high-frequency oscillations in the signal which can mask long-term evolution. Here we refer to the signal that was filtered and averaged in space as (\tilde{UI}).

The \tilde{UI} signal was analyzed by means of a Fast Fourier Transform (FFT) to determine its possible periodicities. A windowing technique ([Press 1992]; [Emery 2002]) was used to detect the relevant frequencies with the highest accuracy. In some cases, the periodicity of the signal was too long to be detected by the FFT analysis. In those cases, a trial and error analysis was used to maximize the correlation between the real and the fitted function.

The signal was fitted to a known frequency determined by the previous FFT analysis and to a lower (unknown) frequency. The significance of the correlation was calculated by means of Student's t-test. The original signal was filtered before calculation, which implies that the resulting degrees of freedom are fewer than the ones corresponding to the original signal. Thus, N being the number of samples and n the number of neighbors used in the running average filter (± 2 in the present study, which results in $n = 5$), the degrees of freedom were $N' = N/n$, which is the value that was used in the significance testing.

A.3 Results and Discussion

A simple linear fitting similar to the ones described by [Álvarez 2008a] and [Pérez 2010] showed a decreasing trend in \tilde{UI} ($7.8 \text{ m}^3 \text{ s}^{-1} \text{ km}^{-1} \text{ per decade}$), with a significance $< 90\%$ (Table ??). This decrease is considerably lower than the one observed by [Pérez 2010] ($\sim 45 \text{ m}^3 \text{ s}^{-1} \text{ km}^{-1} \text{ per decade}$). The discrepancy can be attributed to different factors.

- 1) [Pérez 2010] considered the period 1965–2007.
- 2) They only considered a single point from reanalysis located at the northwestern corner of the Iberian Peninsula ($42.85^\circ N$, $9.37^\circ W$); the validity of this point was corroborated with local data measured at ($43^\circ N$, $11^\circ W$).
- 3) [Pérez 2010] considered the evolution of annual UI instead of the evolution of seasonal UI. This approach can be misleading, since upwelling is a seasonal phenomenon, and a seasonal analysis is more suitable. Otherwise, the trend can be biased by changes in wind intensity and direction during the non-upwelling season. [Lemos 2004]

and [Álvarez 2008a] also described high variability depending on the month under study.

Comparison with previous studies has shown that the observed trends are strongly dependent on the length of the time series, which indicates that the observed behavior is not linear. To investigate the multidecadal variability of upwelling, we calculated trends in groups of *21 yr*, *dashed line* in Fig.A.1. For each year, the trend was computed for itself and for the previous and following *10 yr*, e.g. the trend for 1958 was computed for the sub-period 1948–1968 and so on, (*black line*, in Fig.A.1) This period of *21 yr* is long enough to filter high-frequency variability but short enough to retain multidecadal oscillations. Fig.A.1 shows the trends for the period 1958–1999, calculated from the raw signal without previous filtering. High variability was observed in both signals. Furthermore, the trend can be both positive and negative during the period under study, although the mean trend was negative ($-11.1 \text{ m}^3 \text{ s}^{-1} \text{ km}^{-1} \text{ per decade}$). Note that this mean trend differs slightly from the one shown above ($-7.8 \text{ m}^3 \text{ s}^{-1} \text{ km}^{-1} \text{ per decade}$), since the periods of study are different.

As previously mentioned, the \tilde{UI} signal is nonlinear, which makes it difficult to distinguish between changes due to natural variability and trends. The FFT analysis using a windowing technique shows a main peak between 10.7 and 12.8 *yr*. The length of the record only allows a coarse discretization in terms of frequency (period).

This period is close to the Schwabe cycle of solar activity, which is 10.7 *yr* [Usoskin 2009]. This fact does not necessarily suppose that changes in solar irradiance directly result in changes in wind (upwelling) patterns. Some authors ([Haigh 1996];[White 1997]) have proposed indirect mechanisms (cloud coverage, atmospheric wind) to link sea surface temperature to changes in solar irradiance. Thus, in the case of the UI, the changes can

A.3. RESULTS AND DISCUSSION

	R	P	Trend
Linear function	0.36	85%	-7.8
Linear function and sinusoid (T_s)	0.53	95%	-8.5
Linear function and double sinusoid ($T_s T_l$)	0.78	99%	16.2

Table A.1: Summary of fitting strategies. R : correlation coefficient; significance calculated with Student's t-test. Trends are in $m^3 s^{-1} km^{-1}$ per decade. Periodicities: $T_s = 10.9$ and $T_l = 89$ yr

be modulated via changes in the teleconnection patterns ([Barnston 1987]; [Hurrell 1995];[deCastro 2008a]). According to [Stephenson 2000], the North Atlantic Oscillation (NAO) also shows decadal variations that are unlikely to be obtained from sampling a white noise process. The most recent solar cycles were analyzed in an exploratory way to study their possible relationship with the peaks in the upwelling signal (*solid line* in Fig.A.2). The last solar cycles ended in April 1954, October 1964, June 1976, September 1986, May 1996, and December 2008. On the other hand, peaks in $\tilde{U}I$ signal used were observed in 1955, 1963, 1974, 1989, 1996, and 2009. Thus the peaks in both signals do not exactly coincide, although they are relatively close. On average, the length of the last solar cycles (from the 1950s on) is 10.9 *yr*, which is the periodicity that was considered in the present analysis.

$\tilde{U}I$ can be fitted to a sinusoidal function with a possible linear trend following:

$$\tilde{U}I = a + bt + c \cos\left(\frac{2\pi}{T_s}t + \varphi_s\right) \quad (\text{A.1})$$

where a , b , c , and φ_s are a set of unknowns to be computed, and time of the short period, $T_s = 10.9$ *yr* is the imposed periodicity. This fitting shows a decreasing trend in $\tilde{U}I$ ($8.5 m^3 s^{-1} km^{-1} dec^{-1}$) with a significance of 95%

A. UPWELLING ALONG THE WESTERN COAST OF THE IBERIAN PENINSULA

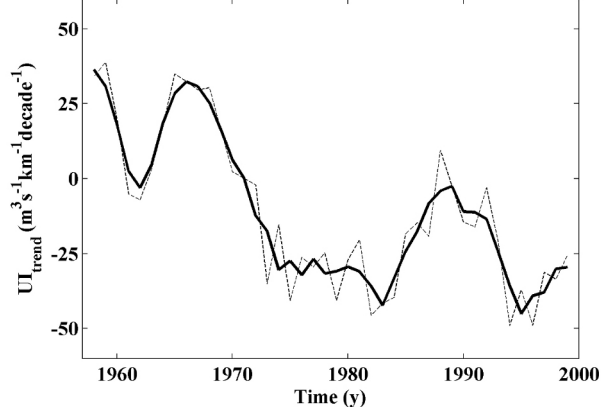


Figure A.1: Trends in upwelling index (UI) along the western coast of the Iberian Peninsula (WIP) for the period 1958–1999. Data were grouped in intervals of 21 *yr* prior to linear fitting. The *dashed line* corresponds to the raw trends, and the *solid line* to the trends smoothed with a running average (± 1 *yr*)

(see *Table A.1*). This value is close to the one calculated by simple linear fitting, albeit with a higher significance, since the sinusoidal part is able to reproduce the decadal periodicity of the signal. Nevertheless, the different amplitude of the peaks cannot be satisfactorily reproduced assuming only periodicity.

The \tilde{UI} signal was then fitted to a double sinusoid with a possible linear trend following:

$$\tilde{UI} = a + bt + c\cos\left(\frac{2\pi}{T_s}t + \varphi_s\right) + d\cos\left(\frac{2\pi}{T_l}t + \varphi_l\right) \quad (\text{A.2})$$

where a , b , c , d , φ_l , and φ_s are a set of unknowns to be computed, and T_l and T_s represent the long and short period, respectively. Note that T_l was not determined by the previous Fast Fourier Transform (FFT) analysis, due to the limited extent of the series, so its value was determined by computing the value of T_l that provided the highest correlation coefficient (R) between \tilde{UI} and the fitted signal. The best estimate, $R = 0.78$ with a significance

A.3. RESULTS AND DISCUSSION

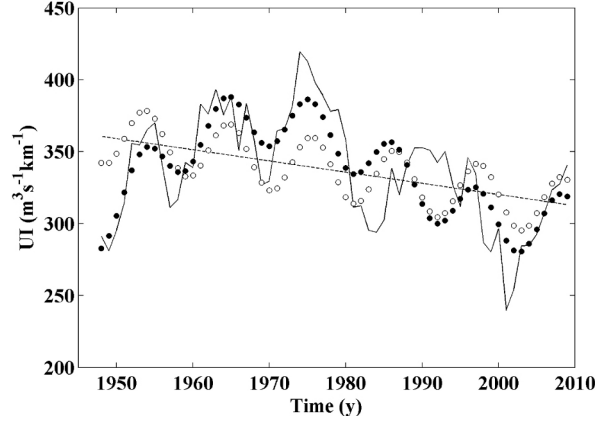


Figure A.2: Comparison between the upwelling index signal that was filtered and averaged in space ($\tilde{U}I$; *solid line*) and the different fitting functions. Linear (*dashed line*); linear and sinusoidal (*open circles*); Linear and double sinusoid (*closed circles*)

higher than 99%, was obtained for $T_l = 89 \text{ yr}$, considering $T_s = 10.9 \text{ yr}$ to be a constant. However, this fit does not result in a negative trend in $\tilde{U}I$, but rather in a positive one ($16.2 \text{ m}^3 \text{ s}^{-1} \text{ km}^1 \text{ per decade}$). This periodicity can be related to the Gleissberg cycle of solar activity, which is around 87 yr ($70\text{--}100 \text{ yr}$; [Peristykh 2003];[Braun 2005]). According to some authors (e.g. [Yousef 2006]), several prominent teleconnection patterns such as the NAO or El Niño Southern Oscillation, the levels of different lakes, and even fisheries can be influenced by this cycle. Finally, the trend is variable and our result cannot be considered an absolute value. Actually, any T_l between 70 and 100 yr resulted in a correlation coefficient similar to the one obtained for $T_l = 89 \text{ yr}$ (1% lower at most), although the trends ranged from 4 to $25 \text{ m}^3 \text{ s}^{-1} \text{ km}^1 \text{ per decade}$ and were always positive.

A.4 Conclusions

The $\tilde{U}I$ signal was fitted to different equations to analyze the variability in upwelling observed during the last decades. Both a simple linear fitting and a more complex, sinusoidal ($T_s = 10.9 \text{ yr}$) and linear fitting resulted in a negative trend in upwelling intensity. In contrast, the fit of the signal to a straight line and to a double sinusoid ($T_s = 10.9$ and $T_l = 89 \text{ yr}$, respectively) resulted in a positive trend in upwelling intensity. This last fitting function provided the best estimate, with a significance $> 99\%$. Moreover, observed periodicities did not correspond to the mathematical values that maximized the correlation coefficient between $\tilde{U}I$ and the fitting function, but rather coincided with periodicities in solar activity, the Schwabe and Gleissberg cycles.

The present study does not elucidate whether the long periodicity is real or a mathematical artifact. None of the approaches is comprehensive, since the linear assumption is too coarse and the single sinusoid does not explain the amplitude of the different peaks.

In summary, it is still unclear which part of the observed changes in coastal upwelling is related to natural causes and which part is linked to shifts with a possible anthropogenic cause.

Acronym and abbreviation list

- *AABW*: Antarctic Bottom Water.
- *AAO*: Antarctic Oscillation.
- *AMSR*: Advanced Microwave Scanning Radiometer.
- *AMO*: Atlantic Multidecadal Oscillation.
- *AO*: Arctic Oscillation.
- *AVHRR*: Advanced Very-High Resolution Radiometer.
- *BUE*: Benguela Upwelling Ecosystem.
- *CFSR*: Climate Forecast System Reanalysis.
- *CPC*: Climate Prediction Center.
- *CTD*: Conductivity Temperature Depth.
- *CUE*: Canary Upwelling Ecosystem.
- *EA*: Atlantic Pattern.
- *EA/WR*: Atlantic Pattern / Western Russia Pattern.

B. ACRONYM AND ABBREVIATION LIST

- *ENACW*: Eastern North Atlantic Central Water.
- *EOF*: Empirical Orthogonal Functions.
- *FFT*: Fast Fourier transform.
- *HadISST*: Hadley Center Ice Sea Surface Temperature.
- *IP*: Iberian Peninsula.
- *IPCC*: Intergovernmental Panel on Climate Change.
- *LSW*: Labrador Sea Water.
- *MBT*: Mechanical Bathythermograph.
- *MW*: Mediterranean Water.
- *NADW*: North Atlantic Deep Water.
- *NAO*: North Atlantic Multidecadal Oscillation.
- *NCEP/NCAR*: National Center of Atmospheric Research / National Center for Environmental Prediction.
- *NCDC*: National Climatic Data Center.
- *NOAA*: National Oceanographic Atmospheric Administration.
- *NOMADS*: National Operational Model Archive and Distribution System.
- *NWABW*: North-West Atlantic Bottom Water.
- *OI*: Optimum interpolation.
- *PFEL*: Pacific Fisheries Environmental Laboratory.

- *POL*: Polar / Eurasia Pattern.
- *RPCA*: Rotated Principal Component Analysis.
- *SAM*: Southern Hemisphere Annular Mode.
- *SCA*: Scandinavia Pattern.
- *SLP*: Sea Level Pressure.
- *RPCA*: Rotated principal component analysis.
- *SODA*: Simple Ocean Data Assimilation.
- *SST*: Sea Surface Temperature.
- *THC*: Thermohaline Circulation.
- *UI*: Upwelling Index.
- *WIP*: Western Iberian Peninsula.
- *XBT*: Expendable Bathythermograph.

B. ACRONYM AND ABBREVIATION LIST

Appendix C

List of Publications

[Gesteira2013] Gómez–Gesteira, M., deCastro, F., Santos, M., Álvarez, Changes in the frequency of extreme sea temperature events along the west iberian peninsula from 1982 to 2011, “Submitted Journal Geophysical Research, (2013).

[Gesteira 2013a] Gómez–Gesteira, M. deCastro, F. Santos and I. Álvarez, “Changes in ENACW observed in the Bay of Biscay over the period 1975-2006, “Submitted Contineltal Shelf Research (2013)

[Santos 2011a] Santos, F., Gómez–Gesteira, M., deCastro, M., Álvarez, I., “Upwelling variability along the western coast of the Iberian Peninsula: can trends be accurately calculated?, “Climate Research, (2011).

[Santos 2011b] Santos, F., Gómez–Gesteira, M., deCastro, M., “Coastal and oceanic variability along the western Iberian peninsula,“Continental Shelf Research, **31**, 2012–2017, (2011).

[Santos 2011c] Santos, F., Gómez–Gesteira, M., deCastro, M., Álvarez, I.,“Upwelling along the western coast of the Iberian Peninsula: dependence of trends on fitting strategy, “Climate Research, **48** 213–218, (2011).

[Santos 2012a] Santos F., Gómez-Gesteira, M., deCastro, M. Álvarez I,“Variability

C. LIST OF PUBLICATIONS

of coastal and ocean water temperature in the upper 700 m along the Western Iberian Peninsula from 1975 to 2006, “Plos One, **7(12)**, 1–7, (2012).

[Santos 2012b] Santos F., Gómez-Gesteira, M., deCastro, M. Álvarez I, “Differences in coastal and oceanic SST trends due to the strengthening of coastal upwelling along the Benguela current system, “Continental Shelf Research, **34**, 79–86, (2012)

[Santos 2012c] Santos, F., deCastro, M., Gómez-Gesteira, M., Álvarez, I., “Differences in coastal and oceanic SST warming rates along the Canary upwelling ecosystem from 1982 to 2010, “Continental Shelf Research, **47** 1–6, (2012).

Bibliography

- [Acken 1996] Acken, H.M. van and Becker, G., “Hydrography and through-flow in the northeastern North Atlantic Ocean: the NANSEN project, “Progress in Oceanography, **38**, 297–346, (1996).
- [Álvarez 2008a] Álvarez, I., Gomez-Gesteira, M., deCastro, M., Dias, J.M., “Spatio temporal evolution of upwelling regime along the western coast of the Iberian Peninsula, “Journal of Geophysical Research, **113**, (2008).
- [Álvarez 2008b] Álvarez, I., Gomez–Gesteira, M., deCastro, M., Novoa, E.M., “Ekman transport along the Galician Coast (NW, Spain) calculated from QuikSCAT winds, “Journal of Marine Systems, **72**, 101–115. (2008).
- [Álvarez 2010] Álvarez, I., Gomez-Gesteira, M., deCastro, M., Gomez-Gesteira, J.L., and Dias, J.M., “Summer upwelling frequency along the western Cantabrian coast from 1967 to 2008, “ Journal of Marine Systems, **79**, 218–226,(2010).
- [Ambar 1979a] Ambar, I. and Howe, M.R. “Observations of the Mediterranean outflow I. Mixing in the Mediterranean outflow, “Deep Sea Research, **26**, 535–54, (1979).

BIBLIOGRAPHY

- [Ambar 1979b] Ambar, I. and Howe, M.R. “Observations of the Mediterranean outflow II. The deep circulation in the vicinity of the Gulf of Cadiz, “ *Deep Sea Research*, **26A**, 555–68, (1979).
- [Ambar 1983] Ambar, I., “A shallow core of Mediterranean water off western Portugal, “*Deep Sea Research*,**30**, 677–80, (1983).
- [Ambar 2002] Ambar, I., Serra, N., Brogueira, M.J., Cabecadas, G., Abrantes, F., et al., “ Physical-Chemical and sedimentological aspects of the Mediterranean outflow off Iberia, “*Deep Sea Research Part II*, **49**, 4163–4177, (2002).
- [Aristegui 1994] Arístegui, J., Sangra, P., Hernández–León, S., Canton, M., Hernández–Guerra, A., Kerling, J.L., “Island induced eddies in the Canary islands, “*Deep Sea Research*, **41**,1509–1525, (1994).
- [Aristegui 2009] Arístegui, J., Barton, E.D., Álvarez–Salgado, X.A., Santos, A.M.P., Figueiras, F.G., Kifani, S., Hernández–León, S., Mason, E., Machú, E., Demarq, H., “Subregional ecosystem variability in the Canary current upwelling, “*Progress in Oceanography*, **83**, 33–48, (2009).
- [Bakun 1990] Bakun, A., “Global climate change and intensification of coastal upwelling, “*Science*, **247**, 198–201, (1990).
- [Baldwin 2001] Baldwin, M.P., “Annular modes in global daily surface pressure, “*Geophysical Research Letters*, **28**, 4115–4118, (2001).
- [Barnston 1987] Barnston, A.G., Livezey, R.E., “ Classification, seasonality and persistence of low–frequency atmospheric circulation patterns, “*Monthly Weather Review*, **115**, 1083–1126, (1987).

BIBLIOGRAPHY

- [Barriopedro 2011] Barriopedro, D., Fischer, E.M., Luterbacher, J., Trigo, R.M., García-Herrera, M., “The hot summer of 2010: redrawing the temperature record map of Europe, “*Science*, **332**, 220–224, (2011).
- [Barton 1998] Barton, E.D., Aristegui, J., Tett, P., et al., “The transition zone of the Canary current upwelling region, “*Progress in Oceanography*, **41**, 455–504, (1998).
- [Blanton 1984] Blanton, J.O., Atkinson, L.P., Castillejo, F., Montero, A.L., “Coastal upwelling of the Rias Bajas, Galicia, northwest Spain, I; hydrographic studies, “*Rapports et procès-verbaux des réunions / Conseil permanent international pour l’exploration de la mer*, **183**, 179–190, (1984).
- [Bojariu 2003] Bojariu R., Gimeno, L., “Predictability and numerical modelling of the North Atlantic Oscillation, “*Earth Science Reviews*, **63(1)**, 145–168, (2003).
- [Braun 2005] Braun, H., Christl, M., Rahmstorf, S., Ganopolski, A., and others, “Possible solar origin of the 1,470 *year* glacial climate cycle demonstrated in a coupled model, “*Nature*, **438**, 208–211, (2005).
- [Brohan 2006] Brohan P, Kennedy JJ, Harris I, Tett SFB, Jones PD, “Uncertainty estimates in regional and global observed temperature changes: a new data set from 1850, “*Journal of Geophysical Research*, **111**, D21206, (2006).
- [Carton 2000a] Carton, J.A., Chepurin, G.A., Cao, X., Giese, B.S., “A Simple Ocean Data Assimilation analysis of the global upper ocean 1950-1955, ”Part 1: Methodology, *Journal Geophysics Research*, **30**, 294–309, (2000).

BIBLIOGRAPHY

- [Carton 2000b] Carton, J.A., Chepurin, G.A., Cao, X., “A Simple Ocean Data Assimilation analysis of the global upper ocean 1950-1955,” Part 2: Methodology, *Journal Geophysics Research*, **30**, 311–326, (2000).
- [Carton 2008] Carton, J.A., Giese, B.S., “A reanalysis of ocean climate using Simple Ocean Data Assimilation (SODA),” *Monthly Weather Review*, **136**, 2999–3017, (2008).
- [Casey 2001] Casey, K.S., Cornillon, P., “Global and regional sea–surface temperature trends,” *Journal of Climate*, **14**, 3801–3818, (2001).
- [Castro1994] Castro, C.G., Perez, F.F., Alvarez-Salgado, X.A., Roson, G., Rios, A.F., “Hydrography conditions associated with the relaxation of a upwelling event off the Galician coast (NW Spain),” *Journal of Geophysical Research*, **99**, 5135–5147, (1994).
- [Cole 2000] Cole J.E., Dunbar R.B., McClanahan T.R., Muthiga NA, “Tropical pacific forcing of decadal SST variability in the Western Indian Ocean over the past two centuries,” *Science*, **287**, 617–619, (2000).
- [Czaja 2002] Czaja A., Marshall J., “Observed impact of Atlantic SST anomalies on the North Atlantic Oscillation,” *Journal of Climate*, **15**, 606–623, (2002).
- [deCastro 2006] deCastro M., Lorenzo N., Taboada J.J., Sarmiento M., Alvarez I., Gómez-Gesteira M., “Influence of teleconnection patterns on precipitation variability and on river flow regimes in the Miño River basin (NW Iberian Peninsula),” *Climate Research*, **32**, 63–73, (2006).
- [deCastro 2008a] deCastro, M., Gomez–Gesteira, M., Lorenzo, M.N., Alvarez, I., Crespo, A.J.C., “Influence of atmospheric modes on coastal

BIBLIOGRAPHY

- upwelling along the western coast of the Iberian Peninsula, 1985 to 2005, "Climate Research, **36**, 169–179, (2008).
- [deCastro 2008b] deCastro, M., Gomez–Gesteira, M., Alvarez, I., Lorenzo, M.N., Cabanas, J.M., Prego, R., Crespo, A.J.C., "Characterization of fall–winter upwelling recurrence along the Galician western coast (NW Spain) from 2000 to 2005: dependence on atmospheric forcing, "Journal of Marine Systems, **72**(1–4), 145–158, (2008).
- [deCastro 2009] deCastro, M., Gomez–Gesteira, M., Alvarez, I., Gesteira, J.L.G., "Present warming within the context of cooling&warming cycles observed since 1854 in the Bay of Biscay, "Continental Shelf Research **29**, 1053–1059, (2009).
- [deCastro 2011] deCastro, M., Gomez–Gesteira, M., Alvarez, A.J.C. Crespo., "Atmospheric modes influence on Iberian poleward current variability, "Continental Shelf Research, **31**, 425–432, (2011).
- [Delworth 1993] Delworth, T.L., Manabe, S., Stouffer, R.J., "Interdecadal variability of the thermohaline circulation in a couple ocean–atmosphere model, "Journal of Climate, **6**, 1993 –2001, (1993).
- [Dessai 2002] Dessai S., " Heat stress and mortality in Lisbon. Part I: model construction and validation, "International Journal of Biometeorology, **47**, 6 –12, (2002).
- [DiazdelRio 1998] Diaz del Rio, G., Gonzalez, N., Marcote, D., "The intermediate Mediterranean water inflow along the northern slope of the Iberian Peninsula, "Oceanologica Acta, **21**, 157–163, (1998).
- [desChamps 1984] desChamps, P.Y., Frouin, R., Crepon, M., "Sea surface temperatures of the coastal ones of France observed by the HCMM satellite, "Journal of Geophysical Research, **89**, 8123–8149, (1984).

BIBLIOGRAPHY

- [Diaz 2006] Díaz J, Garcia-Herrera R, Trigo RM, Linares C, Valente MA, De Miguel JM, Hernandez E., “The impact of summer 2003 heat wave in Iberia: how should we measure it?,” *International Journal of Biometeorology*, (2006).
- [Diederich 2005] Diederich, S., G. Nehls, J. E. E. van Beusekom, K. Reise, “ Introduced Pacific oyster (*Crassostrea gigas*) in the northern Wadden Sea: Invasion accelerated by warm summers?,” *Helgoland Marine Research*, **59**, 97–106, (2005).
- [diLorenzo 2005] Di Lorenzo, E., Miller, A.J., Schneider, N., McWilliams, J.C., “The warming of the California current system: dynamics and ecosystem implications,” *Journal of Physical Oceanography*, **35**, 336–362, (2005).
- [Dima 2001] Dima, M., Lohmann, G., “A hemispheric mechanism for the Atlantic Multidecadal Oscillation,” *Journal of Climate*, **20**, 2706–2719, (2007).
- [Domingues 2008] Domingues CM, Church JA, White NJ, Gleckler PJ, Wijffels SE, et al., “ Rapid upper-ocean warming helps explain multidecadal sea-level rise,” *Nature*, **453**, 1090–1093, (2008).
- [Enfield 2001] Enfield, D.B., Mestas-Nunhez, A.M., Trimble, P.J., “The Atlantic multidecadal oscillation and its relation to rain fallan driver flows in the continental *U.S.*,” *Geophysical Research Letters*, **28(10)**, 2077–2080, (2001).
- [Emery 1986] Emery, W.J. and Meinke, J. “Global water masses: summary and review,” *Oceanological Acta*, **9**, 383–91, (1986).
- [Emery 2002] Emery, W.J., Thompson, R.E., “Data analysis methods in physical oceanography, 2nd edn,” Elsevier, Amsterdam, (2004).

BIBLIOGRAPHY

- [Fennel 1999] Fennel, W., "Theory of the Benguela upwelling system, "Journal of Physical Oceanography, **29**, 177–190, (1999).
- [Fiuza 1983] Fiuza, A.F.G., "Upwelling patterns off Portugal. In: Suess, E., Thiede, J.(Eds.), Coastal Upwelling .Its Sediment Records (PartA), "Plenum, NewYork, 85–98, (1983).
- [Folland 1984] Folland C, Parker D, Kates F., "Worldwide marine temperature fluctuations 1985–1981, "Nature, **310**, 670–673, (1984).
- [Folland 1990] Folland, C., Karl, T., Vinnikov, K., "Observed climate variations and change In: Houghton, J., Jenkins, G., Ephraums, J. (Eds.), "Climate Change: The IPCC Scientific Assessment, "Cambridge University Press, 195–238, (1990).
- [Folland 1992] Folland C, Nicholls N, Nyenzi B, Parker B, Vinnikov K., "Observed climate variability and change in: Houghton, J., Jenkins, G., Ephraums., J. (Eds.), " Climate Change 1992: The Supplementary Report to the IPCC Scientific Assessment Cambridge University Press, 135–170, (1992).
- [Folland 1995] Folland C.K., Parker D.E., "Correction of instrumental biases in historical sea surface temperature data, " Q. J. R. Meteorological Society, **121**, 319–367, (1995).
- [Folland 2001] Folland, C., Colman, A.W., Rowell, D.P., Davey, M.K., "Predictability of northeast Brazil rain fall and real-time forecast skill, 1987–1998, "Journal of Climate, **14**, 1937–1958, (2001)
- [Fraga 1982] Fraga, F., Mouriño, C. and Manríquez, M., " Las masas de agua en la costa de Galicia: junio-octubre, "Resultados de Expediciones Científicas, **10**, 51–77, (1982).

BIBLIOGRAPHY

- [Frank 2005] Frank, K. T., B. Petrie, J. S. Choi, and W. C. Leggette, “Trophic cascades in a formerly cod-dominated ecosystem,” *Science*, **308**, 1621–1623, (2005).
- [GarciaHerrera 2005] García-Herrera R, Diaz J, Trigo RM, Hernandez E., “Extreme summer temperatures in Iberia: health impacts and associated synoptic conditions,” *Annual Geophysics*, **23**, 239–251, (2005).
- [GarciaSoto 2002] García-Soto, C., Pingree, R.D., Valdés, L., “Navidad Development in the Southern Bay of Biscay: climate change and Swoddy structure from remote sensing and in situ measurements,” *Journal of Geophysical Research*, **107(C8)**, 3118 (2002).
- [Ganachaud 2000] Ganachaud, A., Wunsch, C. “Improved estimates of global ocean circulation, heat transport and mixing from hydrographic data,” *Nature*, **408**, 453–457, (2000).
- [Gesteira 2006] Gómez-Gesteira, M., Moreira, C., Alvarez, I., deCastro, M., “Ekman transport along the Galician coast (NW, Spain) calculated from forecasted winds,” *Journal of Geophysical Research*, **111**, (2006).
- [Gesteira 2008a] Gómez-Gesteira, M., deCastro, M., Álvarez, I., Gómez-Gesteira, J.L., “Coastal sea surface temperature warming trend along the continental part of Atlantic Arc (1985–2005),” *Journal Geophysical Research*, **113**, C04010, (2008).
- [Gesteira 2008b] Gómez-Gesteira, M., deCastro, M., Álvarez, I., Lorenzo, M.N., Gesteira, J.L.G., Crespo, A.J.C, “Spatio-temporal upwelling trends along the Canary upwelling system (1967–2006), Trends and Directions in Climate Research,” *Annals New York Academy Science*, **1146**, 320–337, (2008).

BIBLIOGRAPHY

- [Gesteira 2011] Gómez–Gesteira, M., Gimeno, L., deCastro, M., Lorenzo, M.N., Alvarez, I., Nieto, R., Taboada, J.J., Crespo, A.J.C., Ramos, A.M., Iglesias, I., Gómez–Gesteira, J.L., Santo, F.E., Barriopedro, D., Trigo, I.F., “The state of climate in North–West Iberia,” *Climate Research*, **48**, 109–144, (2011).
- [Gesteira 2013] Gómez–Gesteira, M., deCastro, F., Santos, I., Álvarez, Changes in the frequency of extreme sea temperature events along the west iberian peninsula from 1982 to 2011, “Submitted Journal Geophysical Research, (2013).
- [Gesteira 2013b] Gómez–Gesteira, M. deCastro, F. Santos and I. Álvarez, “Changes in ENACW observed in the Bay of Biscay over the period 1975-2006,” *Submitted Continental Shelf Research* (2013)
- [Gill 1982] Gill, A.E., “Atmospheric–Ocean Dynamics,” Elsevier, New York, 662, (1982).
- [Ginzburg 2004] Ginzburg A.I., Kostianoy A.G., Sheremet N.A., “ Seasonal and interannual variability of the Black sea surface temperature as revealed from satellite data (1998–2000),” *Journal of Marine Systems*, **52**, 33–50, (2004).
- [Giese 2011] Giese B.S., Ray S., “ El Niño variability in simple ocean data assimilation (SODA), 1981–2008,” *Journal of Geophysical Research*, **116**, C02024, (2011).
- [Goikoetxea 2009] Goikoetxea, N., Borja, A., Fontán, A., González, M., Valencia, V., “Trends and anomalies in sea surface temperature, observed over the last 60 years, within the south eastern Bay of Biscay,” *Continental Shelf Research*, **29**, 1060–1069, (2009).

BIBLIOGRAPHY

- [Goldenberng 2001] Goldenberng, S.B., Landsea, C.W., Mestas Nunhez, A.M., Gray, W.M., “The recent increase in Atlantic hurricane activity: causes and implications,” *Science*, **293**, 474–479, (2001).
- [Gong 1999] Gong, D.Y., Wang, S.W., “Definition of Antarctic oscillation index,” *Geophysical Research Letters*, **26**, 459–462, (1999).
- [GonzalezPola 2005] González–Pola, C., Lavín, A., Vargas–Yáñez, M., “Intense warming and salinity modification of intermediate water masses in the southeastern corner of the Bay of Biscay for the period 1992–2003,” *Journal of Geophysical research*, **10**, C05020, (2005).
- [Gordon 2000] Gordon, C., Cooper, C., Senior, C.A., Banks, H., Gregory, J.M., Johns, T.C., Mitchell, J.F.B., Wood, R.A., “The simulation of SST, sea ice extents and ocean heat transports in a version of the Hadley Centre coupled model with out flux adjustments,” *Climate Dynamics* **16**,147–168, (2000).
- [Haigh 1996] Haigh, J., “On the impact of solar variability on climate,” *Science*, **272**, 981–984, (1996).
- [Hall 2002] Hall, A., Visbeck, M., “Synchronous variability in the Southern Hemisphere atmosphere, sea ice, and ocean resulting from the annular mode,” *Journal of Climate*, **15**, 3043–3057. (2002).
- [Halpert 1997] Halpert, M.S., Bell, G. D., “Climate Assessment for 1996. Bull, “*America Meteorologica Society*, **78**, S1–S49, (1997).
- [Haynes 1993] Haynes, R., Barton, E.D., Pilling, I., “Development, persistence and variability of upwelling filaments off the Atlantic coast of the Iberian peninsula,” *Journal of Geophysical Research*, **98**, 22681–22692.

BIBLIOGRAPHY

- [Honkoop 1998] Honkoop, P. J. C., J. Van der Meer, J. J. Beukema, D. Kwast, “Does temperature-influenced egg production predict the recruitment in the bivalve *Macoma balthica*?, “ Marine Ecology Progress Series, **64**, 229–235, (1998).
- [Hurrell 1995] Hurrell, J.W., “ Decadal trends in the North Atlantic Oscillation: regional temperatures and precipitation, “ Science, **269**, 676–679, (1995)
- [IPCC 1990] Intergovernmental Panel on Climate Change, “ The IPCC Scientific Assessment 1990, “Report prepared for Intergovernmental Panel on Climate Change by Working Group I J.T. Houghton, G.J. Jenkins and J.J. Ephraums (eds.), Intergovernmental Panel on Climate Change, “ Cambridge University Press, Cambridge, Great Britain, New York, NY, USA and Melbourne, Australia 410 pp. (1991).
- [IPCC 1996] Intergovernmental Panel on Climate Change, “ Climate Change 1995: The Science of Climate Change, “Contribution of Working Group I to the Second Assessment Report of the Intergovernmental Panel on Climate Change. Cambridge University Press, “Cambridge, Reino Unido y Nueva York, EE.UU., pp. 572, (1996).
- [IPCC 2001] Intergovernmental Panel on Climate Change, “ Climate Change 2001: The Scientific Basis, “Contribution of Working Group 1 to the Fourth Assessment Report of the Intergovernmental Panel on Climate Change Cambridge University Press, “Cambridge, university press. UK, (2001).
- [IPCC2007] Intergovernmental Panel on Climate Change, “ Climate Change 2007: The Physical Science Basis, “Contribution of Working Group 1 to the Fourth Assessment Report of the Intergovernmental

BIBLIOGRAPHY

Panel on Climate Change Cambridge University Press, “Cambridge, UK (2007).

- [Jones 2001] Jones, P.D., Osborn, T.J., Briffa, K.R., Folland, C.K., Horton, E.B., Alexander, L.V., Parker, D.E., Rayner, N.A., “ Adjusting for sampling density in grid box land and ocean surface temperature time series, “Journal of Geophysical Research **106**, 3371–3380. (2001).
- [Johnson 2007] Johnson, G.C. and Gruber, N., “Decadal water mass variations along $20^{\circ}W$ in the northeastern Atlantic Ocean,“ Progress in Oceanography, **73**, 277–295, (2007).
- [Josey 2002] Josey S.A., Kent E.C., Taylor P.K., “Wind stress forcing of the ocean in the SOC climatology: comparisons with the NCEP–NCAR, ECMWF, UWM/COADS, and Hellerman and Rosenstein datasets, “Journal Physics Oceanographic, **32**, 1993–2019, (2002).
- [Kaplan 1997] Kaplan, A., Y. Kushnir, M. Cane, and M. Blumenthal, “Reduced space optimal analysis for historical data sets: 136 years of Atlantic sea surface temperatures, ”Journal Geophysics Research, **102**, 27,835–27.860, (1997).
- [Kapala 1998] Kapala A., Machel H., Flohn H., “Behaviour of the centres of action above the Atlantic since 1881. II. Associations with regional climate anomalies, “International Journal of Climatology, **18**, 23–36, (1998).
- [Kara 2000] Kara, A.B., Rochfor, P.A., Hurlburt, H.E., “An optimal definition for ocean mixed layer depth, “Journal of Geophysical research, **105**, 16803–16821, (2000).

BIBLIOGRAPHY

- [Katsman 2011] Katsman C.A., van Oldenborgh G.J., “ Tracing the upper ocean’s missing heat, “ *Geophysical Research Letters*, **38**, L14610, 2011.
- [Kent 2005] Kent, E., Berry, D.I., “ Quantifying random measurement errors in voluntary observing ships’ meteorological observations, “ *International Journal of Climatology*, **25**, 843–856, (2005).
- [Kent 2006a] Kent, E., Challenor, P.G., “Toward estimating climatic trends in SST. PartII: random errors, “ *Journal of Atmospheric and Oceanic Technology*, **23**, 476–486, (2006).
- [Kent 2006b] Kent ,E., Taylor, P.K., “Toward estimating climatic trends in SST. PartI: methods of measurements, “*Journal of Atmospheric and Oceanic Technology*, **23**, 464–475, (2006).
- [Kerr 2000] Kerr, R.A., “A North Atlantic climate pacemaker for the centuries, “*Science*, **288 (5473)**, 1984–1986, (2000).
- [Kidson 1999] Kidson, J.W., “Principal modes of Southern Hemisphere low frequency variability obtained from NCEP–NCAR reanalysis, “*Journal of Climate*, **12**, 2808–2830, (1999).
- [Kilpatrick 2001] Kilpatrick, K., Podestá , G., Evans, R., 2001, “Over view of the NOAA/NASA pathfinder algorithm for sea surface temperature and associated match-updatabase, “*Journal of Geophysical Research*, **106**, 9179–9198, (2001).
- [Knight 2005] Knight, J.R., Allan, R.J., Folland, C.K., Vellinga, M., Mann, M.E., “Asignature of persistent natural thermohaline circulation cycles in observed climate, “*Geophysical Research Letters* **32**, L20708, (2005).

BIBLIOGRAPHY

- [Koutsikopoulos 1998] Koutsikopoulos, C., Beillois, P., Leroy, C., Taillefer, F., “Temporal trends and spatial structures of the sea surface temperature in the Bay of Biscay, “*Oceanologica Acta*, **21**, 335–344, (1998).
- [Kushnir 1994] Kushnir Y., “Interdecadal variations in North Atlantic sea surface temperature and associated atmospheric conditions, “ *American Meteorological Society*, 141–157, (1994).
- [Lemos 2004] Lemos, R.T., Pires, H.O., “The upwelling regime off the west Portuguese coast, 1941~2000, “*International Journal of Climatology*, **24**, 511–524, (2004).
- [Lemos 2006] Lemos, R.T., Sansó, H.O., “Spatio-temporal variability of ocean temperature in the Portugal current system, “*Journal of Geophysical Research*, **111**, C04010, (2006).
- [Levitus 1994] Levitus, S., Boyer, T., “World Ocean Atlas 1994“, Vol. 4: Temperature. NESDIS Atlas series, NOAA, “Washington, DC, 117 pp, (1994).
- [Levitus 2000] Levitus S, Antonov J, Timothy P.B., Stephens C., “Warming of the World Ocean, “*Science*, **287**, 2225–2229, (2000).
- [Levitus 2001] Levitus, S., Antonov, J.I., Boyer, T.P., Locarnini, R.A., Garcia, H.E., et al., “Global ocean heat content 1955–2008 in light of recently revealed instrumentation problems,“*Geophysical Research Letters*, **36**, L07608, (2001).
- [Levitus 2005] Levitus, S., Antonov, J., Boyer, T., “Warming of the world ocean, 1955–2003, “*Geophysical Research Letters*, **32**, L02604, (2005).
- [Levitus 2009] Levitus S, Antonov JI, Boyer TP, Locarnini RA, Garcia HE, et al.“ Global ocean heat content 1955â2008 in light of recently re-

BIBLIOGRAPHY

- vealed instrumentation problems, “ *Geophysical Research Letters*, **36**, L07608, (2009).
- [Levitus 2012] Levitus, S., Antonov, J.I., Boyer, T.P., Baranova, O.K., Garcia, H.E., et al., “World ocean heat content and thermosteric sea level change (0–2000 m), 1955–2010, “*Geophysical Research Letters*, **39**, L10603, (2012).
- [Lima 2006] Lima, E.P., Queiroz, N., Ribeiro, P.A., Hawkins, S.J., Santos, A.M., “Recent changes in the distribution of a marine gastropod, *Patella rustica* Linnaeus, 1758, and their relationship to unusual climate events, “ *Journal Biogeography*, **33**, 812–822, (2006).
- [Lima 2007] Lima, E.P., Ribeiro, P.A., Queiroz, N., Hawkins, S.J., Santos, A.M., “Do distributional shifts of northern and southern species of algae match the warming pattern?, “*Global Change Biology*, **13**, 2592–2604, (2007).
- [Lima 2012] Lima, F.P., Wethey, D.S., “Three decades of high-resolution coastal sea surface temperatures reveal more than warming, “*Nature Communications*, **3**, 704, (2012).
- [Llope 2006] Llope, M., Anadón, R., Viesca, L., Quevedo, M., González-Quiros, R., Stenseth, N.C., “Hydrography of the Southern Bay of Biscay shelf- break region: Interacting the multiscale physical variability over the period 1993–2003, “*Journal of Geophysical Research*, **111**, C09021, (2006).
- [Lorenzo 2008] Lorenzo M.N., Taboada J.J., Gimeno L., “Links between circulation weather types and teleconnection patterns and their influence on precipitation patterns in Galicia (NW Spain), “*International Journal of Climatology*, **28**(11), 1493–1505, (2008).

BIBLIOGRAPHY

- [Lyman 2010] Lyman, J.M., Good, S.A., Gouretski, V.V., Ishii, M., Johnson, et al., “Robust warming of the global upper ocean,” *Nature*, **465**, 334–337, (2010).
- [McGregor 2007] McGregor, H.V., Dima, M., Fischer, H.W., Mulitza, S., “Rapid 20th-century increase in coastal upwelling off northwest Africa,” *Science*, **315**, 637–663, (2007). doi:10.1126/science.1134839.
- [Marshall 2003] Marshall, G.J., “Trends in the southern annular mode from observations and reanalysis,” *Journal of Climate*, **16**, 4134–4143, (2003).
- [Mendelsohn 2002] Mendelsohn, R., Schwing, F.B., “Common and uncommon trends in SST and wind stress in the California and Peru–Chile current Systems,” *Progress in Oceanography*, **53**, 141–16, (2002).
- [Michel 2009] Michel, S., Treguier, A.M., Vandermeirsch, F., “Temperature variability in the Bay of Biscay during the past 40 years, from an insitu analysis and a 3D global simulation,” *Continental Shelf Research*, **29**(8), 1070–1087, (2009).
- [Nan 2003] Nan, S., Li, J., “The relationship between the summer precipitation in the Yangtze River valley and the boreal spring Southern Hemisphere annular mode,” *Geophysical Research Letters*, **30**(24), (2003).
- [Nelson 1983] Nelson, G., Hutchings, L., “The Benguela upwelling area,” *Progress in Oceanography*, **12**, 333–356, (1983).
- [Nerem 1999] Nerem R.S., Chambers D.P., Leuliette E.W., Mitchum G.T., Giese B.S., “Variations in global mean sea level associated with the 1997–1998 ENSO event: implications for measuring long-term sea level change,” *Geophysical Research Letters*, **26**, 3005–3008, (1999)

BIBLIOGRAPHY

- [Nicholls 1996] Nicholls N, Gruza GV, Jouzel J, Karl T, Ogallo L, et al. "Observed climate variability and change. In: Houghton, J., Jenkins, G., Ephraums., J. (Eds.), " Climate Change 1995: The Science of Climate Change, Cambridge University Press, 133–1992, (1996).
- [Nykjaer 1994] Nykjaer, L., VanCamp, L., "Season a land interannual variability of coastal upwelling along north west Africa and Portugal from 1981 to 1991, "Journal of Geophysical Research, **99(C7)**, 14197–14207, (1994).
- [Occhipinti 2007] Occhipinti-Ambrogi, A, " Global change and marine communities: Alien species and climate change, " Marine Pollution Bulletin, **55**, 342–352, (2007).
- [OSPAR2000] OSPAR, "Quality Status Report. Region IV– Bay of Biscay and Iberian coast, "Published by OSPAR Commission, London, (2000).
- [Palttridge 1981] Palttridge G., Wooddruff S., " Changes in global surface temperature from 1880 to 1977 derived from historical records of sea surface temperature, "Monthly Weather Review, **109**, 2427–2434, (1981).
- [Pardo 2011] Pardo, P.C., Padín, X.A., Gilcoto, M, Farinna–Busto, L., Pérez, F.F., "Evolution of upwelling systems coupled to the long term variability of sea surface temperature and Ekman transport, "Climate Research, **48**, 231–246, (2011).
- [Parker 1994] Parker, D.E., Jones, P., Folland, C., Bevan, A., " Interdecadal changes of surface temperature since the late nineteenth century, "Journal of Geophysical Research, **99**, 14339–14373, (1994).
- [Patti 2008] Patti, B., Guisande, C., Vergara, A.R., Riveiro, I., Maneiro, I., Barreiro, A., Bonanno, A., Buscaino, G., Cuttita, A., Basilone, G.,

BIBLIOGRAPHY

- Mazzola, S., “Factors responsible for the differences in satellite-based chlorophyll a concentration between the major global upwelling areas,” *Estuarine Coastal and Shelf Science*, **76**, 775–786, (2008).
- [Patti 2010] Patti, B., Guisande, C., Riveiro, I., Thejll, P., Cuttita, A., Bonanno, A., Basilone, G., “Effect of atmospheric CO_2 and solar activity on wind regime and water column stability in the major global upwelling areas,” *Continental Shelf Research*, **88**, 49–52, (2010).
- [Pauly 1995] Pauly, D., Christensen, V., “Primary production required to sustain global fisheries,” *Nature*, **374**, 255, (1995).
- [Pérez 1995] Pérez, F.F., Rios, A.F., King, B.A. & Pollard, R.T., “Decadal changes of the q–S relationship of the Eastern North Atlantic Central Water,” *Deep Sea Research, Part I*, **42**, 1849–1864, (1995).
- [Pérez 2010] Pérez, F.F., Padin, X.A., Pazos, Y., Gilcoto, M., Cabanas, M., Pado, P.C., Doval, M.D., Fariña-Bustos, L., “Plankton response to weakening of the Iberian coastal upwelling,” *Global Change Biology*, **16**, 1258–1267, (2010).
- [Peristykh 2003] Peristykh, A.N., Damon, P.E., “Persistence of the Gleissberg 88 *year* solar cycle over the last 12,000 years: evidence from cosmogenic isotopes,” *Journal of Geophysical Research*, **108**, 1003, (2003).
- [Philippart 2003] Philippart, C. J. M., H. van Aken, J. J. Beukema, O. G. Bos, G. C. Cade'e, R. Dekker, “Climate-related changes in recruitment of the bivalve *Macoma balthica*,” *Limnology and Oceanography*, **48**(6), 2171–2185, (2003).
- [Planque 2003] Planque, B., Beillois, P., Jegou, A.M., Lazure, P., Petitgas, P., Puillat, I., “Large-scale hydroclimatic variability in the Bay of Bis-

BIBLIOGRAPHY

cay: the 1900s in the context of interdecadal changes, "ICES Marine Science. Symposium, **219**, 61–70, (2003).

[Pollard 1996] Pollard, R.T., Griffiths, M.J., Cunningham, S.A., Read, J.F., Pérez, F.F. & Ríos, A.F. "Vivaldi 1991—A study of the formation, circulation and ventilation of Eastern North Atlantic Central Water, "Progress in Oceanography, **37**, 167–192, (1996).

[Pingree 1997] Pingree, R.D., "The eastern subtropical gyre (North Atlantic): Flow rings recirculations structure and subduction, "Journal of the Marine Biological Association of the UK, **78**, 351–376, (1997).

[PozoVázquez 2005] Pozo-Vázquez D, Gámiz-Fortis SR, Tovar-Pescador J, Esteban-Parra MJ, Castro-Díez Y., "El Niño-Southern Oscillation events and associated European winter precipitation anomalies,"International Journal of Climatology, **25**, 17–31, (2005).

[Press 1992] Press, W.H., Teukolsky, S.H., Vetterling, W.T., Flannery, B.P., "Numerical recipes in C: the art of scientific computing, "Cambridge University Press, Cambridge, (1992).

[Rayner 2003] Rayner, N.A., Parker, D.E., Horton, E.B., Folland, C.K., Alexander, L.V., Rowell, D.P., Kent, E.C., Kaplan, A., "Global analyses of sea surface temperature, sea ice, and night marine air temperature since the late nineteenth century, "Journal Geophysical Research, **108**, (2003).

[Rayner 2006] Rayner, N.A., et al., "Improved analyses of changes and uncertainties in sea surface temperature measured in situ since the mid-nineteenth century: the HadSST2 data set,"Journal of Climate, **19**, 446–469, (2006).

BIBLIOGRAPHY

- [Relvas 2009] Relvas, P., Luis, J., Santos, A.M.P., “Importance of the mesoscale in the decadal changes observed in the northern Canary upwelling system, “*Geophysical Research Letters* **36**, L2260, (2009)
- [Reynolds 1994] Reynolds, R.W., Smith, T.M., “ Improved global sea surface temperature analysis using optimum interpolation, “*Journal of Climate*, **7**, 929–948. (1994)
- [Reynolds 2009] Reynolds, R. W., “ What’s new in Version 2, “<http://www.ncdc.noaa.gov/oa/climate/research/sst/papers/whatsnewv2.pdf>, (2009).
- [Reynolds 2010] Reynolds, R. W., Chelton, D.W., “Comparisons of daily sea surface temperature analysis for 2007–08, “*Journal of Climate*, **23**, 3545–3562, (2010).
- [Rios 1992] Ríos, A.F., Pérez, F.F. and Fraga, F., “Water masses in the upper and middle North Atlantic Ocean east of the Azores, “*Deep-Sea Research*, **39**, 645–58, (1992).
- [Rodo 1997] Rodó X., Baert E., Comin F.A., “Variations in seasonal rainfall in southern Europe during the present century: relationships with the North Atlantic Oscillation and the El Niño–Southern Oscillation, “*Climate Dynamics*, **13**, 275–284, (1997).
- [RodriguezPuebla 1988] Rodríguez–Puebla C, Encinas AH, Nieto S, Garmendia J., (1998), “Spatial and temporal patterns of annual precipitation variability over the Iberian Peninsula, “*International Journal of Climatology*, **18**, 299–316, (1988).
- [RodriguezPuebla 2001] Rodríguez–Puebla C., Encinas A.H., Sáenz J., “Winter precipitation over the Iberian Peninsula and its relationship to

BIBLIOGRAPHY

- circulation indices, “Hydrology and Earth System Sciences, **5**, 233–244, (2001).
- [Saenz 2001] Saenz J., Zubillaga J., Rodríguez–Puebla C., “Interannual winter temperature variability in the north of the Iberian Peninsula, “Climate Research **16**, 169–179, (2001).
- [Saha 2010] Saha, Suranjana, et al, “The NCEP Climate Forecast System Reanalysis, “ Bulletin of the American Meteorological Society, **91**, 1015–1057, (2010).
- [Santos 2011a] Santos, F., Gómez–Gesteira, M., deCastro, M., Álvarez, I., “Upwelling variability along the western coast of the Iberian Peninsula: can trends be accurately calculated?, “Climate Research, (2011).
- [Santos 2011b] Santos, F., Gómez–Gesteira, M., deCastro, M., “Coastal and oceanic variability along the western Iberian peninsula,“Continental Shelf Research, **31**, 2012–2017, (2011).
- [Santos 2011c] Santos, F., Gómez–Gesteira, M., deCastro, M., Álvarez, I.,“Upwelling along the western coast of the Iberian Peninsula: dependence of trends on fitting strategy, “Climate Research, **48** 213–218, (2011).
- [Santos 2012a] Santos F., Gómez-Gesteira, M., deCastro, M. Álvarez I,“Variability of coastal and ocean water temperature in the upper 700 m along the Western Iberian Peninsula from 1975 to 2006, “Plos One, **7(12)**, 1–7, (2012).
- [Santos 2012b] Santos F., Gómez-Gesteira, M., deCastro, M. Álvarez I,“Differences in coastal and oceanic SST trends due to the strengthening of coastal upwelling along the Benguela current system,“Continental Shelf Research, **34**, 79–86, (2012)

BIBLIOGRAPHY

- [Santos 2012c] Santos, F., deCastro, M., Gómez-Gesteira, M., Álvarez, I., “Differences in coastal and oceanic SST warming rates along the Canary upwelling ecosystem from 1982 to 2010, “Continental Shelf Research, **47**, 1–6, (2012).
- [SantosA 2005] Santos A.M.P., Kazmin A.S., Peliz A., “Decadal changes in the Canary upwelling system as revealed by satellite observations: their impact on productivity,“Journal of Marine Research, **63**, 359–379, (2005).
- [Saunders 2008] Saunders, M.A., Lea, A.S., “Large contribution of sea surface warming to recent increase in Atlantic hurricane activity, “Nature, **451**, 557–560, (2008).
- [Schwing 1997] Schwing, F.B., Mendelsohn, R., “Increased coastal upwelling in the California Current System,“Journal Geophysical Research, **102B**, 3421–3438, (1997).
- [Slonosky 2002] Slonosky V., Yiou P., “Does the NAO index represent a zonal flow? The influence of the NAO on North Atlantic surface temperature,“Climate Dynamics, **19**, 17–30, (2002).
- [Smith 1994] Smith, T.M., Reynolds, R.W., Ropelewski, C.F., “Optimal averaging of seasonal sea-surface temperatures and associated confidence intervals (1860–1989), “Journal of Climate, **7**, 949–964, (1994).
- [Smith 2002] Smith, T.M., Reynolds, R.W., “Bias corrections for historic sea-surface temperatures based on marine air temperatures, “Journal of Climate, **15**, 73–87, (2002).
- [Smith 2003] Smith, T.M., Reynolds, R.W., “Extended reconstruction of global sea-surface temperatures based on COADS data (1854–1997), “Journal of Climate, **16**, 1495–1510, (2003).

BIBLIOGRAPHY

- [Smith 2004] Smith, T.M., Reynolds, R.W., “Improved extendedre construction of SST (1854–1997), “*Journal of Climate*, **17**, 2466–2477, (2004).
- [Smith 2005] Smith T.M., Reynolds R.W., “ A global merged land&air&sea-surface temperature reconstruction based on historical observations (1880–1997), “*Journal of Climate*, **18**, 2021–2036, (2005).
- [Smith 2008] Smith T.M., Reynolds R.W., Lawrimore J., “Improvements to NOAA’s historical merged land-ocean surface temperature analysis (1880–2006), “*Journal of Climatic*, **21**, 2283–2296, (2008).
- [Stephenson 2000] Stephenson, D.B., Pavan, V., Bojariu, R., “Is the North Atlantic Oscillation a random walk?, “*International Journal of Climatology*, **20**, 1–18, (2000).
- [Strong 2000] Strong A.E., Kearns E.J., Gjovig K.K., “ Sea-surface temperature signals from satellite an update, “ *Geophysical Research Letters*, **27**, 1667–1670, (2000).
- [Sutton 2005] Sutton, R.T., Hodson, D.L.R., “Atlantic Ocean forcing of North American and European summer climate, “*Science*, **290**, 2133–2137, (2005).
- [Sutton 2007] Sutton, R.T., Dong, B., Gregory, J.M., “Land/sea warming ratio in response to climate change: IPCC AR4 model results and comparison with observations, “*Geophysical Research Letters*, **34**, L02701, (2007)
- [Timmermann 1998] Timmermann,A., Latif, M., Voss, R., Grotzner, A., “Northern hemispheric interdecadal variability: a couple dair-sea mode, “*Journal of Climate*, **11**, 1906–1931, (1998).

BIBLIOGRAPHY

- [Thieltges 2006] Thieltges, D. W., “Parasite induced summer mortality in the cockle *Cerastoderma edule* by the trematode *Gymnophallus cholechus*,” *Hydrobiologia*, **559** (1), 455–461, (2006).
- [Thompson 2000] Thompson D.W.J., Wallace, J.M., “Annular modes in the extratropical circulation. I. Month-to-month variability,” *Journal of Climate*, **13**, 1000–1016, (2000).
- [Tome 2004] Tome, A.R., Miranda, P.M.A., “Piecewise linear fitting and trend changing points of climate parameters,” *Geophysical Research Letters*, **31**, L02207, (2004).
- [Trenberth 2006] Trenberth, K.E., Shea, D.J., “Atlantic hurricanes and natural variability in 2005,” *Geophysical Research letters*, **33**, L12704, (2006).
- [Trigo 2004] Trigo R.M., Pozo–Vázquez D., Osborn T.J., Castro–Díez Y., Gámiz–Fortis S., Esteban–Parra M.J., “North Atlantic Oscillation influence on precipitation, river flow and water resources in the Iberian Peninsula,” *International Journal of Climatology*, **24**, 925–944, (2004).
- [Trigo 2009] Trigo R M, Ramos A M, Nogueira P J, Santos F D, Garcia-Herrera R, Gouveia C, Santo F E, “Evaluating the impact of extreme temperature based indices in the 2003 heatwave excessive mortality in Portugal,” *Environmental Science & Policy*, **12**, 844–854, (2009).
- [Usoskin 2009] Usoskin, I.G., Mursula, K., Arlt, R., Kovaltsov, G.A., “A solar cycle lost in 1793–1800: early sunspot observations resolve the old mystery,” *Astrophys Journal Letters*, **700**, L154, (2009).
- [VanCamp 1991] VanCamp, L., Nykjaer, L., Mittelstaedt, E., Schlittenhardt, P., “Upwelling and boundary circulation off northwest Africa

BIBLIOGRAPHY

as depicted by infrared and visible satellite observations, “Progress in Oceanography, **26**, 357–402, (1991).

[Vellinga 2002] Vellinga, M., Wood, R.A., “Global climatic impacts of a collapse of the Atlantic thermohaline circulation, “Climate Change, **54**, 251–267, (2002).

[White 1997] White, W.B., Lean, J., Cayan, D.R., Dettinger, M.D., “A response of global upper ocean temperature to changing solar irradiance, “Journal Geophysics Research, **102**, 3255–3266, (1997).

[Wethey 2011] Wethey, D.S., et al., “ Response of intertidal populations to climate: effects of extreme events versus long term change, “Journal of Experimental Marine Biology and Ecology, **400**, 132–144, (2011).

[Wooster 1976] Wooster, W.S., Bakun, A., McLain, D.R., “The seasonal upwelling cycle along the eastern boundary of the north Atlantic, “Journal of Marine Research, **34**, 131–141, (1976).

[Worley 2005] Worley, S.J., Woodruff, S.D., Reynolds, R.W., Lubker, S.J., Lott, N., “ICOADS release 2.1 data and products, “International Journal of Climatology, **25**, 823–842, (2005).

[Yousef 2006] Yousef, S.M., “ 80–120 *yr* long-term solar induced effects on the earth, past and predictions, “Physics and Chemistry of the Earth, **31**, 113–122, (2006).

[Zheng 2009] Zheng Y., Gies B.S., “Ocean heat transport in Simple Ocean Data Assimilation: structure and mechanisms, “ Journal Geophysical Research, **114**, C11009, (2009).

BIBLIOGRAPHY

- [Zheng 2010] Zheng Y., Shinoda T., Kiladis G.N., Lin J., Metzger E.J.,
“Upper-Ocean Processes under the Stratus Cloud Deck in the South-
east Pacific Ocean,” American Meteorological Society, (2010).